FORECASTING DRY WEATHER FLOW TO ASSESS FUTURE WATER EXTRACTION CAPACITIES AT KOLEIMODARA INTAKE IN KUDA GANGA, KALU GANGA

Warushahennadige Rangika Sajeewani Fernando

(208351R)

Degree of Master of Science

Department of Civil Engineering

University of Moratuwa
Sri Lanka

February 2022

FORECASTING DRY WEATHER FLOW TO ASSESS FUTURE WATER EXTRACTION CAPACITIES AT KOLEIMODARA INTAKE IN KUDA GANGA, KALU GANGA

Warushahennadige Rangika Sajeewani Fernando

(208351R)

Supervised by

Mr A. H. R. Ratnasooriya

Thesis submitted in partial fulfillment of the requirements for the degree Master of Science in Civil Engineering

UNESCO Madanjeet Singh Centre for
South Asia Water Management (UMCSAWM)
Department of Civil Engineering

University of Moratuwa
Sri Lanka

February 2022

DECLARATION OF THE CANDIDATE AND SUPERVISOR

"I declare that this is my own work and this thesis/dissertation2 does not incorporate without acknowledgement any material previously submitted for a Degree or Diploma in any other University or institute of higher learning and to the best of my knowledge and belief it does not contain any material previously published or written by another person except where the acknowledgement is made in the text".

Also, I hereby grant to University of Moratuwa the non-exclusive right to reproduce and distribute my thesis, in whole or in part in print, electronic or other medium. I retain the right to use this content in whole or part in future works (such as articles or books).

UOM Verified Signature

Warushahennadige Rangika Sajeewani Fernando

03/02/2022

Date

The above candidate has carried out research for the Masters/~~MPhil/PhD~~ thesis/ ~~Dissertation~~ under my supervision

UOM Verified Signature

Mr A. H. R. Ratnasooriya

03/02/2022

Date

ABSTRACT

Forecasting Dry Weather Flow to Assess Future Water Extraction Capacities at Koleimodara Intake in Kuda Ganga, Kalu Ganga

Kalu Ganga is the primary source of potable water supply in the greater Colombo area and total Kalutara District. Kethhena water treatment is supposed to cover the water demand in the middle and southern parts of the Kalutara district, which is estimated as 1.5 m^3/s, including the subsequent explanation to covet 2030 to 2060 design horizon. The new intake at Koleimodara in Kuda Ganga is supposed to extract water during the dry weather period the as the old intake at Thebuwana is impacted by salinity intrusion. Therefore, this study was formulated to assess the possibility of extracting water from the Koleimodara intake during the subsequent design horizon.

A hydrological model was developed using Hydrologic Engineering Centre's Hydrologic Modelling System (HEC HMS) to estimate river discharge at Koleimodara with Deficit and Constant loss method, linear reservoir baseflow method, Snyder Unit Hydrograph transform method, and Muskingum routing method. The calibration and validation events were selected as the water cycle having prolonged dry spells i.e.,2006/2007 and 2011/2012 for calibration and 2008/2009, 2009/2010, 2013/2014 and, the continuous stimulation from 2005 to 2015 for validation. Kukule Ganga run-off-the-river plant operations were included for the model with elevation-capacity-discharge relationship considering environmental flow (0.5 m^3/s) and maximum turbine discharge. The objective functions, Relative Nash-Sutcliff (NSE_{rel}), Mean Ratio of Absolute Error (MRAE), Root mean square error (RMSE), and Percent bias (PBIAS) were used to evaluate model performance. Future precipitation projections were derived from Regional Climate Model (RCM) ICTP-RegCM4-7 based on NCC-NORESM1-M Global Climate Model (GCM) under Coupled Model Intercomparison Project Phase 5 (CMIP5) project. Two future scenarios of Representative Concentration Pathways (RCP) 2.6 and 8.5 were used to assess the future precipitation in the basin and streamflow at the intake location. The Standard Precipitation Index (SPI) and low flow indices i.e., Probability exceedance flow of 90^{th} percent (Q_{90}) and 50^{th} percent (Q_{50}), Mean 7-day annual minima (MAM7) and Mean 30-day annual minima (MAM30), Baseflow index (BFI), deficit duration, deficit volume, and intensity were applied to assess the future (2030-2060) climatic and low flow conditions of the project area relative to the observed data simulations of the 2005 to 2020 period.

The SPI indicated a possibility of the dry months becoming drier (June, July, and August under RCP 2.6 and July and August under RCP 8.5) or prevail the same dry conditions (January and February under both RCPs), and the wet month May receives more precipitation (under RCP 8.5). All indices indicated a possibility of low flows decreasing with deficit durations becoming more prolonged under both RCPs particularly during 2030-2040. Deficit analysis results and MAM7, MAM30 results indicated that the first inter-monsoon and Northwest monsoon periods continue to be the dry period. The intake is projected as facing a maximum deficit volume of 4.9 MCM for 47 days with the intensity of 105 thousand m^3/day and with a deficit volume of 4.4 MCM for 42 days with the intensity of 105 thousand m^3/day respectively, under RCP 2.6 and 8.5 during 2030 to 2040. Deficit events are projected as two during the base period (2005-2020) and nine and twelve respectively, under RCP 2.6 and 8.5 from 2030 to 2060. Based on the results of this study, it is recommended to select another water source for the next design horizon extractions or maintain storage of about 4.9 MCM to cater to the dry period water deficit to provide an uninterrupted water supply.

Keywords: Climate change, HEC HMS, Kukule Ganga, low flow, RCM, water intake

DEDICATION

I would like to dedicate this study to my parents for all the efforts and dedications they made, and the encouragement and support given which no words can express to make me and my sister who we are today.

ACKNOWLEDGEMENT

I would like to offer my sincere gratitude to the late Sri Madanjeet Singh for founding South Asia Foundation (SAF) and offering scholarships through UNESCO Madanjeet Singh Center for South Asia Water Management (UMCSAWM). The efforts by SAF chapter of Sri Lanka are highly appreciated which paved the way for obtaining the scholarship and processing of the documents.

I take this opportunity to express my sincere gratitude to my research supervisor, Mr. Harsha Rathnasooriya, for continuous guidance, valuable advice, and support and for guiding me to get support from relevant expertise. I must convey my heartfelt appreciation to the research coordinator, Dr. Janaka Bamunawala for the valuable advice, encouragement, fullest support given throughout this study, and coordination for even arranging other expertise to get advice.

Further, I wish to express my deep appreciation to Prof. R. L. H. Lalith Rajapakse, Director/center Chairman of UMCSAWM for his valuable advice, and for being always responsive and supportive to complete this study successfully. I must convey my sincere gratefulness to all the research panel members as their valuable comments had always helped me to direct this study on the correct path and to continuously improve it. Moreover, I must show my sincere appreciation to Dr. Nimal Wijayaratna for his valuable support, advice given especially in hydrological modeling. I am very much grateful to Dr. Jeewanthi Sirisena for her valuable advice and heartfelt encouragement to move forward during the hard times.

Further, I wish to acknowledge the help provided by the technical and support staff in the UMCSAWM center of the University of Moratuwa.

I am grateful to the Director of Irrigation (Hydrology), Irrigation Department for providing me with streamflow data as well as the Deputy General Manager (Samanala Complex) and Civil Engineer of DGM (Samanala Complex) office, Ceylon Electricity Board for providing me with Elevation-Area-Capacity details and other relevant data of the Kukule Ganga weir which were very important data for this study.

Further, I must acknowledge Ms. Kumari Alahapperuma, the immediate superior of my workplace, Chief Engineer (Planning and Design), and also Deputy General Manager (Western-South) and the General Manager of the National Water Supply and Drainage Board for granting me to apply for this scholarship and acquire this valuable knowledge.

I must sincerely acknowledge my heartiest fellow batch mates for their support and encouragement. Even though we had to manage with distance learning their support was always there when needed.

Finally, I must gratefully remind my husband and my son for all the support and encouragement given and for baring me being fully engaged with studies in times and also my mother and parents in-law who supported me in every possible way to complete this study successfully.

TABLE OF CONTENTS

LIST OF FIGURES

LIST OF TABLES

LIST OF ABBREVIATIONS

ADB: Asian Development Bank, ... 1
AED: Atmospheric Evaporative Demand, ... 36
AMAIWSP: Aluthgama Mathugama Agalawatta Integrated Water Supply Project, . 4
AMF: Absolute Minimum Flow, ... 10
AOGCM: Atmosphere-Ocean coupled General Circulation Model, ... 34
AR 5: Fifth Assessment Report, ... 32
CCCR-IITM: Centre for Climate Change Research - Indian Institute of Tropical Meteorology, ... 33
CE: Coefficient of Efficiency, ... 19
CEA: Central Environmental Authority, ... 14
CGCM: Coupled General Circulation Models, ... 32
CMIP 5: Coupled Model Intercomparison Project Phase 5, ... 32
CORDEX: Coordinated Regional Downscaling Experiment, ... 6
C_p: Peaking Coefficient, ... 30
C_t: basin coefficient, ... 30
DC: Deficit and Constant, ... 27
DSD: District Secretariate Division, ... 3
EIA: Environmental Impact Assessment, ... 4
EMC: Environmental Management Classes, ... 14
ESGF: Earth System Grid Federation, ... 34
ET_o: Reference Evapotranspiration, ... 36
FDC: Flow Duration Curve, ... 10
FSL: Full Supply Level, ... 76
GCM: Global Climate Models, ... 33
HEC HMS: Hydrologic Engineering Centre's Hydrologic Modelling System, ... 23
IEE: Initial Environmental Examination, ... 13
IPCC: Inter-governmental Panel for Climate Change, ... 6
IWMI: International Water Management Institute, ... 14
JICA: Japan International Cooperation Agency, ... 1

CHAPTER 1

1 INTRODUCTION

1.1 General

Sufficient, safe, and convenient water supply and sanitation services are required to facilitate economic development, protect health, and ensure the participation of all citizens in society. Drinking water is the primary need of water supply, and Sri Lanka currently covers its drinking water requirement through different sources, i.e., 49.2% from pipe-bone water, 36.4% from protected wells, 5.4% from reservoirs or rivers, 4.4% from unprotected wells, 3.2% from tube wells, 1% from rainwater (Fan, 2015). The Government of Sri Lanka, through the Ministry of Water Supply with the support of development partners such as the World Bank, Asian Development Bank (ADB), Japan International Cooperation Agency (JICA), and China has substantially invested in improving water supply and sanitation services. These projects cover urban and semi-urban schemes implemented by the National Water Supply and Drainage Board (NWSDB) in all parts of the country.

As a result of the infrastructure development with economic opportunities and continuing effective urbanization in areas connected to the cities, more people have migrated to these urban and semi-urban areas making some 57% of the population live in urban or semi-urban areas. Households are rapidly adopting urban characteristics aspiring to better housing, transport, and reliable utility services such as water supply and sanitation (CSIP, 2019).

National development objectives and strategies are gradually shifting from agriculture to service sector, export-oriented industries, tourism, and financial services. Efficient services in water supply and sewerage are needed to support this transformation. The growth of the Colombo metropolis and the surrounding towns requires substantial water and wastewater services (CSIP, 2019). When considering the annual water

consumption in Sri Lanka (513 MCM), the Greater Colombo area in the Western province accounted for 39% of portable water consumption. Manufacturing water demand also growing high in the Western province and 87% of total annual water consumption in the Manufacturing Sector (15 MCM) is consumed within the Western Province (CSIP, 2019). Raw water requirement for the Western province is mainly covered by the Kelani River and Kalu River. Therefore, the water extraction capacity in the rivers will be critical for future developments in the area. The water treatment plants further downstream of both rivers already started facing salinity intrusion issues during the low flow periods and among many other reasons the reduction of flow during this period would be a possible reason which should be considered.

1.2 Climate Change Effects Related to the Wet Zone of Sri Lanka

The Global Climate Risk Index 2020 has listed Sri Lanka under the ten countries which were most affected by the extreme events due to climate change in 2018. Due to climate change, significant shifts in weather patterns have been observed in Sri Lanka, bringing new challenges to water resources managers. The temperature in Sri Lanka is increasing at a rate of 0.0164°C/year (Chen & Costa, 2017), intensifying the evaporation, directly affecting the water retention capacity of inland water bodies and soil. According to the past studies, the mean annual precipitation (MAP) of Sri Lanka has decreased by 144 mm (~7%) between 1961 and 1990 compared to the period 1931 – 1960 (Chandrapala, 1996; Jayatillake et al., 2005). The western slope of the central highlands, which receive the highest MAP (often exceeds 5000 mm), has indicated a significant decline in rainfall from 1900 to 2002, mainly due to the reduction in SWM rainfall. Country-wide statistics indicate that the number of consecutive dry days expanded, whereas continuous wet days reduced (Pathirana et al., 2007; Premalal, 2009). Wet zone and intermediate zone rainfall are projected to be increased while the dry zone i.e., north and southwestern region rainfall to be decreased by 2050 (Basnayake & Vithanage, 2004). Marambe et al. (2015) and Punyawardena et al. (2013) also recently projected that the climate pattern in Sri Lanka would be getting polarized as the wet zone areas be wetter and dry zones be drier.

Extended dry weather periods decrease the river flow discharges, which enhances the salinity intrusion and drastically decreases the other water quality parameters by increased pollutant loads due to inadequate dilution water factor (Dasgupta et al., 2014). Many water supply schemes in the wet zone's coastal belt would face a water deficit by 2030 unless new sources are added because the abstraction from the Kelani River is already limited during dry spells.1 Besides the quantity limitations, a quality crisis is also due to salinity intrusion. The water supply sector engaged in supplying water to drinking and other industrial purposes is one of the critical sectors which needs urgent attention regarding these climate-change-driven impacts, as its adverse consequences are already evident.

1.3 Background and Context

The Kalu Ganga is the primary source of water used by NWSDB, to provide potable and industrial water to the Southern part of Colombo district, whole Kalutara District, and also covering part of Bentota District Secretariate Division (DSD). There are two water intakes in Kalu Ganga located at Thebuwana and Kandana, operated by NWSDB to supply water to Western South Region. The Thebuwana water intake, which supplies raw water to Kethhena Water Treatment Plant (WTP), is located at Kalu Ganga around 17 km upstream of the river's outfall (Figure 1-1).

Present maximum treatment of Kethhena intake is 12.5 Million Gallons per Day (MGD) (i.e., 0.7 m^3/s or 56,850 m^3/day to serve 250,000 people) and it will be upgraded to 15.5 MGD (i.e., 0.82 m^3/s or 70,450 m^3/day) under Aluthgama Mathugama Agalawatta Integrated Water Supply Project (AMAIWSP).

Salinity intrusion to Thebuwana Intake has become a significant problem. During the dry weather conditions in February, March, and August, salinity intrusion severely affects this intake, creating numerous operational problems in the water supply schemes. To solve this significant social and health problem, the NWSDB has proposed constructing a salinity barrier across Kalu Ganga around 200 m downstream to the existing Kethhena Intake at Thebuwana. Hydraulic and Environmental study for the Environmental Impact Assessment (EIA) report was carried out by Lanka Hydraulic Institute (LHI). However, NWSDB could not obtain the necessary approval

from the Irrigation Department to construct a salinity barrier due to the severe flood-prone nature of the Kalu River.

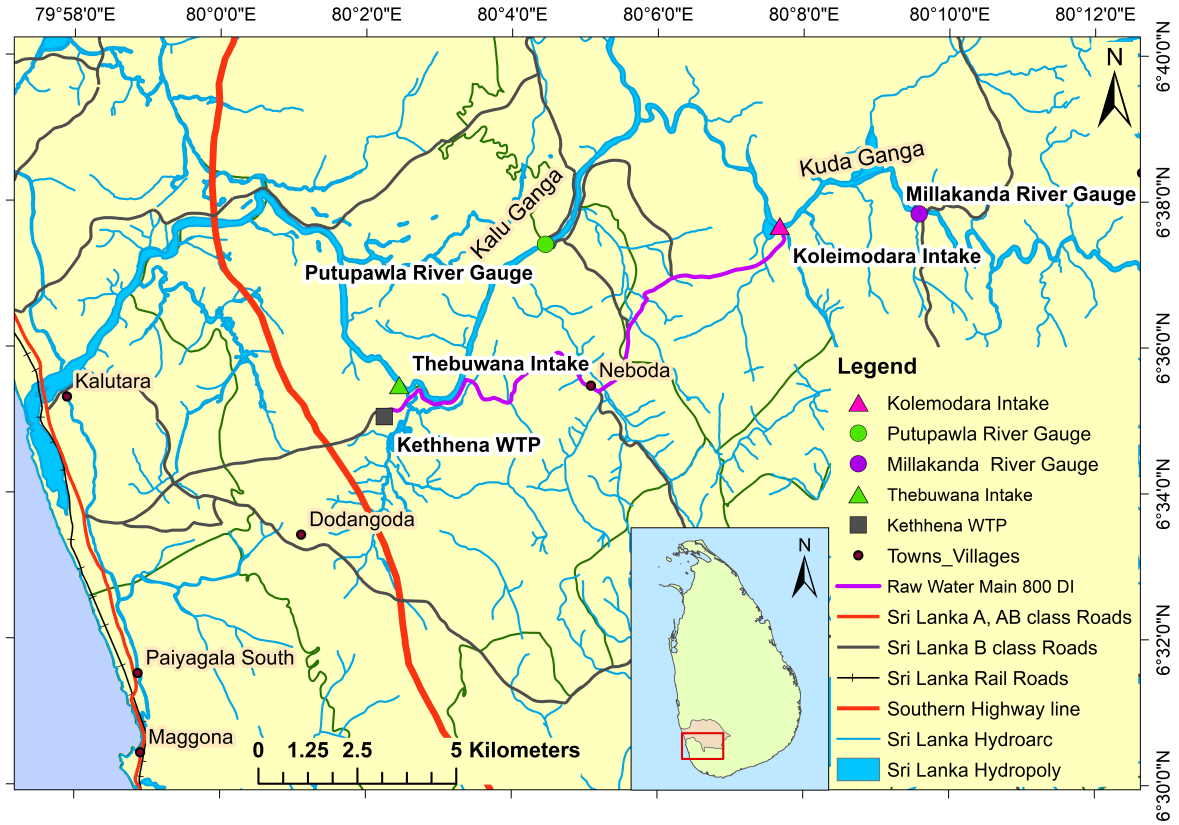

Figure 1-1: The Location map of intakes and river gauging stations

Source: Survey Department of Sri Lanka

A new water intake structure has been constructed by NWSDB with a capacity of 16.5 MGD (i.e., 0.87 m^3/s or 75,000 m^3/day) at Koleimodara in Kuda Ganga under AMAIWSP to extract water during the salinity intrusion period. It is about 4.8 km downstream of the Millakanda river gauging station (Figure 1-1). The minimum annual daily average discharge at Millakanda varies between 8.4 m^3/s to 26.1 m^3/s during the 1990-2017 period. Koleimodara has been identified as the most feasible location for the new water intake, considering the recorded minimum daily average discharges at Millakanda river gauging station during 1991-2008 and water quality conditions during dry periods at the proposed intake. This Intake structure has been designed considering a 20-year design horizon to cater to the water demand up to 2030 (*Pre-Feasibility Report - Aluthgama Mathugama Agalawatta Integrated Water Supply Project*, 2011). According to the latest project formulation decisions of NWSDB, the

design horizon of a water supply project would be panned and designed for 30 years design horizon (*P1 Manual – Project Planning Feasibility*, 2019). By the time of 2030, the water extraction capacity of the Intake structure will have to be improved for the next 30 years. The subsequent intake capacity requirement has been estimated as 50,000 m^3/day according to the Masterplan of NWSDB (CSIP, 2019). The low flow period of the Kuda Ganga will be critical for the functioning of the intake at its total capacity while maintaining environmental flow. Therefore, it is required to assess the low flow thresholds of Kuda Ganga to check the adequacy for future water demands.

Kukule Ganga run-off-the-river type power plant, commissioned in November 2003, was built in the Kukule Ganga which is a tributary of Kuda Ganga (Sonoda, 2007). Considering the yearly minimum flow of the Millakanda river gauging station, a decrease in the magnitude of yearly minimum flow could be identified after introducing a run-off-the-river type power plant in Kukule Ganga in 2003. The data period after 2003 is not adequate to perform frequency analysis and predict the subsequent 30-year minimum flows. Therefore, this study was undertaken to calibrate and validate a suitable hydrological model using 2005 to 2020 data sets to simulate runoff at the Koleimodara intake location using the Millakanda River gaging data for model calibration. Future precipitation projections were derived by Regional Climate Model (RCM) extracted from the regional climate model (Coordinated Regional Downscaling Experiment - CORDEX) (CORDEX; http://cordex.org/) under Inter-governmental Panel for Climate Change (IPCC) fifth assessment (Giorgi et al., 2012). A low-end Representative Concentration Pathways (RCP) 2.6 and high-end RCP 8.5 were selected for the future projections of precipitation to assess the low flows from the hydrological models for the next design horizon up to 2060.

1.4 Problem Statement

Yearly minimum seven-day moving average daily flow at Millakanda streamflow gauging station in Kuga Ganga indicates a decreasing trend from 1990 to 2015 (Figure 1-2), before and after the Kukule Ganga run-off-the river power plant operation. Koleimodara intake in Kuga Ganga is located 4.8 km downstream of the Millakanda streamflow gauging station. Therefore, the possibility of water extraction from the

intake to meet increasing future demands of the coverage area (Southern part of Kalutara district) will be critical in the future. According to the latest project formulation decisions of NWSDB, the design horizon of a water supply project would be planned and designed for 30 years design horizon (*P1 Manual – Project Planning Feasibility*, 2019). By the time of 2030, the water extraction capacity of the Intake structure will have to be improved for the subsequent 30 years. The knowledge of the future water extraction capacities on the location is very important as it facilitates correct decisions and convinces the other stakeholders.

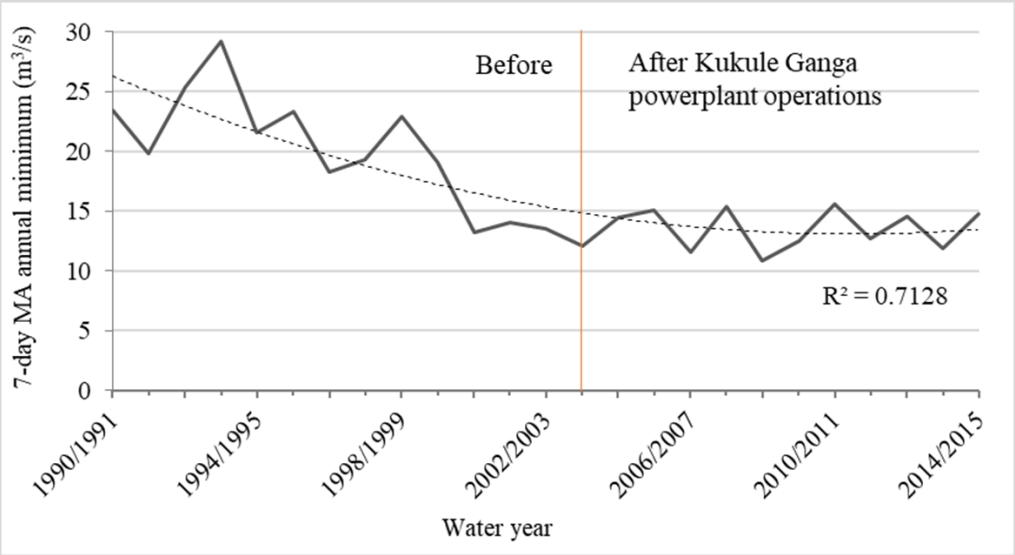

Figure 1-2: Annual minimum of seven-day moving average daily discharge at Millakanda gauging station for total data period before (1991-2001) and after (2003 -2017) the Kukule Ganga run-off-the-river powerplant establishment

1.5 Research Objectives

1.5.1 Main objective

This research aims to assess and predict low flow thresholds of Kuda Ganga at Koleimodara intake and check the possibility of water extraction throughout the next design horizons, considering the latest climate change scenarios.

1.5.2 Specific objectives

The specific objectives related to this study are identified as follows;

- To study streamflow characteristics and identify the low flow period of Kuda Ganga using Millakanda river flow gauging station data.
- To develop a hydrological model to estimate river flow at Koleimodara Intake.
- To determine minimum flow threshold values at Koleimodara intake.
- To assess future low flow using extracted data from RCM under higher-end climate scenario (RCP8.5) and lower-end climate scenario (RCP 2.6).
- To obtain recommendations regarding the possibility of water extraction at Koleimodara intake for the next design horizon (2030 to 2060).

CHAPTER 2

2 LITERATURE REVIEW

Low flow can be identified in different ways relative to the group of interest as described by Smakhtin (2001). He simply describes it as the river discharge during the dry period of the annual water cycle or it may depend on the conditions of the river regime and time periods between flood events. Environmental Protection Agency also figure out the definition of low according to the definition of the World Meteorological Organization which is the "flow of water in a stream during prolonged dry weather".

2.1 **Low Flow Hydrology**

The low flow of a particular river is usually derived from the groundwater discharge or from the surface discharges from surface storages such as lakes, marshes, or by the melting of glaciers. Low flow hydrology of a particular river basin is essential for planning and designing of water supply, estimating the potential for waste dilution, reservoir capacity designing, for recreation and wildlife conservation, for quality wise and quantity wise estimating of other water withdrawal capacities such as for irrigation and other industrial purposes (Smakhtin, 2001; (WMO), 2009). This study mainly focused on the significance of low flow hydrology in the planning and designing activities concerning the water supply sector.

The low flow regime of a river is affected by natural factors such as the level of distribution of the aquifers, and their hydraulic characteristics, recharge amount, rate, and frequency, the infiltration rate of the soil, rate of evapotranspiration, vegetation types, climate, and topology. It is followed by various anthropogenic activities such as groundwater and surface water abstractions, diversions and damming, all kinds of land-use changes, and effluent discharges (Smakhtin, 2001).

2.1.1 Low flow estimation

The lowest recorded daily discharge is termed as the Absolute Minimum Flow (AMF). Absolute Minimum Flow depends on the record length of the streamflow data gauge measuring limits. Analysis of the low flow regime of a river depends on the type of data availability and the nature of the output requirement. The flow duration curve (FDC) method is used in different temporal resolutions of the whole data period, such as average annual FDCs', long-term average monthly FDC', monthly FDC, or long-term average seasonal FDC. The FDC illustrates the duration characteristics of a river flow with frequency distribution for a given period and does not refer to the sequence of occurrence of the event (Mngodo, 1997; Vogel & Fennessey, 1994).

Low flow frequency analysis fills the above-mentioned shortcoming of FDC and demonstrates the recurrence interval of the low flow event relative to a defined discharge. The low flow Frequency Curve (LFFC) is plotted using the annual minimum flow value (daily or monthly) from an available continuous flow series data, or the minimum low flow value selected from the seasons considered for low flow frequency analysis. The problem in frequency analysis is the unavailability of sufficient observed data for reliable extreme event quantification for a required return period. Extrapolation of data beyond the observed period needed various theoretical distribution functions, such as different forms of Weibull, Gumbel, Pearson Type III, and log-normal distributions. However, a specific or worldwide recognized distribution function is not existing for low-flows and is unlikely to be identified (Smakhtin, 2001).

2.1.2 Low flow deficit analysis

Flow Duration Curves (FDC) or LFFC do not determine the length of low flow relative to a specified interested flow or the deficit of flow volume. Two methods are used for streamflow deficit analysis: the threshold-level method and the sequent peak algorithm (WMO, 2009). The determination of the threshold value depends on the purpose of the study. Smakhtin (2001) used 70–90% exceedance on FDC as the drought analysis threshold value of perineal rivers. The Manual on Low-flow Estimation and Prediction Operational Hydrology Report (WMO No.1029) suggests 70–95% exceedance on

FDC as a suitable threshold. The streamflow deficit starts when the streamflow reduces below the selected threshold value and ends as the flow increases beyond the threshold value. Several characteristics are defined and used by the researchers to analyze the low flow conditions, namely; (i) The duration d_i in the number of days which discharge $Q \leq Q_o$;(ii) The drought volume or severity, v_i [m^3]; (iii) The intensity, also referred as drought magnitude if the ratio between deficit volume and deficit duration m_i; (iv) The minimum flow of each drought event [Q_{min}]; (v) The time of occurrence or the drought onset (Figure 2-1)(Demuth, S. Heinrich, 1997; Smakhtin, 2001; (WMO), 2009).

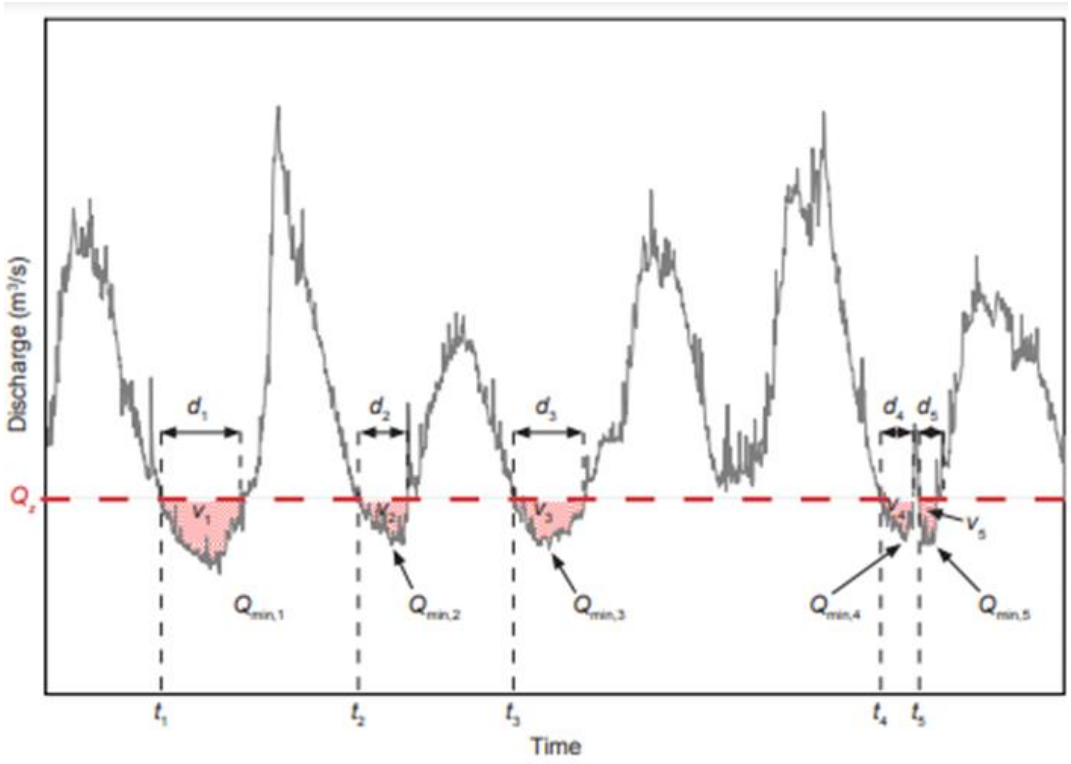

Figure 2-1: Commonly used deficit characteristics defined by the threshold level method

Source: Fleig et al. (2006)

When using the daily data, there is a problem of exceedance of flow beyond the threshold level for a brief period, dividing a lengthy deficit period into short time durations. Moving average (MA) procedure can be adopted to overcome this by pooling the intermediate dependant drought. The moving average for n-day intervals smoothens the discharge series and filters the short access periods ((WMO), 2009). Bardsley (1994) recommended stopping testing distinctive dissemination capacities in

low-flow recurrence investigation and pushed a subjective extrapolation utilizing an intuitive computer design.

2.1.3 Baseflow index (BFI)

Baseflow can be identified as a relatively stable component of streamflow, which is essential for sustaining the streamflow (Miller et al., 2016), while overland flow and the interflow are the other two streamflow components. Baseflow is a result of slowly responding components of streamflow possibly by groundwater reserves or surface water resources such as lakes, reservoirs, or melted snow (Tan et al., 2020). Baseflow is a critical component for water resource planning and management. Therefore, understanding the baseflow and its contribution to the streamflow is important for sustainable planning and management of water resources.

The baseflow index (BFI) is defined as the ratio of the baseflow component of the streamflow to the total streamflow. BFI can be estimated annually or for a certain period of concern (entire observation period) (Gustard et al., 1992). The BFI may get close to 1 in the catchments with high groundwater contribution or high storage capacity, whereas BFI values close to 0 can be identified as a stream of rapidly responding to the rainfall with basin characteristics of impermeable soil properties and geological structure (Gustard et al., 1992; Sapač et al., 2019; Smakhtin, 2001).

2.2 Environmental Flow Assessment

The requirement of freshwater resources for human consumption, such as irrigation, power generation, and potable water, keeps increasing and imposing stresses on water resources. These impacts get even worsen with the uncertainties arising due to climate change. It has been globally accepted that water resources should not be stressed over human needs (Petts, 2009). Riverine ecosystems undergo unacceptable impacts due to the deviation from the natural flow regime of the river system, mainly due to the development activities such as impounding, temporary or permanent diversion, or inter and trans-basin water transfer (Rosenberg et al., 2000).

The environmental flow (e-flow) concept has evolved to determine the minimum flow required to be released downstream to satisfy the ecological and human water

extractions and activities. The e-flow of a river can be defined as the required river flow regime of that river to sustain the ecosystem functions and the downstream socio-economical and socio-cultural requirements (Petts, 2009). Ecological flow requirement is the water quality and quantity required for healthy habitat maintenance of native fish and wildlife species. Socio-economic and cultural flow requirement includes the flow needed to be maintained downstream for water extraction activities such as irrigation, power generation, potable water supply, industrial water requirements, and activities within the river reach such as washing and bathing, fishing, tourism, and religious activities (CEA, 2018; Eriyagama & Smakhtin, 2015).

The E-flow has been considered for diversion projects in Sri Lanka since the 1990s. According to the National Environmental (Amendment) Act, No. 56 of 1988 (http://www.cea.lk/images/pdf/acts/act56–88.pdf) and Government Gazette No. 772/22 of June 18, 1993 (http://www.cea.lk/images/pdf/eiaregulations/reg772-22.pdf), all large river basin development and irrigation projects should perform an Environmental Impact Assessment (EIA) or an Initial Environmental Examination (IEE) (Eriyagama & Smakhtin, 2015). Water supply projects have been prescribed as the projects which should be conducted under the EIA process depending on the amount of water extraction.

As specified in the Government Gazette No. 772/22 of June 18, 1993; All water supply projects which extract groundwater with a capacity of exceeding 0.5 million cubic meters per day and all water supply projects which consist of treatment plant with a capacity exceeding 0.5 million cubic meters per day are included in this category project list in part I. The EIA process is implemented through designated Project Approving Agencies (PAA) as prescribed by the Minister under Section 23 Y of the National Environmental Act (NEA) in Gazette Extra ordinary No 859/14 of 23 February 1995 Ordinary No 978/13 of 04th June 1997 and Extra-Ordinary No 1373/6 of 29 December (*P1 Manual – Project Planning Feasibility*, 2019). The P1 manual is the guideline of NWSDB for project planning feasibility; under Chapter – 5, Water Resources; it indicates, that the water rights for extraction from the respective water sources shall be obtained, either through a valid document from the legally accepted

custodian or through a memorandum of understanding (MOU) with existing water users and also requirement of environmental flow should be considered.

There are no specific national guidelines with legislative backing in Sri Lanka to follow when determining e-flow related to any development project. Therefore, different project approving agencies have been following various criteria to determine the e-flow requirement of the project (CEA, 2018).

Researchers working with International Water Management Institute (IWMI) have developed an Environmental flow calculation Software tool – Sri Lanka Environmental Flow Calculator (SLEFC) for Sri Lankan River basins. Central Environmental Authority (CEA) has mentioned this as an acceptable guideline for determination for e-flow for river diversion projects (CEA, 2018). In this method, environmental flow results related to the Millakanda river gauging station can be obtained directly from the SLEFC, where gauging station data are already fed for the application, which is termed as "natural flow". Environmental Flow time series is generated based on six 'Environmental Management Classes (EMCs). These can be selected based on the flow regime requirement of the user (named A through F), ranging from 'Unmodified and largely natural' to 'Seriously and critically modified', where water quality requirement varies in ascending order.

Seventeen number of fixed probabilities of exceedance (0.01, 0.1, 1, 5, 10, 20, 30, 40, 50, 60, 70, 80, 90, 95, 99, 99.9 and 99.99%) in the table of flow represent the FDC. Generating of EMC is based on the shift of reference monthly time series FDC of the location-based on "literature sources (e.g., Tennant (1976); Jones (2002)) and partially through limited 'calibration' of EF estimates for Indian rivers against better-tested approaches (Smakhtin & Anputhas, 2006)".

The present FDC curve (17 points) can be derived by feeding the current streamflow data, and the present flow regime of the river can be compared with the EMCs. Streamflow data for before and after the Kukule Ganga powerplant construction were evaluated, and it was found that the flow regime has only varied slightly compared to the natural stage in 1950-1979.

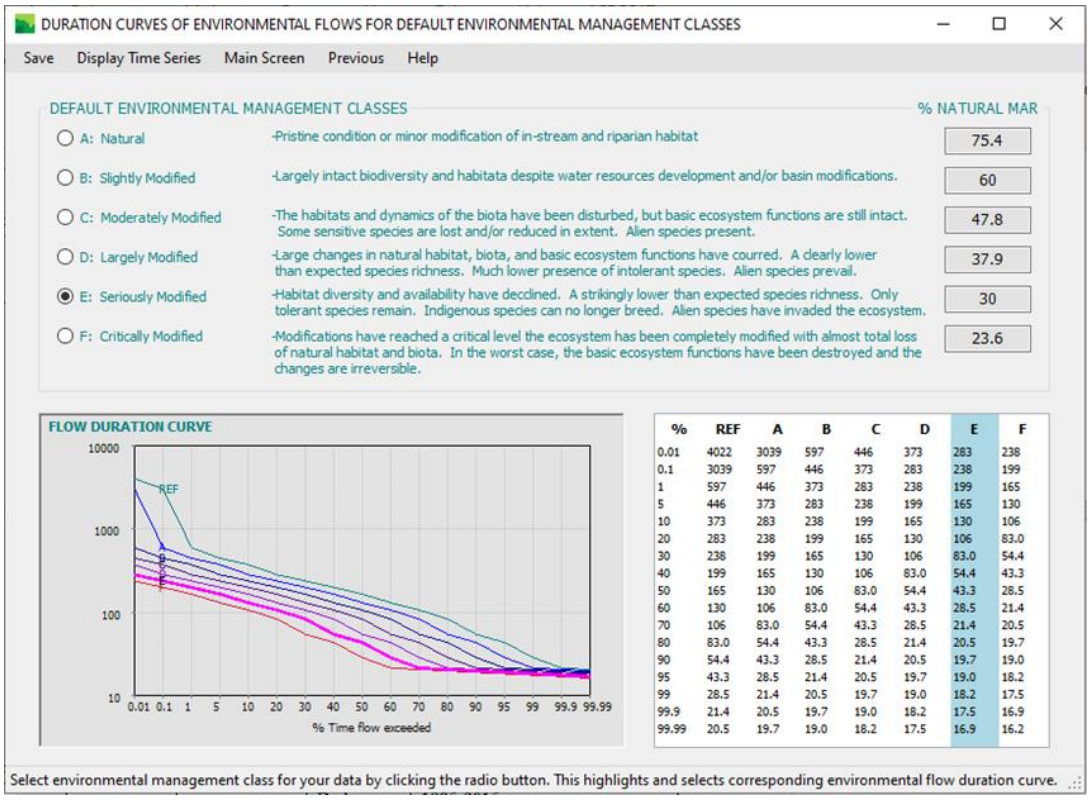

Figure 2-2: Screenshots from the Sri Lanka Environmental Flow Calculator (SLEFC) FDCs of Millakanda data for default EMCs

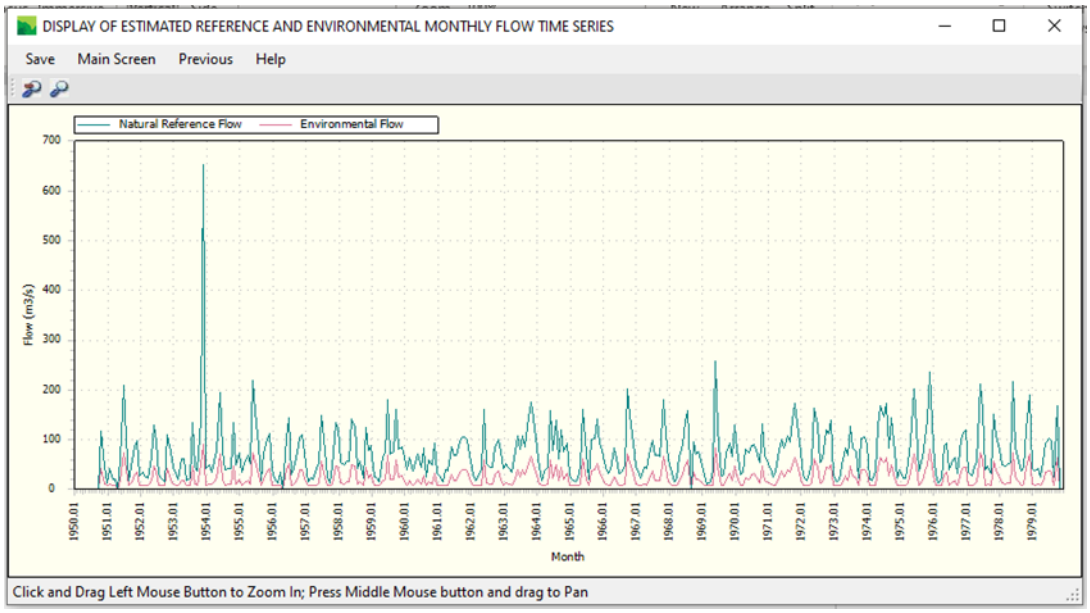

Figure 2-3: Screenshots from the Sri Lanka Environmental Flow Calculator (SLEFC) Reference time series and Environmental time series for EMC – class E for Millakanda

2.3 Hydrological Modelling

Sorooshia (2008) describes the model as a simplified representation of the real-world system. Hydrological models are developed to understand various hydrological processes and predict the system's behaviour. A runoff model consists of various parameters depending on the user's requirement, which are used as the functions of the set of equations (Devia, Ganasri, & Dwarakish, 2015). Hydrological models are used in many applications: flood and drought-related studies, planning and designing of water-related structures and water quality, hydro – ecology, and climate studies.

2.3.1 Types of hydrological models

Hydrological models are categorized based on the parameters fed into the model and theories or principles utilised for model development, and hence, they are classified into many types. When the models are classified based on input parameters as a function of space and time, it is classified as lumped and distributed model (Devia et al., 2015).

Chow et al. (1988) classified hydrological models as physical and abstract or mathematical models. As Devia et al. (2015) describe, a physical model is an idealized representation of real-world phenome, including the principles of physical processes. It does not require extensive hydrological and meteorological data in calibration but physical character describing parameters such as soil moisture content, initial water depth, topography, topology, and dimensions of the river network. Physical models can be advanced isolated into two bunches: scale and analogue models. A scale shows could be a physical representation of a natural system that keeps up connections between critical viewpoints of the system. Analogue models represent the analogue way of representing the modelling process, such as the analogues to fluid flow are the flux of electricity, heat, and solutes, respectively. Abstract or mathematical models are developed based on mathematical theories by utilising programming languages to model the terrestrial phase of the hydraulic cycle relative to space and time (Jajarmizadeh, Harun, & Salarpour, 2012).

Hydrological models can be classified based on randomness as deterministic and stochastic models. A deterministic model generates unique output based on a single

input value set without accounting for input randomness. On the contrary, stochastic models generate different outputs for a single set of inputs with randomness (Devia et al., 2015). A deterministic model can be subdivided as lumped, distributed, and semi-distributed, as expressed by Cunderlik (2003).

In lump models, the whole river basin is considered as one unit disregarding the spatial variability. In contrast, the river basin is divided into small units, usually square cells or triangulated irregular networks, and input spatially varied parameters in distributed models. Distributed models can produce spatially varied outputs (Moradkhani & Sorooshian, 2008). Distributed models easily become over-parameterized and become unrealistic compared to the input data. A common problem in distributed models is uncertainty in parameter estimation and hence identification of model (Madsen, Wilson, & Ammentorp, 2002). Semi-distributed models comprise some advantages of both lumped and distributed types. Division of catchment into sub-catchments partly accounts for spatial variation. This model type utilises minimum data compared to the distributed models as well as it is more physical based than the lumped model (Jajarmizadeh et al., 2012).

Continuous simulation model and event-based model is another classification of models whereas event-based models consider one hydrological even such as soil moisture or flood for a shorter period giving the peak discharge and volume emphasising only the infiltration and surface runoff and continuous simulation account for a series of such events for a longer period. Continuous simulation models consider a longer period of simulation, and they interpret hydrological processes such as evapotranspiration, canopy interception, the shallow sub-surface flow, which are sometimes neglected in the event-based models. It simulates drought and water balance.

There are numerous models accessible for different types of applications. The selection of a particular model is based on criteria such as the possibility of self-learning with less time, user-friendly, generated results are at a satisfactory level, rationalisation of hydrological systems, a reasonable level of data demands, and affordability of resource requirements (Pratik, 2016).

2.4 Objective Function

The purpose of using an objective function in any scientific study is to distinguish how much of the simulated results match with the observed data or with reality. In the case of hydrological modelling, the confidence level of the model is determined by using objective functions during the calibration and validation periods and is further useful for justifying its ability to perform in the required purpose (Guo et al., 2002).

The selection of objective functions depends on the purpose of the modelling. As an example, when peak flow is more important low flow and shape of the hydrograph are less accounted whereas hydrograph shape is important (rising and falling limbs) when routing effect is more concerned. On the other hand, the hydrograph volume should be considered if storage is contemplated (Green & Stephenson, 1986). In single event modelling, Green & Stephenson (1986) recommended using a percent error in peak, percent error in volume, and the sum of squares/ sum of absolute residuals objective functions. Further, they recommend using the coefficient of efficiency or Nash Sutcliff objective function to check the model performance over a series of different events when a dimensionless measure of fit is required. They also discussed 21 objective functions, and below mentioned are the recommended ones.

I. Percent Error in Peak (PEP)

$$\text{PEP} = \frac{Q_{op} - Q_{cp}}{Q_{op}} \times 100 \quad [2\text{-}1]$$

II. Percent Error in Volume (PEV)

$$\text{PEV} = \frac{V_o - V_c}{V_o} \times 100 \quad [2\text{-}2]$$

III. Sum of Squared Residuals (SSR)

$$\text{SSR} = \sum (Q_{obs} - Q_{cal})^2 \quad [2\text{-}3]$$

IV. Sum of Absolute Residuals (SAR)

$$\text{SAR} = \sum ABS(Q_{obs} - Q_{cal})^2 \quad [2\text{-}4]$$

V. Coefficient of Efficiency (CE) or Nash-Sutcliff (NSE)

$$\mathrm{CE} = 1 - \frac{\sum(Q_{obs} - Q_{cal})^2}{\sum(Q_{obs} - \overline{Q_{obs}})^2} \quad [2\text{-}5]$$

2.4.1 Percent bias (PBIAS)

Percent bias (PBIAS) is a percentage-wise comparison of the amount of average simulated flow being greater than or less than the observed flow (Gupta et al., 1999).

$$\mathrm{PBIAS}\ (\%) = \frac{\sum_i^n (Q_{obsi} - Q_{simi}) \times 100}{\sum_i^n Q_{obsi}} \quad [2\text{-}6]$$

where Q_{obsi} is the observed streamflow, and Q_{simi} is the simulated streamflow.

2.4.2 Percent streamflow volume error (PVE)

Percent streamflow volume error (PVE) (Equation [2-2]) can be used in most hydrological models as a primary metric for the objective function (Jain & Singh, 2003). The whole scale matching between the observed flow and the simulated flow over the required period is illustrated by the PVE.

2.4.3 Mean Ratio of Absolute Error (MRAE)

Mean Ratio of Absolute Error (MRAE) is denoted as the difference between the observed and simulated flow relative to the observed flow concerning each simulation step and finally the average of all steps (Equation [2-7]).

$$\mathrm{MRAE} = \frac{1}{n} \sum \frac{|(Q_{obs} - Q_{cal}|}{Q_{obs}} \quad [2\text{-}7]$$

where Q_{obs} is the observed streamflow, Q_{cal} is the calculated streamflow, and n is the number of observations used for comparison.

This MRAE objective function checks the correlation of observed and simulated flow respective to each simulation step which can be considered as giving a good sign in the presence of contrasting data (Wijesekera & Abeynayake, 2003). Then after this objective function has been used by many researchers (i.e., Dissanayake, 2017; Herath & Wijesekera, 2021; Khandu, 2015; Sharifi, 2015)

2.4.4 Coefficient of determination (R^2)

The coefficient of determination (usually denoted as R^2) is a theory in the variance analysis and the regression analysis (Equation [2-8]). It is also defined as the squared value of the coefficient of correlation (Krause et al., 2005c). The quantity of variance in the observed data which the model explains is explained by the R^2. It represents the closure of the observed and simulated flows by the amount of fit of the regression line. It measures the fraction of the explained variance available in the data. Therefore, a high value of R^2 denotes the better agreement between observed and simulated data. The value range of R^2 depends on the model application and for a standard circumstance such as for least-squares regression models the range of 0 to 1 is used. The value 0 represents correlation as none while the value 1 represents the dispersion of simulation results is equal to the observations (Coffey et al., 2004; di Bucchianico, 2008).

$$R^2 = \left[\frac{\sum_{i=1}^{n}(O_i-\bar{O})(P_i-\bar{P})}{\sqrt{\sum_{i=1}^{n}(O_i-\bar{O})^2}\sqrt{\sum_{i=1}^{n}(P_i-\bar{P})^2}}\right] \quad [2\text{-}8]$$

The level of acceptance is reached when the R^2 value is above 0.5. Althoff & Rodrigue (2021) have cited other researchers' findings regarding R^2. They have discussed that the major drawback of R^2 is being oversensitive to extreme events (Krause et al., 2005a; Legates & McCabe, 1999; Moriasi et al., 2007). This means, the model would generate a high value of R^2 by matching peak flow data during extreme events, which may misinterpret the actual relationship between observed and simulated results (Legates & McCabe, 1999). Also, Moriasi et al. (2007) point out that R^2 inability to capture systematic under or overestimation. Due to the above drawbacks, Krause et al. (2005a) recommend checking the slope of the regression line fit together with the R^2 with the regression line intercept equal to 0 and a slope equal to 1. This should be the reason that the R^2 is more commonly seen associated with the regression plots, but not hydrological model optimization performance evaluations.

2.4.5 Root mean square error (RMSE)

This RMSE (Equation [2-9]), represents the square root of the mean of the squared difference of model-simulated and observed results (Barnston, 1992). It represents the error of the average model performance with the magnitude of the squared of the errors also with the total or average-error magnitude (MAE) (Willmott & Matsuura, 2005).

$$\mathrm{RMSE} = \sqrt{\frac{\sum_{i=1}^{n}\left(Q_{obs,i} - Q_{model}\right)^2}{n}} \qquad [2\text{-}9]$$

where Q_{obs} is the observed value, Q_{model} is the simulated value, and n is the number of observations.

2.4.6 Relative Nash-Sutcliff (NSE_{rel})

The Nash-Sutcliff (NSE) is oversensitive to the peak flow as is produced by the difference between the observed and the predicted values raised to power 2 (Althoff & Rodrigues, 2021). Gupta et al. (2009) and Mizukami et al. (2019) have also stated that the NSE underestimates the variability of the observed flow. Althoff & Rodrigues (2021) discuss Relative Nash-Sutcliff (NSE_{rel}), which is indicated in Equation [2-10] with an advantage of being more sensitive on low-flow conditions and with disadvantages of i) Low effectiveness for matching peak-flows ii) Necessary of adjustments for null values in flow observations.

$$\mathrm{NSE}_{rel} = 1 - \frac{\sum_{i=1}^{n}\left|\frac{O_i - P_i}{O_i}\right|^2}{\sum_{i=1}^{n}\left|\frac{(O_i - \bar{O})}{O}\right|^2} \qquad [2\text{-}10]$$

In equations [2-8] and [2-10], O_i and P_i are observed and predicted (simulated) values at time-step i, and n denotes the total number of time-steps.

2.4.7 Recommended performance ratings for the study

Table 2-1 summarises the ranges of the recommended performance ratings i.e., PBIAS and NSE by Moriasi et al. (2007) and MRAE by Wijesekera & Abeynayake (2003), subjected to their literature review findings. The rating range varies from very good to unsatisfactory. Althoff & Rodrigues (2021) recommend using performance indexes

based on relative values; NSE_{rel}, and Mean Absolute Relative Error (MARE), similar to MRAE for tropical watersheds, where water becomes scarce during the dry periods. The NSE_{rel} value also ranges from -∞ to 1, and the performance rating is ideal when reaching 1.

Table 2-1: General performance ratings for watershed models

Performance rating	R^2	PBIAS/PVE	NSE	MRAE
Very good	$0.75< R^2 \leq 1$	PBIAS≤±10	0.75<NSE≤1	0<MRAE<4
Good	$0.65 < R^2 \leq 0.75$	±10 ≤PBIAS <±15	0.65<NSE≤0.75	0<MRAE<5
Satisfactory	$0.5< R^2 \leq 0.65$	±15 ≤PBIAS <±25	0.50<NSE≤0.65	5<MRAE<7
Unsatisfactory	$R^2 \leq 0.5$	PBIAS≥ ±25	NSE≤0.5	MRAE>7

2.5 HEC HMS Model

The Hydrologic Engineering Centre's Hydrologic Modelling System (HEC-HMS) is an updated version of the HEC-1, both were designed by the United States Army Corps of Engineers (USACE) (Scharffenberg et al., 2018). It is a deterministic, semi-distributed, event-based/continuous, mathematically based (conceptual) model and its modelling process consists of each important element of the precipitation and runoff process i.e., evaporation, infiltration, surface runoff, and groundwater recharge (USACE, 2000). Analysis results of the HEC HMS model are straight away or together with for studies such as checking the water availability, urban drainage, climate change studies, future flow projections, future urbanization impact, designing of reservoir spillways, flood damage reduction, floodplain regulation, and systems operation in values in a wide-spread variety of geographical regions (Scharffenberg et al., 2018).

The three main elements of HEC-HMS which essential to run any project are (1) Basin model, (2) Precipitation model, and (3) Control specification. The role of the basin model is to establish the connectivity between catchment and physical characteristics

transforming the atmospheric condition into streamflow at a specific location. The meteorological model processes the precipitation and evapotranspiration data which are essential for the modelling. The control specification defines the starting and the ending dates of the model simulation and the simulation time interval. The main components of the basin model include the loss model, transform model, baseflow model, and routing model. Details of model structures of HEC-HMS can be found in USACE (2000) and Scharffenberg et al. (2018).

Due to the ease of use, capacity in short-time simulations, and use of standard methods, HEC HMS has become a widely used and reliable hydrologic model for simulating rainfall-runoff correlation (Azmat et al., 2017). The HEC-HMS has been productively used in many studies in Sri Lanka (Table 2-2) and worldwide, including flood forecasting/rainfall-runoff modelling (Oleyiblo & Li, 2010; Xuefeng & Alan, 2009), reservoir management (Anderson et al., 2002), water resources assessment (Hussain et al., 2021; Wang et al., 2016), land-use change impacts (Ali et al., 2011), climate change impact studies (Azmat et al., 2016, 2017; Bai et al., 2019; Meenu et al., 2013) and many others.

Table 2-2: HEC HMS hydrological model studies in Sri Lanka

River Basin Purpose of Modelling	Modelling Outcomes
Attatanagalu oya – Dunamale sub catchment Halwatura & Najim, (2013) studied three different approaches to calibrate HEC HMS hydrologic model, i.e., the SCS curve number loss method, the deficit constant loss method (with the Snyder unit hydrograph (UH), and the Clark UH transform methods), and decided the most suitable method.	The study interpreted that the Snyder unit hydrograph method simulated flows more reliably than the Clark unit hydrograph method. Further, the SCS CN method does not perform well, but the deficit and constant method performed better as the loss method for continuous simulation of the Attanagalu Oya catchment.
Kelani River basin – Hanwella subwatershed De Silva et al., (2014) study the HEC HMS model application for disaster mitigation, flood control, and water management of the Kelani River basin. Flood events in April and May 2008, May and June 2008, and May 2010 are used for the event-based model. Three-month, two-year, and three-year time series are used for continuous simulations.	This model can be effectively used for downstream water resources development, flood control, water supply management for drinking water using long-term continuous simulation runs. They have shown that the HEC HMS successfully reproduced low flows and, therefore, is a useful tool to estimate low flows in advance based on drought forecasts.
Deduru Oya Sampath et al., (2015) has developed HEC-HMS to estimate runoff in the Deduru Oya river by the continuous rainfall-runoff modelling in part of the Deduru Oya basin with intra-basin diversions and storage irrigation systems. They have used the five-layer soil moisture accounting loss method, Clark UH transformation method, and recession base flow method.	The model could successfully capture the seasonal characteristics of streamflow. It proves the model's ability to estimate flow from tropical catchments with intra-basin diversions and irrigation storages and, therefore, a useful tool for water management in the Deduru Oya river basin.

River Basin Purpose of Modelling	Modelling Outcomes
Kalu Ganga - Ratnapura Sub basin Kanchanamala et al., (2016) checked the possibility of increasing the model performance by increasing the no of subbasins when using the model for water management practices.	Three models have been developed as lump model, six basin, and nine basin models. Model performance increased when the number of basins increased to six subbasins from the lumped model. Considering the nine subbasin model performance, it is not useful to have many sub-catchments with more or less similar properties.
Kalu Ganga - Ratnapura Sub basin Jayadeera & Wijesekera, (2019) have carried out a diagnostic HEC HMS model development for the Kalu Ganga after evaluating the studies carried out by Halwatura & Najim, (2013) and Kanchanamala et al., (2016). Continuous model simulation has been carried out using deficit and constant loss method, SCS method as transform method, and Recession baseflow model.	The model can be used for flood management successfully. Further, the model can estimate watershed yield in Yala and Maha seasons and is suitable for Water Resources Management. The model does not give satisfactory results in low flow estimation

2.5.1 Precipitation loss model

Abstraction or the precipitation loss can be defined as the difference between the observed total rainfall hyetograph and the excess rainfall hyetograph (Chow et al., 1988). They also describe the Phi index as a constant rate that produces an excess rainfall hyetograph, whose total depth equals the direct runoff over the watershed, determined by trial and error.

The USACE (2000)) describes the different types of precipitation loss models available with HEC HMS (nine numbers), which are available to simulate precipitation, with their advantages and disadvantages. Out of those loss models, only

the deficit and constant (DC) model and the Soil Moisture Accounting (SMA) can be utilized for continuous hydrologic modelling (Cunderlik & Simonovic, 2004).

The DC method considers three parameters: Initial Deficit, Maximum Storage, and Constant Loss. Initial deficit denotes the water requirement to saturate the soil layer to the maximum storage, while maximum storage considers the water holding capacity of the soil in a specified soil depth. The upper limit of the Maximum storage can be obtained by soil depth multiplied by the porosity of the soil. The constant rate defines the infiltration rate when the soil is saturated while the rainfall occurs. The hydraulic conductivity at the bottom of the root zone is the upper limit of the constant rate parameter (USACE, 2000).

The continuous changes in the soil moisture content are captured by a single soil layer in the deficit constant loss method. The DC method should be combined with a canopy method that will extract water from the soil in response to potential evapotranspiration computed within the meteorologic model. It may also be combined with a surface method that represents the water held by the land surface depressions (USACE, n.d.). As in Figure 2-4, precipitation initially fills the canopy storage up to its total capacity and falls onto storage on the ground. If soil is not saturated, water infiltrates into the soil layer at an essentially infinite rate until the soil layer gets saturated. Percolation occurs at a constant rate until the soil moisture deficit exceeds zero. When rainfall is greater than percolation, runoff is generated (USACE, n.d.).

Halwatura & Najim (2013) developed a HEC HMS model for Attanagalu Oya using the SCS CN method and deficit and constant loss methods and have concluded that the SCS CN not performing well whereas the constant loss method can be accepted as a better alternative.

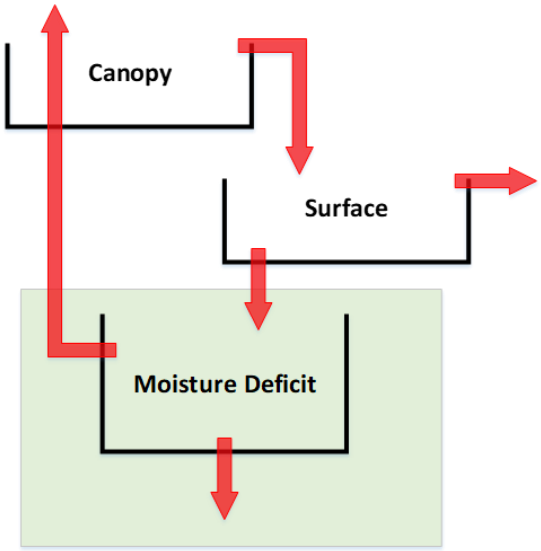

Figure 2-4: Schematic of DC model

Source: USACE (n.d.)

2.5.2 Initial Parameter Estimation

Canopy storage or canopy interception is the precipitation intercepted by vegetation, and it depends on the vegetation structure and meteorological factors. Canopy storage can be calculated using the land-use, land cover classes, and canopy interception values are listed in Table 2-3 (Bennett & Peters, 2004).

Table 2-3: Canopy storage values

Vegetation type	Canopy interception (mm)
General vegetation	1.27
Grasses and deciduous trees	2.032
Trees and coniferous trees	2.54

Source: Fleming & Neary, (2004); Todd Howard Bennett, (1998)

The surface depression storage of the basin can be estimated according to Bennett & Peters (2004), using the slope as categorized in Table 2-4.

Table 2-4: Surface depression storage values

Description	Slope %	Surface storage (mm)
Paved impervious areas	NA	3.2-6.4
Steep, smooth slopes	>30	1
Moderate to gentle slope	5-30	12.7 -6.5
Flat, furrowed land	0-5	50.8

Source: Todd Howard Bennett (1998) *and* Bennett & Peters (2004)

Maximum deficit refers to the driest a soil can become after being drained by gravity, evaporation, and transpiration. According to HEC-HMS Tutorials and Guides, the Maximum deficit can be derived by the difference between the saturation storage and the wilting point storage of soil, and the soil depth is assumed (typically 24 to 36 inches). Soil texture-based porosity and the wilting point of the soil can be derived from Rawls et al. (1983). According to the Survey Department soil classification map, the soil texture can be derived from the Soils of Ceylon by Moormakn & Panabokke (1961).

Table 2-5: Soil data to calculate maximum deficit

Survey department Soil Map	Texture	Saturated Hydraulic Conductivity (in/hr)	Effective Porosity (in^3/in^3)
Red-Yellow podzolic soils with prominent A1 or semi-prominent A1	Sandy Clay Loam	0.06	0.33
	Clay Loam	0.03	0.31
Red-Yellow podzolic soils, steeply dissected, hilly and rolling te'	Sandy Clay Loam	0.06	0.33
	Sandy Clay	0.02	0.32

Source: Moormakn & Panabokke (1961) *and* Rawls et al. (1983)

The DC loss model also requires an impervious percentage of the basin. Percentage impervious of the basin can be calculated based on the land use data described by

Prisloe et al. (2000) based on the impervious surface coefficient for each land use category.

2.5.3 Transform model

The transformed model calculates the actual surface runoff of the subbasin interacting with the other components of the subbasin, i.e., infiltration, and subsurface processes. The HEC HMS model consists of nine transform models (USACE, n.d.). In their study for the Attanagalu Oya basin, Halwatura & Najim (2013) concluded that the Snyder UH method is more reliable with the DC loss method than the Clark UH method.

The parameters of the Snyder UH method consist of standard lag which is the time duration measured from the precipitation mass centroid up to the peak flow of the hydrograph of the precipitation event. The peaking coefficient (C_p) measures the steepness of the hydrograph that results from a unit of precipitation. Basin lag is denoted by the equation [2-11] (Chow et al., 1988).

$$t_p = CC_t(LL_c)^{0.3} \quad [2\text{-}11]$$

here C_t = basin coefficient; L = length of the mainstream from the outlet to the divide; L_c = length along the mainstream from the outlet to a point nearest the watershed centroid; and C = a conversion constant (0.75 for SI and 1.00 for foot-pound system).

Physical basin characteristic parameters (L, L_c) can be directly calculated from HEC HMS 4.7.1 above versions. C_p, C_t values for the Sri Lankan basin can be derived from the Technical Guideline of the Irrigation Department (Ponrajah, 1989).

2.5.4 Baseflow model

The baseflow model computes actual subsurface calculations of the basin model. Six different baseflow methods are available in HEC HMS. Thapa et al. (2020) used linear reservoir (LS) baseflow with DC loss method and Snyder UH method as transform method. They discuss that the deficit and constant loss model successfully captured direct runoff, which is the major portion of streamflow during the wet season. The groundwater storage accounted for the majority of the streamflow during the dry season. The linear reservoirs successfully captured this dry season. Brauer & Fleming (2017) used SMA and DC loss methods for the subbasins with the LR base flow

method for a Russian river and concluded that the model showed good performance at all locations to a level of performance of “very good” level. During this study, the model has produced reliable results of subbasin soil moisture and discharge for testing reservoir reoperation scenarios in the Russian river basin.

The linear reservoir is the only baseflow method that conserves mass within the subbasin. This baseflow model consists of one, two, or three reservoirs, and the infiltration or percolation computed by the loss method is directed to the linear reservoirs as the inflow. Groundwater (GW) fractions determine the amount of inflow passing to each reservoir whereas the total GW fraction is less than or equal to one. The total value of the fraction less than one indicates balance portion of percolated water becomes the aquifer recharge. The total GW fraction precisely equals one indicates that no aquifer recharge would occur. The groundwater storage coefficient is the constant measured in time dimension for each linear reservoir. It denotes the response time of the subbasin in base flow calculation. (USACE, n.d.).

2.5.5 Routing Model

Eight different routing methods are available in HEC HMS: lag, kinematic wave, Lag and K, modified pulse, Muskingum, Muskingum-Cunge, Normal Depth, and straddle stagger routing method. The kinematic wave and Muskingum models cannot capture the influence of backwater in the flood waves. These methods are based on uniform flow assumptions, and only modified pulse methods can simulate the backwater effect (USACE, 2000).

2.5.6 HEC HMS Model calibration

There are two modes of calibration available in HEC HMS: manual and automated parameter optimization methods. Both methods have the functionality to optimize the objective functions. Manual calibration helps to identify parameters that significantly impact results. This can be used to allocate time during model development wisely.

The automatic calibration procedure in the HEC-HMS model follows an iterative method to optimise an objective function. The objective functions can be the sum of the absolute error, the sum of the squared error, the percent error in the peak, and the

peak-weighted root means square error (HEC, 2000). Automatic parameter optimisation in HEC HMS has two search methods: Univariant gradient method, which evaluates one parameter at a time, and Nelder and Mead method that uses a downhill simplex to evaluate all parameters simultaneously and determine which parameter to adjust.

2.6 Climate Change Data for Future Projections

The Coupled Model Intercomparison Project Phase 5 (CMIP5) is a project of the World Climate Research Programme (WCRP) for providing IPCC AR5 (Fifth Assessment Report, IPCC 2013) with time-projected environmental variables. Practically all climate modelling teams in the world have contributed to this project (Taylor et al., 2012). The IPCC was established by the World Meteorological Organization (WMO) and the United Nations Environment Programme (UNEP). The main objective of this organization is to provide scientific information related to climate change among the worldwide governments at all levels to develop climate policies.

A vast amount of time series data needed for scientific studies (daily, monthly, and yearly time steps; from 2006 to 2100, projections even up to 2300 by some models) of physical variables related to climate drivers which were generated by the initiative of CMIP5 project can be accessed through ESGF portal (*The Program for Climate Model Diagnosis and Intercomparison*, 2014). The AR5 expresses the results outcomes of various coupled general circulation models (CGCM) driven by the concentration or emission scenarios under four different representative concentration pathways (RCPs) (i.e., RCP 2.6, RCP 4.5, RCP 6.0, and RCP 8.5). The number followed by RCP resembles the target energy forcing by 2100, in W/m^2 (relative to preindustrial conditions) RCP 8.5 resembles the "high" scenario, RCP 4.5 and RCP 6.0 as the intermediate scenarios, and RCP 2.6 as the low or so-called peak-and-decay scenario, where the radiative forcing is considered as reaching the maximum towards the mid of the twenty-first century and eventually decreasing up to the level of 2.6 W/m^2 (Taylor et al., 2012).

Global Climate Models (GCMs) are used to study and project climatic conditions and have the capacity to simulate the large-scale aspects of climate realistically even with the coarser spatial resolution ranging from 1.0° to 3.8°. However, GCMs do not capture the regional scale climatic conditions and variations of topography, land use (Chen et al., 2019; Ding & Ke, 2013; Sharma et al., 2007). The simulation results from comparatively coarse resolution GCMs climate data can be adequately integrated and improved to a higher resolution by the dynamic and physics of the Regional Climate Models (i.e., RCMs) (Ratna et al., 2014). RCMs are formed by dynamical downscaling (i.e., nesting a physically-based) small spatial resolution regional climate model within the grid of a GCM output. The boundary conditions of the regional models are derived by the relevant GCM outputs. The scale disagreement in the GCMs when studying in the small scale is rectified by the downscaling and with the finer resolution projections resolving the topographical details, coastlines, and land-surface heterogeneities allow the reproduction of climatic information which can be used to study the climate of regions having complex topography (Flato et al., 2013; Wood et al., 2004).

Centre for Climate Change Research - Indian Institute of Tropical Meteorology (CCCR-IITM) is the nodal agency for coordinating the CORDEX modelling activity in South Asia has generated high resolution downscaled projections of regional climate and monsoon over South Asia until 2100 using a regional climate model ICTP-RegCM4 (Giorgi et al., 2012). The RCM model resolutions are available from 25-50 km. These RCM projections have been developed as part of the WMO's World Climate Research Programme (WCRP) regional activity Coordinated Regional Climate Downscaling Experiment (CORDEX; http://cordex.org/). The CCCR-IITM and several international partner institutions have contributed towards the generation and evaluation of regional climate simulations for CORDEX South Asia (http://cccr.tropmet.res.in/home/cordexsa_datasets.jsp). These RCMs comprise downscaled climate scenarios for the South Asia region, derived from the Atmosphere-Ocean coupled General Circulation Model. The AOGCM runs conducted under the Coupled Model Intercomparison Project Phase 5 (CMIP5), using three greenhouse gas emissions scenarios known as Representative Concentration Pathways (RCPs). CORDEX dataset for the South Asia region can be downloaded from Earth System

Grid Federation (ESGF; https://esgf.llnl.gov/) data node (https://esgf-data.dkrz.de/search/cordex-dkrz/). The ESGF is an international collaboration for the software that powers using a system of geographically distributed peer nodes, most global climate change research, notable assessments by the IPCC (Sanjay et al., 2012).

This study (Kuda Ganga Basin) considers a part of the Kalu river with a basin area of about 916 km^2. Therefore, finer resolution RCM data is needed to capture the monsoon precipitation signal. Three models based on the regional climatic model, ICTP-RegCM4-7 simulations based on the GCMs, NCC-NORESM1-M, MPI-M-MPI-ESM-MR, and MIROC-MIROC5 (WAS-22 domain with resolution 25 x 25 km^2) from the CMIP5 ensemble were selected for this study. These models have been successfully used for Kalu Ganga by Sirisena et al. (2021).

2.7 Bias Correction

Bias correction is performed to remove the associated biases with the GCM or RCM output results. Even though the RCMs have a regional scale considerably higher spatial resolution and more reliable results compared to GCMs, the original RCM outputs still contain substantial bias, which is conveyed through the forcing of GCMs or produced by systematic model error (Durman et al., 2001; Herrera et al., 2010).

The mean-based or Linear Scaling (LS) method in the monthly scale is one of the bias correction methods widely used in many studies being a straightforward and comparatively fast method (Lenderink et al., 2007). The LS method can adjust all climatic factors to an acceptable level, where errors in precipitation are adjusted with the use of a multiplier (Ghimire et al., 2019; Lafon et al., 2013; Luo et al., 2018; Mahmood et al., 2018). Linear scaling bias correction method can be applied using the two equations given below ([2-12] & [2-13]), where *cor, his, obs, sim, P,* and *d* stand for bias-corrected data, raw RCM data, observed data, raw RCM simulated data, precipitation and daily, respectively, and μ_m stands for a long-term monthly mean of precipitation data.

$$P_{his,d}^{cor} = P_{his,d} * \frac{\mu_m\left(P_{obs,d}\right)}{\mu_m\left(P_{his,d}\right)} \quad [2\text{-}12]$$

$$P_{sim,d}^{cor} = P_{sim,d} * \frac{\mu_m\left(P_{obs,d}\right)}{\mu_m\left(P_{his,d}\right)} \quad [2\text{-}13]$$

2.8 Bias Corrected RCM Precipitation Data Evaluation (Using Drought Analysis)

Since this study mainly focuses on the low flow conditions of the Kuda Ganga, the agreement of bias-corrected data for the drought conditions of the basin was evaluated. Droughts have become a common problem globally, which has intensified due to climate change. The regions where droughts are not common to have started to show expanding recurrence of summer droughts according to the climate models on which dry spells have become an essential topic (Good et al., 2006; Maracchi et al., 2005; Solberg, 2004). Different methods have been followed by researchers throughout to evaluate the droughts, such as by means of drought indices (Mishra & Singh, 2010; Mukherjee et al., 2018) and modelling duration and frequency analysis of dry spells (Caloiero et al., 2015; Chemeda, 2013; Vicente-Serrano & Beguería-Portugués, 2003).

A dry spell is meteorologically characterized as a grouping of successive dry days with no rainfall or rainfall underneath a specified threshold. Even though dry spells cannot be utilized to decide drought severity, as a result of climatological contrasts, they are exceedingly helpful in assessing climate change-related trends (Raymond et al., 2016) and evaluating spatial contrasts of the drought hazard probability (Lana et al., 2006). A threshold value is required to analyse dry periods of observed precipitation and climate model output, and the frequency distribution of the dry spell length is highly sensitive to the selected threshold. Initially, researchers have used the standard observational threshold of 0.1 mm (Osborn, 1997; Semenov & Bengtsson, 2002). It is acceptable to use threshold values higher than zero to decide a “dry” day that accounts for measurement errors or minimal sums of rain captured by interception and direct evaporation and would not be available for plants or water resources. As a result, a threshold of 1 mm has been adopted by several researchers (Frei et al., 2003; Frich et al., 2002; Klein Tank & Können, 2003; Peterson et al., 2001). Typically, in climate models, many low precipitation values are there compared to observations due to the typical “drizzle effect” of dynamical models, which is also minimized by avoiding very low threshold values (McMahon et al., 2013). On the other hand, fixed threshold

values do not represent the actual ground situation as the evaporation varies spatially and temporally within regions. The atmospheric evaporative demand (AED), together with precipitation, has been used to characterize dry spells as a time and spatially varying threshold. The AED has been calculated using different approaches, such as potential evaporation (McMahon et al., 2013) or the reference evapotranspiration (ET_o)(Allen et al., 1998) and by evaporation pans as well. Rivoire et al. (2019) has studied the effect of applying a fixed threshold value (1 mm/day) and ET_o as the threshold to determine dry spells for the Mediterranean region. During the frequency analysis of seasonal extreme dry spells, it was revealed that the 1 mm fixed threshold underestimated the extreme dry spells compared to the time-varying threshold of ET_o in the extended summer season.

Numerous features of the spell characteristics can be compared using the different indices such as (i) the number of wet/ dry spells with different lengths over the whole study; (ii) the mean and maximum lengths of wet/dry spells; (iii) the contributions of wet/dry spell with different lengths to the total number of wet/dry days; (iv) the amount of precipitation associated with wet spells of a certain length and their contributions to the total amount (Li et al., 2017) and statistical measures such as the Maximum dry spell length across the entire data period; the 99, 95, 90 and 75% quantiles (percentiles) of dry spell length across the entire data period (Lars et al., 2006).

2.9 Past Climate Projected Studies of the Kalu River Basin

According to the recent study by Sirisena et al. (2021), only limited publications are available on the Kalu river basin-scale assessment of future climatic conditions and hydrological variations. Nyunt et al. (2012) have investigated a proper methodology to select GCM (by selecting nine GCMs included in the 4th IPCC assessment report) and setting up a bias correction method considering extreme rainfall, average rainfall, and frequency of no rain day by studying the future climatic conditions Kalu Basin as a case study. All nine GCM ensembles resulted in more intense rainfall in the monsoon season while longer dry spells during the projected 2046-2065 period. (Schulz & Kingston (2017) developed a hydrological model (HBV-Light) with seven CMIP-3 GCMs to study the climate change impact on Kalu river discharge. Their study shows

model uncertainties towards the direction of change of rainfall and runoff, and only the month of June indicated a consistent direction of change (range −17% to −65%).

Sirisena et al. (2021) have studied the disparities in the streamflow and the sediment loads of the Kalu river under climate change projections using high resolution (25 km) regional climate models (RCM) (i.e., RegCM4-MIROC5, MPI-M-MPI-ESM-MR, and NCC-NORESM1-M). Bias corrected (mean-based method) precipitation data of the three RCMs have been forced for the calibrated hydrological model (SWAT) under for the baseline period (1991–2005 and two representative concentration pathways (i.e., RCPs 2.6 and 8.5) for mid-century (2046–2065) and end-century (2081–2099). All three GCMs gave reasonably good, simulated streamflow, but NorESM1-M indicated better agreement in the low flow period (January – March). The study has projected the Kalu river basin to be warmer and wetter than the existing climate conditions (considering the 1991-2005 baseline).

2.10 Analysis of Future Projections with Standardized Precipitation Index (SPI)

Standardized Precipitation Index (SPI) can be used to identify the severity of the potential future drought events. SPI-1 particularly detects the deviation of rainfall patterns due to climate change (Huang et al., 2016).

Mckee et al. (1993) recommend calculating SPI using the Gamma probability distribution. They categorized Drought Severity based on the range of SPI (Table 2-6) and Drought event terminates as the SPI becomes positive. The SPI time scale can be selected based on the study's objective as it represents the differences in magnitude and duration of droughts that generally come in three- to nine-month time scales (Bong & Richard, 2020). The three-month SPI (SPI-3) compares the rainfall for a specific three-month period with the total rainfalls from the same three-month period for all the years chosen in the historical record. The SPI-1 can be used to describe meteorological droughts, SPI-6 for agricultural droughts, and SPI-12 for hydrological droughts (Huang et al., 2016). The SPI-3 specifies short time scale trends and can be used to analyse moisture conditions hence used to describe the seasonal estimation of precipitation. The SPI-9 is also denoted as the hydrological drought index and can be utilized in monitoring of surface resource management (Bong & Richard, 2020).

Table 2-6: Categorising drought events based on SPI values

SPI Values	Drought Category
0 to -0.99	mild drought
-1.00 to -1.49	moderate drought
1.50 to -1.99	severe drought
≤ -2.00	extreme drought

Source: Mckee et al. (1993)

CHAPTER 3

3 METHODOLOGY

The methodology followed in the research is shown in Figure 3-1.

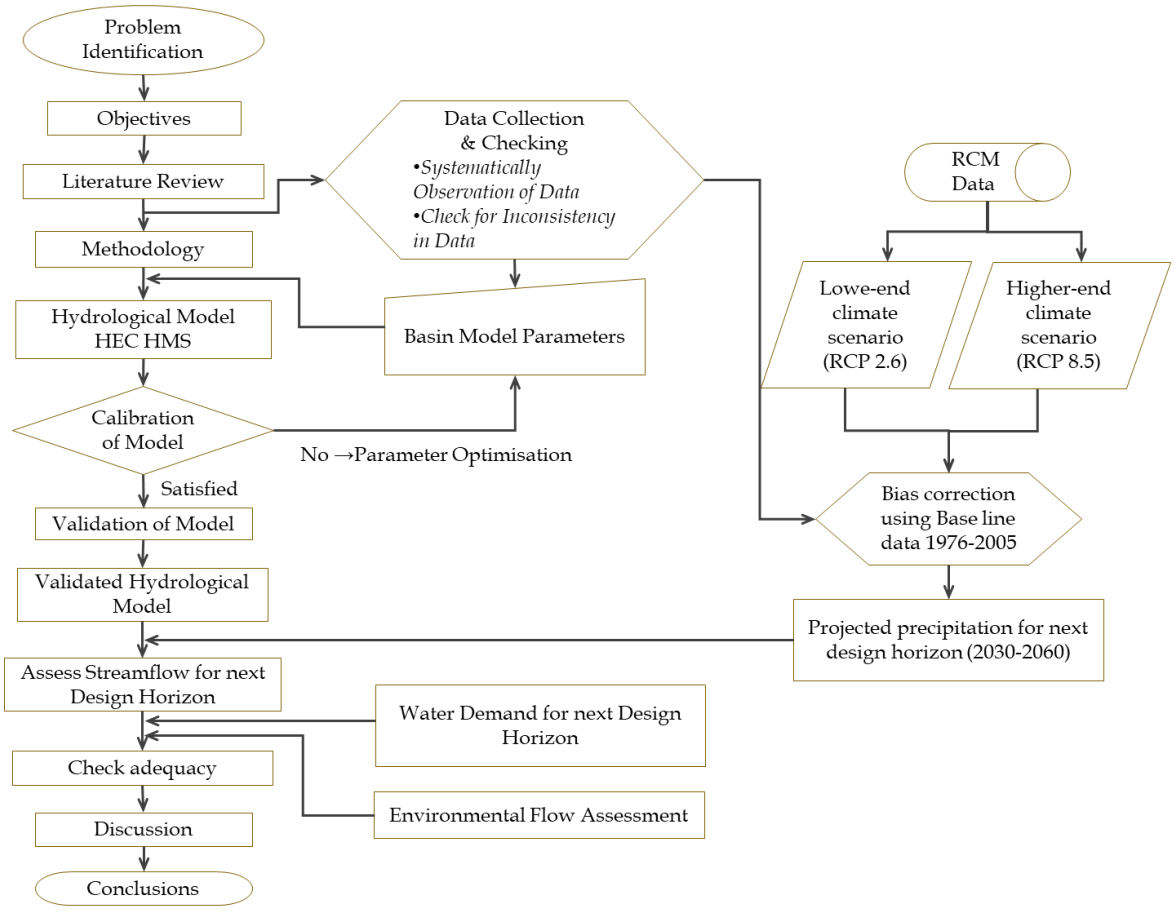

Figure 3-1: Methodology Flowchart of the study

The research problem was selected based on an applicable requirement of NWSDB to assess whether the future water requirement can be extracted from the Koleimodara intake since the minimum annual flow already shows a decreasing trend. The main objective of this study was decided based on the identified problem, and specific objectives were identified tentatively and conformed based on the literature review. The literature review was performed to review and get knowledge related to this study

by looking into the past studies as described in Chapter 2. A hydrological model was developed in HEC HMS to model the Kuda Ganga river basin as the primary outlet at Koleimodara intake. Millakanda river gauging station data was used to calibrate and validate the HEC HMS model. Four rain gauging station data were used for the model: Galatura Estate, Depadena (Rakwana), Usk Valley, and Sirikandura. Data were systematically checked for missing values and inconsistencies and analysed to identify catchment-specific characteristics as described in Section 4 in detail.

The hydrological model was developed using the HEC HMS as a six-basin semi-distributed model with Koleimodara intake as the main outlet (Sink) and Millakanda Junction as the calibration point as described in detail under Section 5. The model was simulated as a continuous model for a single water cycle. The HEC HMS basin model consists of several sub-models as canopy storage, surface storage, loss, base flow, and channel routing in the reach elements. Deficit and constant loss method followed by the simple canopy and simple surface models with Snyder UH transform method was used for continuous flow analysis based on previous study recommendations and model requirements as described in the literature review. Kukule Ganga run-off-the river powerplant effect is also considered as this study mainly focuses on the dry flow period. Kukule Ganga powerplant discharges were added to the model based on the reservoir's elevation-capacity-discharge relationship. Since this is a small impounding reservoir, total tunnel capacity was considered between MOL and FSL.

Model calibration period was selected after the operation of the Kukule Ganga run-off-the river power plant starts its operation. The model was calibrated and validated considering separate waster cycles (October to September) having more extended dry periods as it is necessary to emphasize the capturing dry periods more accurately as described in Section 5.3.1. Two and three separate continuous water cycles were selected for calibration and validation respectively between October 2005 and September 2015. Finally, the model was evaluated for continuous simulation from 2005 to 2015. Simulated flow data of the calibration data set is evaluated based on the objective functions. The goodness of fit of the simulated runoff series of calibration and validation was evaluated using the Root Mean Square Error (RMSE) Mean Ratio of Absolute Error (MRAE), the percentage bias (PBIAS), and relative Nash-Sutcliffe

(NSE_{rel}) (Section 5.3.2). Parameters were optimized until the goodness of fit was reached during the calibration. The model was then validated for the same parameters. If the model performance is satisfactory during validation, the model can be used for further studies. Else constraints of model and data are to be identified and proceed until satisfactory calibration and validation results are obtained.

Precipitation data for the next design horizon period (until 2060) were obtained for the Kuda Ganga Basin using RegCM4-7 RCM model of NCC-NORESM1-M GCM under RCP 8.5 (high-end scenario) and RCP 2.6 (low-end scenario). Four grid point data were selected to extract RCM data (Figure 4-4). The Mean-biased method is used to bias-correct the RCM precipitation data using monthly means of observed and RCM model data for the baseline period (1976-2005) (Section 4.5). Five years (2001 – 2005) period was considered to evaluate bias correction results. Thiessen average rainfall for each sub-basin with the Thiessen average RCM data related to each sub-basin was used to simulate future streamflow projection at Koleimodara intake. The monthly mean of each month and the seasons for each sub-basin were evaluated for the calibration period (2001-2005) using the objective functions RMSE, R^2, and PBIAS. Also, different indices of spell characteristics and statistical measures such as maximum mean and standard deviation of dry spell length across the entire data period; the 99, 95, and 90% quantiles (percentiles) of dry spell length were compared for the baseline period (1976-2005) (Section 4.6). The reference evapotranspiration (ET_o) has been used as the threshold to determine dry spells. The ET_o of the study area has been obtained from the latest publication of the Irrigation Department (Hydrology Division (ID), 2019). Projected streamflow based on the RCM scenarios was compared with calculated future water extraction requirements.

Assessing the streamflow for the next design horizon was performed by studying the behaviour of several low flow incidences (i.e., Probability exceedance flow of 90^{th} percent (Q_{90}) and 50^{th} percent (Q_{50}), Mean 7-day and 30-day annual minima (MAM7 and MAM30), Baseflow index (BFI), deficit analysis by taking deficit duration, deficit volume, or the severity, and intensity relative to the flow threshold (3 m^3/s). Low flow analysis was performed at the Koleimodara intake location, taking the sum of the environmental flow (1.5 m^3/s) and the water extraction requirement (1.5 m^3/s) as a

threshold value as described in Section 4.3. The projected precipitation was also analysed using the one-month Standard Precipitation Index (SPI-1) from 1992 to the projected period of 2030 to 2060 under both RCPs 2.6 and 8.5. The flow characteristics were analysed relative to the simulated flow forced by the observed precipitation during the base period (2005-2020) as the model simulation period starts from 2005. The low flow indices were analysed throughout the design period, decades-wise and in annual, and season-wise, as described in Section 6. Finally, the extraction capacity of the intake location was assessed relative to the deficit duration, volume, and intensity during the design horizon relative to the base period as described in Section 6.3.4.

CHAPTER 4

4 DATA CHECKING AND ANALYSIS

4.1 Study Area

Kalu River begins in the Samanala mountain range in the central hills of Sri Lanka and flows through two administrative districts, namely, Ratnapura and Kalutara, and emerges into the Indian Ocean at Kalutara. The total river length is about 100 km, and the basin area is about 2,778 km^2. The Kalu River is the third-longest river in the country; besides, it discharges the largest annual volume of water into the sea with a magnitude of about 4,000 MCM. The Kalu river basin entirely lies within the wet zone of the country. The average annual rainfall in the basin is about 4,000 mm, reaching up to about 6,000 mm in mountainous areas and even becomes 2,000 mm in the low plain areas. The riverbed level drops from 2,250 to 14 m within the first 36 km of its path before reaching Ratnapura town. It meets the Wey River at Ratnapura and then flows along 76.5 km at a very low gradient of 0.15 m/km to get into the sea at Kalutara (Ampitiyawatta & Guo, 2010; Nandalal, 2009). The study area lies in the Kuda Ganga, one of Kalu Ganga's main tributaries in the Southern part of the Kalu river basin. The watershed area of Koleimodara intake is about 916 km^2. The basin boundaries, gauging station locations, and other important locations are as shown in Figure 1-2 and Figure 4-3.

4.2 Data and Data Checking

The data required for this study can be categorized as historical data and future projections of climate data and further as hydrological, meteorological, topographical, and terrain data. Data resolutions and data sources are listed in Table 4-1.

Table 4-1: Data sources and resolution

Data type	Station	Resolution	Data Period	Source
Rainfall	Sirikandura	Daily	Oct/1976 to Sep/2020	MD
	Usk Valley	Daily		
	Galatura Estate	Daily		
	Depedana (Rakwana)	Daily		
Evaporation	Rathnaputa	Monthly	Oct/2001 to Sep/2015	MD
Streamflow	Millakanda	Daily	Oct/1990 to Sep/2020	ID
Land use data	Kalutara District	1:50,000	Updated 2012	SD
	Ratnapura District	1:50,000	Updated 2001	SD
Soil map	Sri Lanka	1:50,000	Updated 2001	SD
DEM Terrain Data	Sri Lanka	30m		SD

MD - Meteorological Department; ID - Irrigation Department; SD - Survey Department

4.2.1 Land use and soil data

Land use maps and soil maps were retrieved from the Survey Department, Sri Lanka (details are given in Table 4-2). Land use of the studying basin can be classified as in Table 4-2. About one-third of the area is covered under Forest – Unclassified (33.1%), whereas rubber covers 23.2% and Chena covers 12.9 %. Homesteads/Garden covers only 12.9%, and Scrubland and Paddy cover 7.7% and 6.3%, respectively (Figure 4-1). The soil in the Koleimodara basin consists of three types, as shown in Figure 4-2 and Table 4-3.

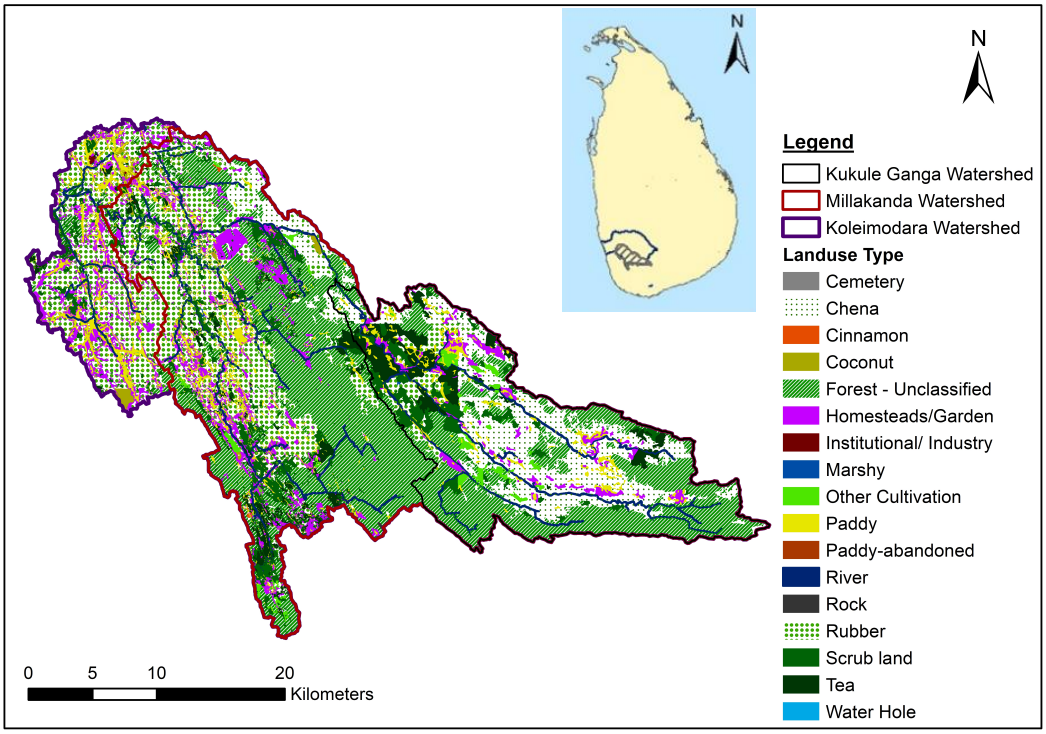

Figure 4-1: Land use map of Koleimodara catchment

Source: Survey Department of Sri Lanka

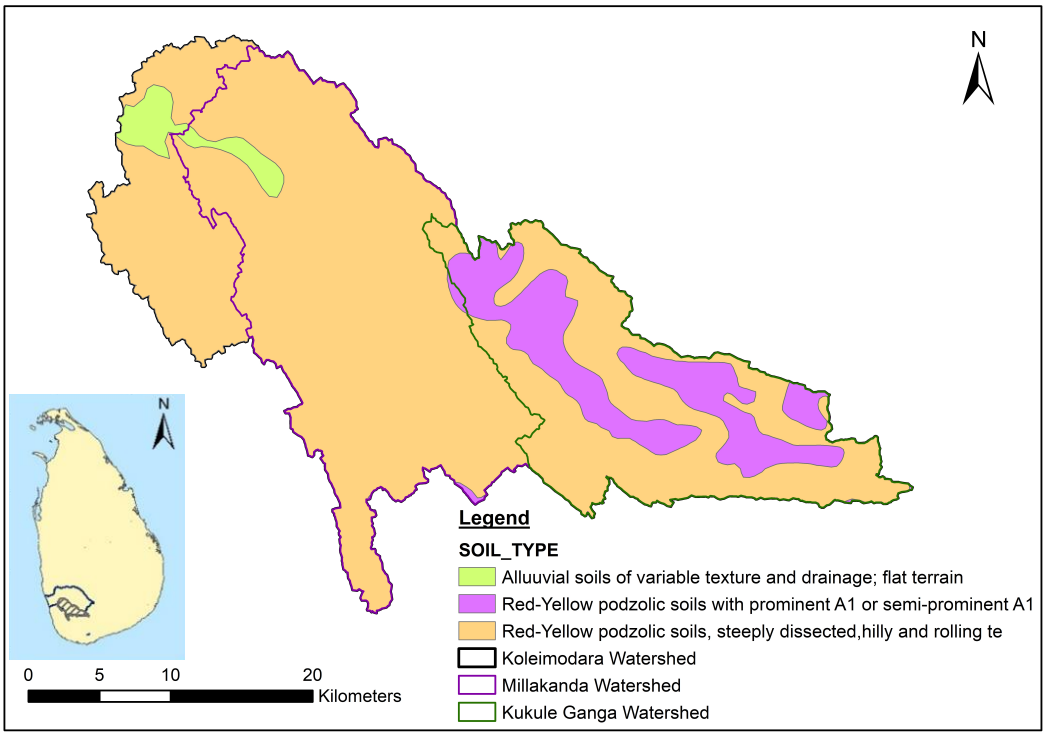

Figure 4-2: Soil map of Koleimodara catchment

Source: Survey Department of Sri Lanka

Table 4-2: Land use distribution of Koleimodara catchment

Land use type	Area (Ha)	Area (%)
Forest – Unclassified	30,319.21	33.10
Rubber	21,228.71	23.20
Chena	11,860.27	12.90
Homesteads/Garden	7,924.22	8.70
Scrub land	7,066.14	7.70
Paddy	5,755.20	6.30
Tea	4,231.70	4.60
Other Cultivation	1,162.89	1.30
River	1,071.60	1.20
Coconut	717.67	0.80
Rock	113.02	0.10
Marshy	48.31	0.10
Cinnamon	36.44	0.00
Industry	26.07	0.00
Cemetery	8.21	0.00
Park / Playground	6.15	0.00
Institutional	3.58	0.00
Paddy-abandoned	2.64	0.00
Water Hole	2.41	0.00
Factory Building	1.67	0.00
Commercial	0.36	0.00
Waste Land	0.25	0.00
Tank	0.06	0.00

Source: Survey Department of Sri Lanka

Table 4-3: Soil types of Koleimodara catchment

Soil type	Area (Ha)	Area (%)
Alluvial soils of variable texture and drainage; flat terrain	2,385.4	2.60
Red-Yellow podzolic soils with prominent A1 or semi-prominent A1	11,604.9	12.70
Red-Yellow podzolic soils, steeply dissected, hilly and rolling terrain	77,596.4	84.70

Source: Survey Department of Sri Lanka

4.2.2 Hydrological and meteorological data

Millakanda river gauging station data, four rain gauging stations data, namely: Galathuta Estate, Sirikandura, Rakwana (Depadena), and Usk Valley, and two evaporation stations data at Ratnapura and Agalawatta were used for this study. Data resolutions and data sources are listed in Table 4-1. The coordinates of the gauging stations are listed in Table 4-4.

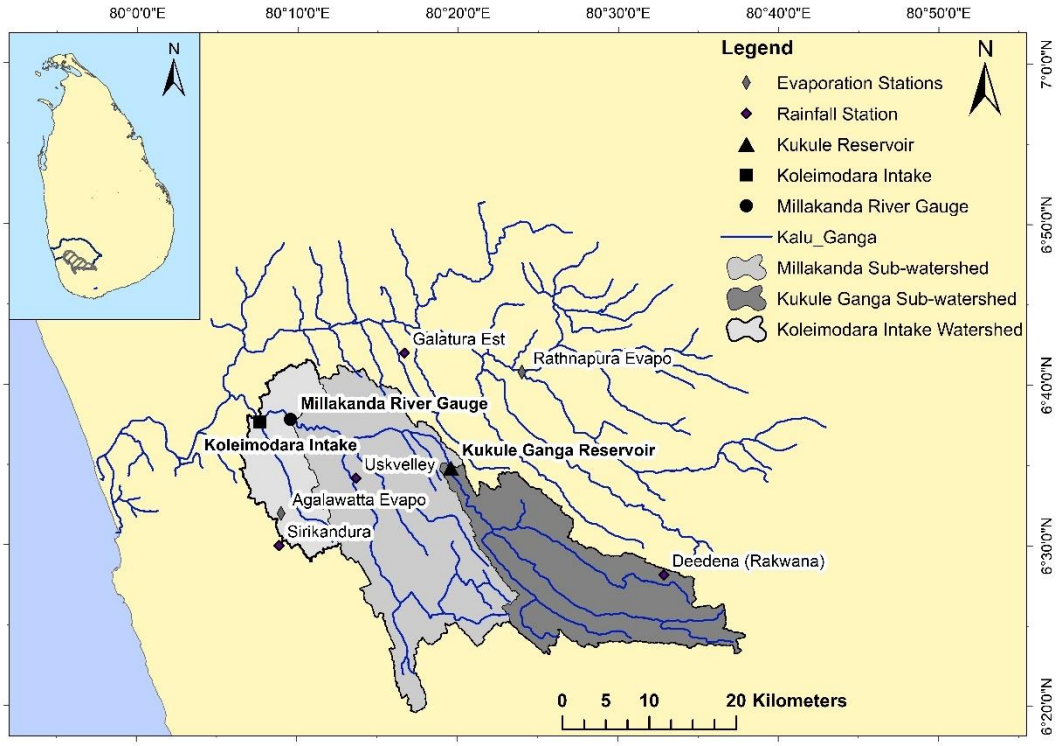

Figure 4-3: Kalu Ganga with Koleimodara basin map and gauging stations

Table 4-4: Coordinates of gauging stations

Data type	Stations Name	Coordinates (Decimal Degrees)
Rainfall	Sirikandura	80.15E, 6.50N
	Usk Valley	80.23E, 6.57N
	Galatura Estate	80.28E, 6.70N
	Depedana (Rakwana)	80.55E, 6.47N
Streamflow	Millakanda	80.16E, 6.63N
Evaporation	Ratnapura	80.40E, 6.68N
	Agalawatta	80.15E, 6.53N

Source: Meteorological Department of Sri Lanka

4.2.3 RCM data for future projections

The hindcasted precipitation data for the historical period and future projections for the next design horizon (until 2060) were derived from the CORDEX dataset for South Asia under ICTP-RegCM4-7 simulations based on three GCMs (Table 4-5). Four grid points were used to extract data (Figure 4-4). Three data sets were downloaded from the same RCM under three different GCMs based on the two available RCPs. The domain WAS 22 was selected as it has the finest resolution data for the South Asia region (0.22 degree or 25 x 25 km^2). Selection details of RCM data are also described in Section 2.6.

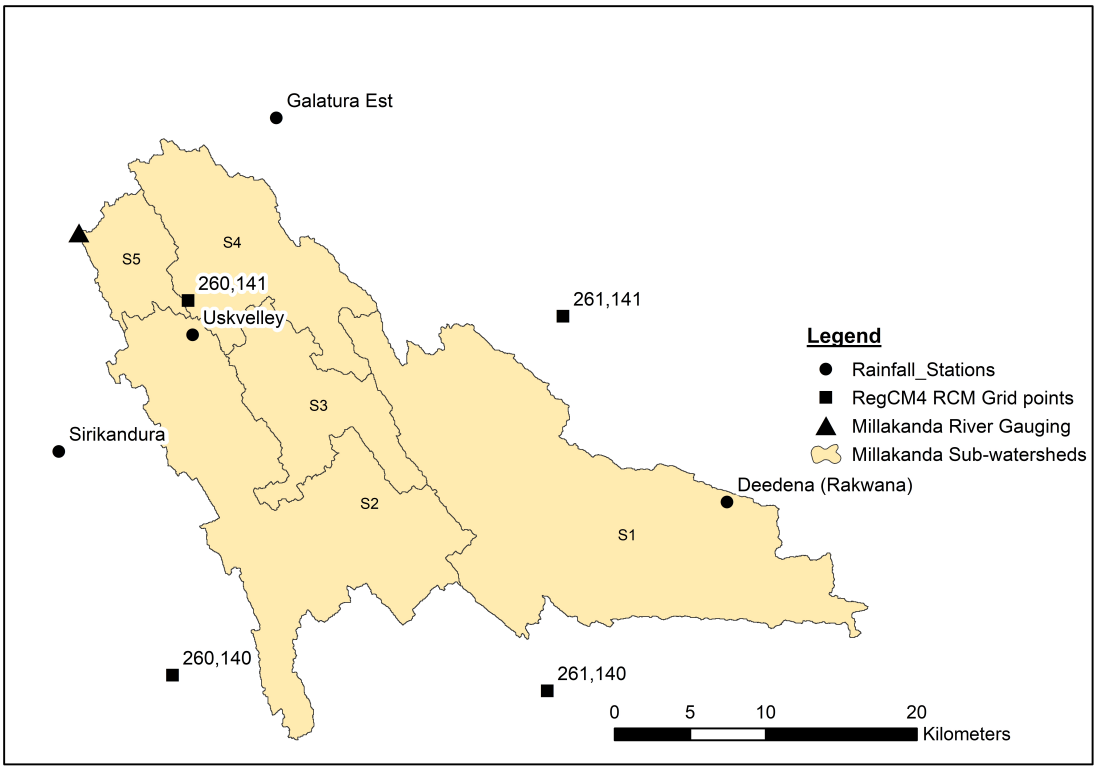

Figure 4-4: RegCM4-7 RCM grid points in the study area (resolution 25 x 25 km^2)

Table 4-5: Details of the RCM and related GCM from the CMIP5 ensemble

RCM	GCM	Resolution	RCP's	Data Period
ICTP - RegCM4-7	NCC-NORESM1-M MIROC-MIROC5 MPI-M-MPI-ESM-MR	25 x 25 km^2	RCP 2.6 RCP 8.2	Historical (1976-2005) Future Projections (2030-2060)

Source: Data downloaded from, https://esgf-data.dkrz.de/search/cordex-dkrz/

4.2.4 Visual data checking

Visual checks were carried out to find inconsistencies in the data with the graphical representation of rainfall corresponding to streamflow. Streamflow was converted to mm, and the rainfall versus streamflow was plotted in a semi-log, and red circles identified areas of concern. The mismatching of rainfall and runoff can be roughly

identified with the help of visual checking. The visual checking was performed for the whole hydrological modelling period (i.e., from 2005 to 2020), and each rainfall station and Thiessen rainfall at the Millakanda sub-watershed. All four rain gauging station data (Galatura Estate, Sirikandura, Rakwana, and Usk Valley) were checked with the Millakanda river flow gauging station data for each water year (October to September) of the modelling period.

Figure 4-5 presents the runoff response in the Millakanda watershed for each rainfall station record from October 2009 to September 2010. The streamflow at the end of September does not respond to the Rakwana and Usk Valley rainfall data, and it only corresponds to the rainfall in Galatura and Sirikandura, which has very low influence according to Thiessen weights. On the contrary, high rainfall recorded in Sirikandura in the middle of May does not correspond to the streamflow records. The highest recorded streamflow for the whole study period with a magnitude of 1,211 m^3/s on 02nd June 2012 does not correspond to the rainfall records. When selecting yearly water cycles for model calibration and validation, these irregular periods were avoided. All the visual data checking plots concerning all water cycles are presented in ANNEXURE I. There are inconsistencies in the low flow data in water cycles 2015/2016, 2016/2017, 2019/2020, with the sudden flow dropping to very low values (Figure I-12, Figure I-15).

The minimum recorded low flow before 2015 October was 9.3 m^3/s, which is also doubtful as its sudden drawdown from 18.4 to 9.3 m^3/s and again rise to 18.5 m^3/s on 01-Jan-2014 in consecutive days without rainfall event from 26-Dec-2013 (Refer Figure I-9). The other minimum recorded streamflow has occurred on 22-Feb-2009 (10.3 m^3/s).

Figure 4-6 shows inconsistency in streamflow after 2015, where the minimum values decreased even below 1.0 m^3/s. Such low values were not recorded before 2015 with similar rainfall conditions. There were no water extractions upstream or any significant land-use changes recorded after 2015 to cause this much flow decreasing variations. Hence, these inconsistent data periods were not used for hydrological model calibration and validation.

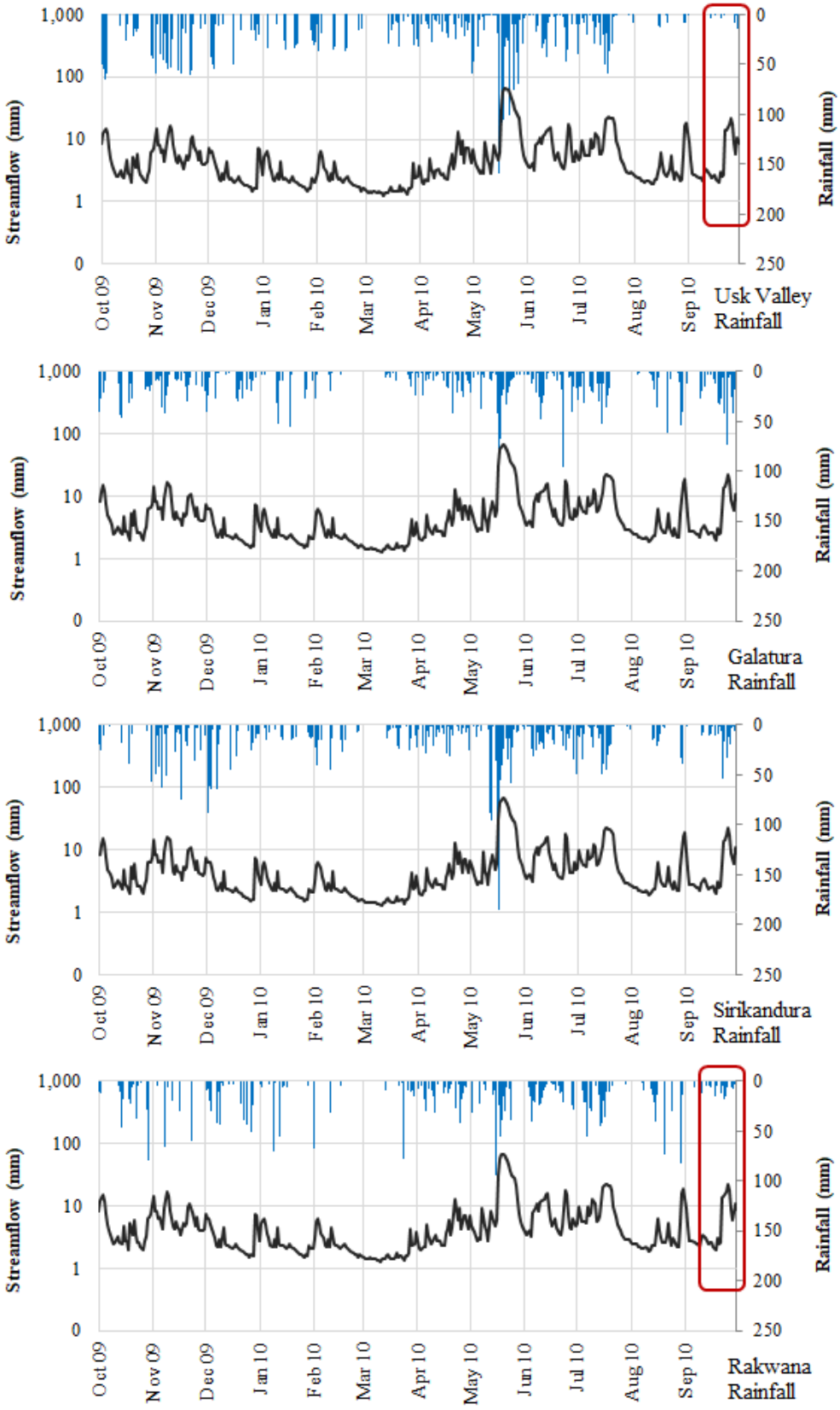

Figure 4-5: Streamflow response to rainfall in Millakanda watershed in 2009/2010

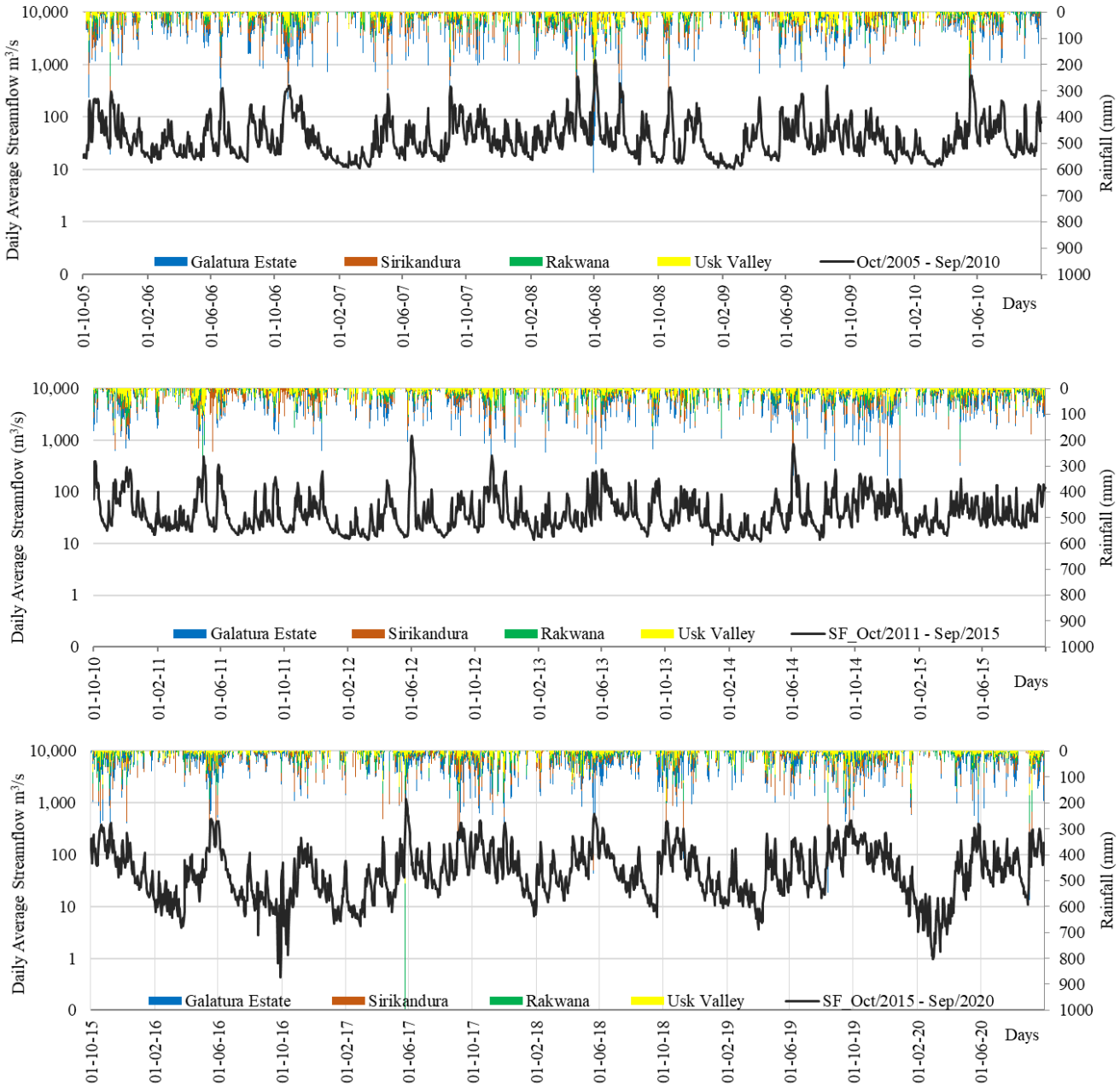

Figure 4-6: Variation of daily rainfall of all stations with Millakanda streamflow; comparing three 5year water cycles (Oct/2005 to Sep/2020)

4.2.5 Thiessen average rainfall

Thiessen Average rainfall for the Millakanda watershed and other sub-watersheds were obtained according to Chow et al. (1988). Thiessen polygons of the Millakanda watershed were derived using the Arc GIS tools, and the weighted averages are listed in Table 4-6.

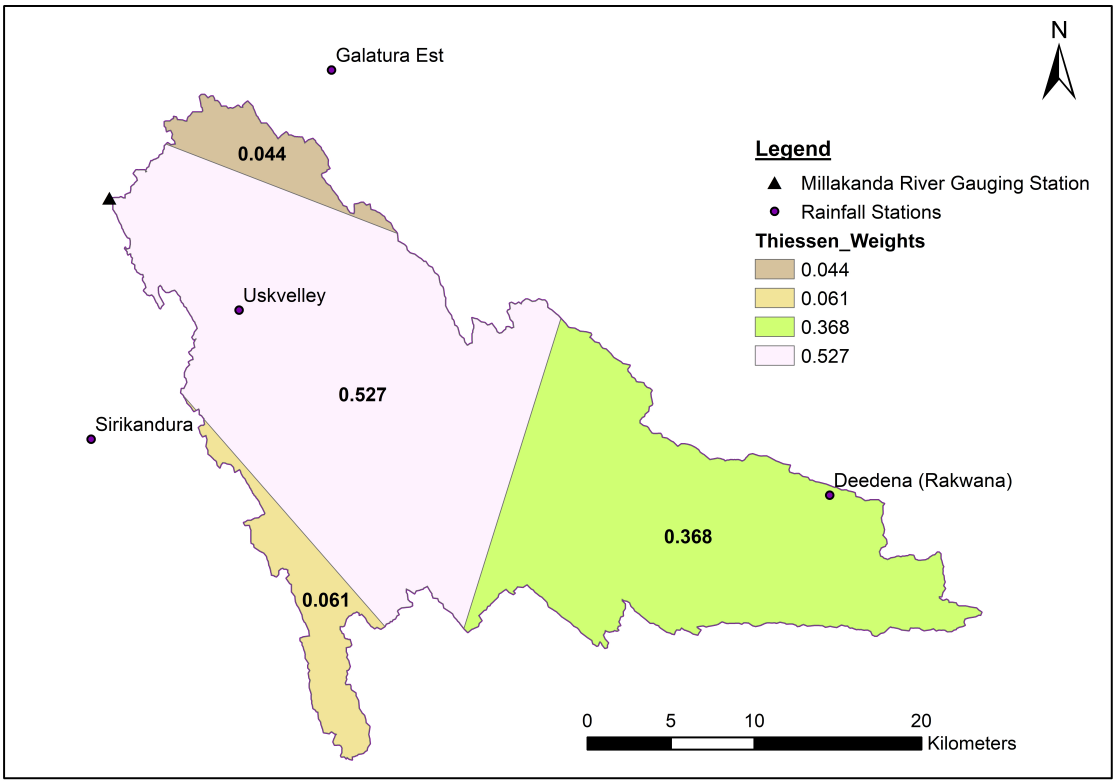

Figure 4-7: Thiessen polygons of Millakanda watershed

Table 4-6: Thiessen weights of rain gauging stations – Millakanda watershed

Rainfall Stations	Area (km^2)	Thiessen weight
Sirikandura	46.94	0.061
Usk Valley	405.64	0.527
Galatura Estate	33.81	0.044
Depedana (Rakwana)	283.28	0.368

Thissen average rainfall of Millakanda watershed also plotted against the Millakanda Streamflow data similarly as described in Visual data checking under Section 4.2.4. The inconsistencies in streamflow with rainfall could be observed in Thiessen Rainfall also as described in the same section. Similarly, the graphs were plotted with Thiessen average rainfall against streamflow for each annual water cycle for the period of

October 2005 to September 2020 which are compiled in APPENDIX 1, Figure I-16 to Figure I-19.

4.2.6 Annual and monthly rainfall variations

Annual rainfall variation of Galatura Estate, Sirikandura, Rakwana, and Usk Valley rain gauging stations for the whole data period (1976 to 2020) was analysed at an annual scale (Figure 4-8). There is an inconsistency in the annual rainfall of Usk Valley station in years 1989/1990, 1990/1991, 1991/1992 compared to the other stations. Rakwana station received the least rainfall of all the stations, 13% less than the Usk Valley which has the highest average annual rainfall (about 4,500 mm). The annual rainfall of Galatura shows an irregular pattern in 1981/1982 compared to the other stations. The annual rainfall of Galatura station is 7,030 mm, which is not realistic when considering the average basin rainfall of 4,130 mm.

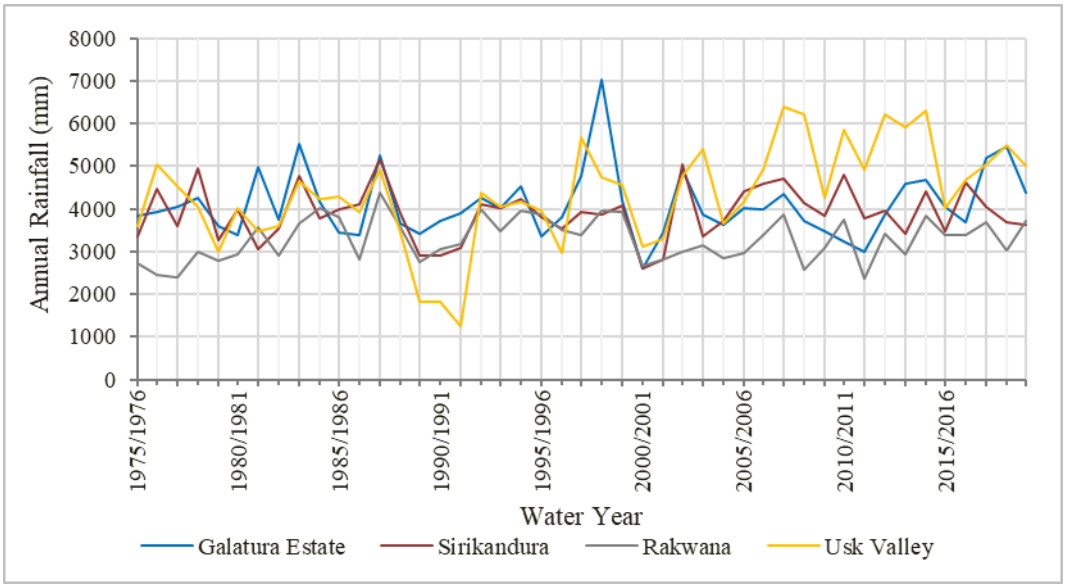

Figure 4-8: Variation of the annual rainfall of Millakanda watershed

The monthly average rainfall of Galatura Estate, Sirikandura, Rakwana, and Usk Valley rainfall stations over 20 years (October 2000 to September 2020) were considered to avoid inconsistent data periods. The results are listed in Table 4-7.

.

Table 4-7: Monthly average rainfall comparison Oct/2000 to Sep/2020

Month	Monthly average rainfall (mm)			
	Galatura Estate	Sirikandura	Rakwana	Usk Valley
October	519	552	425	529
November	410	395	396	441
December	267	288	236	333
January	136	155	121	187
February	148	138	137	180
March	179	188	200	260
April	383	331	383	412
May	514	513	376	579
June	460	370	278	457
July	312	255	231	310
August	336	257	234	326
September	466	445	294	492
Annual Total	**4129**	**3886**	**3310**	**4507**

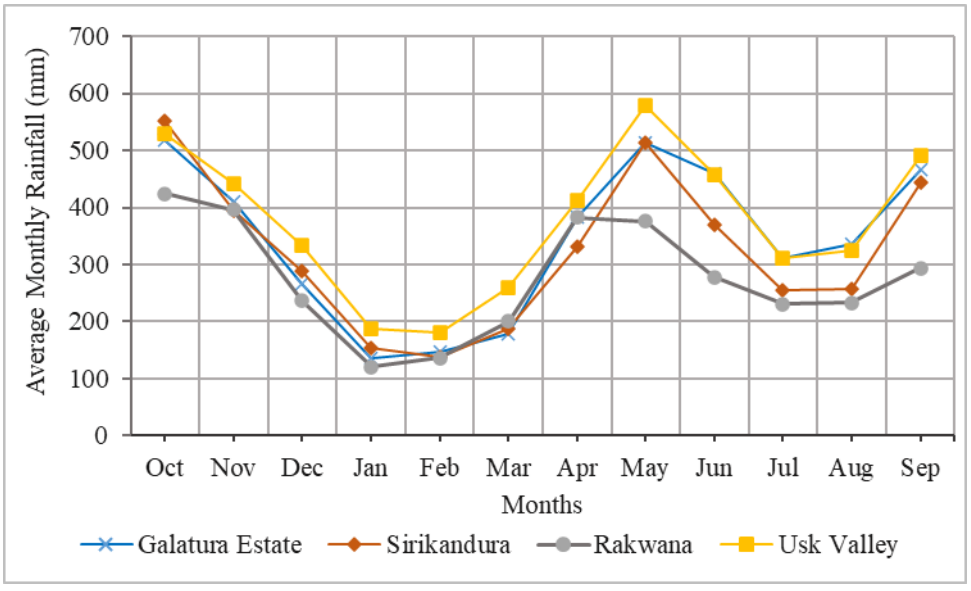

Figure 4-9: Variation of average monthly rainfall of Millakanda watershed (2000-2020)

Figure 4-9 illustrates that the catchment receives most of its rainfall during the seasons of the Southwestern Monsoon (May to September) and Second Inter Monsoon (October to November). Usk Valley rainfall station receives the highest rainfall during these 20 years, whereas Rakwana receives the least.

4.2.7 Single mass curve

Single mass curves were plotted to check the consistency of the rainfall throughout time. Single mass curves of each rainfall station are attached in the ANNEXURE II. There are inconsistencies in the data of Usk Valley for three years (Figure II-1), which is also observed in the annual rainfall data plots.

4.2.8 Double mass curve

The double Mass curve is plotted to compare single station cumulative annual rainfall with the average of the surrounding stations of the catchment. The consistency of the rainfall data can be evaluated using the double mass curve plots. The change in the slope of the double mass curve shows the inconsistency of the data. The drop in the double mass curve of Usk Valley station is due to inconsistent annual rainfall in 1989/1990, 1990/1991, 1991/1992 water years (Figure II-2). The slope of the curve is not changed. Therefore, Usk Valley data can be used to model simulations from 2005 to 2020. The other three rainfall station data do not show any inconsistency. Therefore, the available rainfall data can be used for hydraulic modelling without modification (Figure II-2).

4.2.9 Filling of missing rainfall data

Missing rainfall data should be filled in to obtain time series for rainfall-runoff modelling. In this study, two methods were used to fill the missing data based on the average annual value of the rainfall stations, as described in The AIT Manual on Hydrology: Measurement and Analysis (Shrestha & Deb, n.d.). Percentage of missing rainfall and streamflow data during the model simulation period (October/2005 to September/2020) are as shown in Table 4-8.

Table 4-8: Percentage of missing rainfall and streamflow data of total model simulation period (September/2005 to October/2020)

Data type	Stations Name	% of missing data
Rainfall	Sirikandura	4 %
	Usk Valley	6 %
	Galatura Estate	3 %
	Depedana (Rakwana)	2 %
Streamflow	Millakanda	< 1 %

The arithmetic average method can be used when the average annual rainfall of the station with missing data is within 10% of the average annual rainfall at the adjoining stations. Simple averages of the surrounding stations are used to fill the missing data of the station as in the equation [4-1].

$$P_x = \frac{1}{m}(P_1 + P_2 + \cdots + P_m) \quad [4\text{-}1]$$

where P_x is the rainfall under consideration and P_1, P_2, ……, P_m are rainfall corresponding to 'm' neighbouring stations.

The normal ratio method is used if any index station has an annual rainfall of magnitude that varies more than 10% of the interpolation station. Missing rainfall data (P_x) of the stations X are filled by the 'm' number of stations. Then the missing precipitation P_x is estimated as per the equation [4-2].

$$P_x = \frac{1}{m}\sum_{i=1}^{m}\left[\frac{N_x}{N_i} * P_i\right] \quad [4\text{-}2]$$

Other than the equation [4-1] notations, the average annual precipitations N_1, N_2, …, N_i at each of the above stations, including station X, are known.

4.3 Determination of Flow Threshold for Low Flow Deficit Analysis

Threshold or truncation concepts are one way of estimation of flow deficit based on a particular objective, as described in section 2.1.1. The minimum flow threshold based

on the objective of this study at the Koleimodara intake location is the future water extraction requirement by NWSDB plus the environmental flow required by the downstream river section. Present intake capacity at the Koleimodara intake is 75,000 m^3/day or 0.9 m^3/s. The NWSDB has identified the next intake capacity extension requirements on the region's future water demands, which is estimated as 50,000 m^3/day or 0.6 m^3/s according to the Masterplan of NWSDB (CSIP, 2019). Therefore, the total water extraction requirement for the next design horizon would be 1.5 m^3/s.

The Kukule Ganga run-off-the-river powerplant hydropower generation project has used the environmental flow as 0.5 m^3/s. The reservoir has a catchment area of 322 km^2, whereas the catchment area of the Koleimodara intake location is 916 km^2. Assuming the same ecological conditions downstream the Millakanda outlet and Koleimodara outlet locations of the river, e-flow can be taken as proportionate to the watershed area, which is 1.5 m^3/s. The flow threshold for low flow analysis was taken as the sum of water extraction and environmental flow requirement, which is 3.0 m^3/s.

4.4 Seasonal Distribution of Streamflow in Kuda Ganga

Millakanda streamflow records (since 1990) are available at the Irrigation Department. As described in the Problem Statement in Section 1.4, there is a decreasing trend in the yearly minimum seven-day moving average daily flow as illustrated in Figure 1-2, which has become much stabilized after the construction of Kukule Ganga run-off-the river power still with a slightly decreasing trend.

Since the main objective of this study is to assess low flow conditions in the future, streamflow data starting from the operation of the Kukule Ganga run-off-the river power plant from 2005 to 2015 was used for hydrological model development. Data after 2015 was not used in model calibration and validation due to the inconsistencies described in Section 4.2.4. Knowledge of the seasonal distribution of the streamflow is essential as this study mainly focuses on the low flow period water availability. Figure 4-10 indicates that the low flow months are January, February, March, and August.

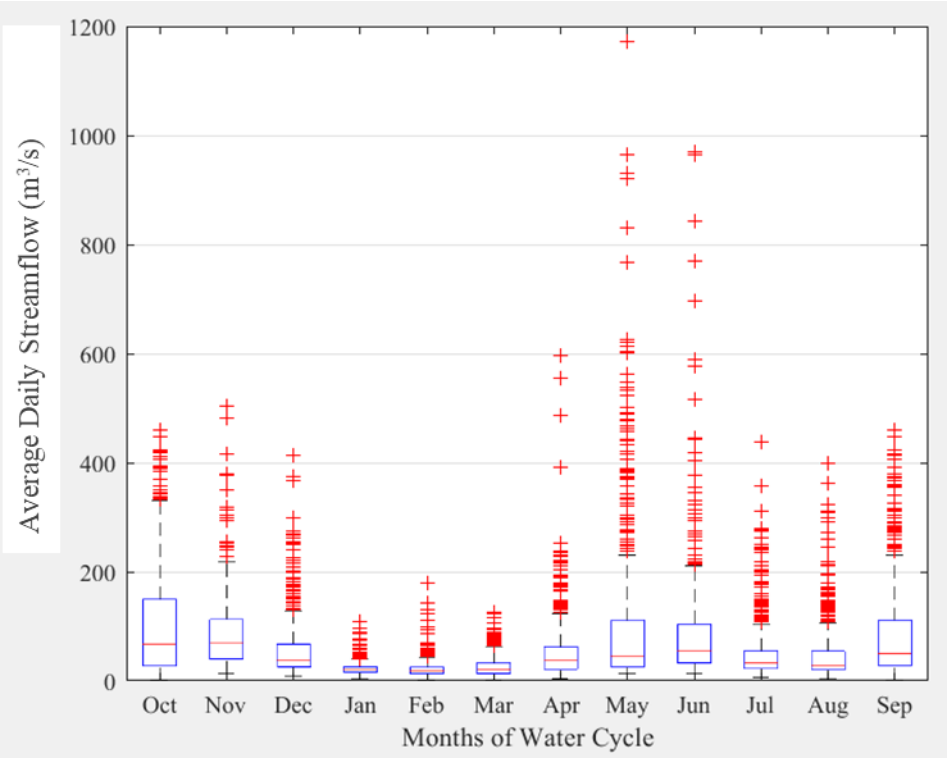

Figure 4-10: Seasonal variation of streamflow at Millakanda gauging station (2005 to 2020)

4.5 Bias Correction of RCM Data and Model Selection

Three RCM data sets were bias-corrected with the mean-based method described in Section 2.7. Thiessen average of the RCM historical precipitation of the four grid points over the Millakanda sub-basin (Figure 4-4) was bias-corrected using the mean-based method of the Thiessen average rainfall Millakanda subbasin as the observed data set. Thiessen weights of four RCM grid points over the Millakanda watershed is given in Table 4-9.

Table 4-9: Thiessen weights of RCM grid points over Millakanda watershed

Grid point	Thiessen weights
(260,141)	0.40
(261,141)	0.20
(260,140)	0.12
(261,140)	0.28

The monthly mean of the observed and bias-corrected precipitation data during the 2001-2005 period (five years) was evaluated using the statistical parameters RMSE, R^2, and PBIAS. The NCC-NorESM1-M model indicates the best results based on the statistical indicators of the bias-corrected data, and, the average annual rainfall varies 2% from the observed as summarized in Table 4-10. According to Figure 4-11, NCC-NorESM1-M shows a better correlation with observed data during the low flow months other than the other two models considering the total 30-year data period (1976 to 2005). Therefore, the NCC-NorESM1-M model was selected for further evaluation.

Table 4-10: Statistics of bias correction result over the evaluation period (2001-2005)

Model Name	Average Annual Rainfall (mm)	RMSE (mm) (Before BC)	RMSE (mm) (After BC)	R^2 (Before BC)	R^2 (After BC)	PBIAS % (Before BC)	PBIAS % (After BC)
NCC-NorESM1-M	**3,578**	**236**	**55**	**0.0001**	**0.77**	**25**	**-3.1**
MIROC-MIROC5	4,111	501	85	0.018	0.74	114	11.3
MPI-M-MPI-ESM-MR	4,210	412	106	0.050	0.65	106	14.0
Observed	3,660						

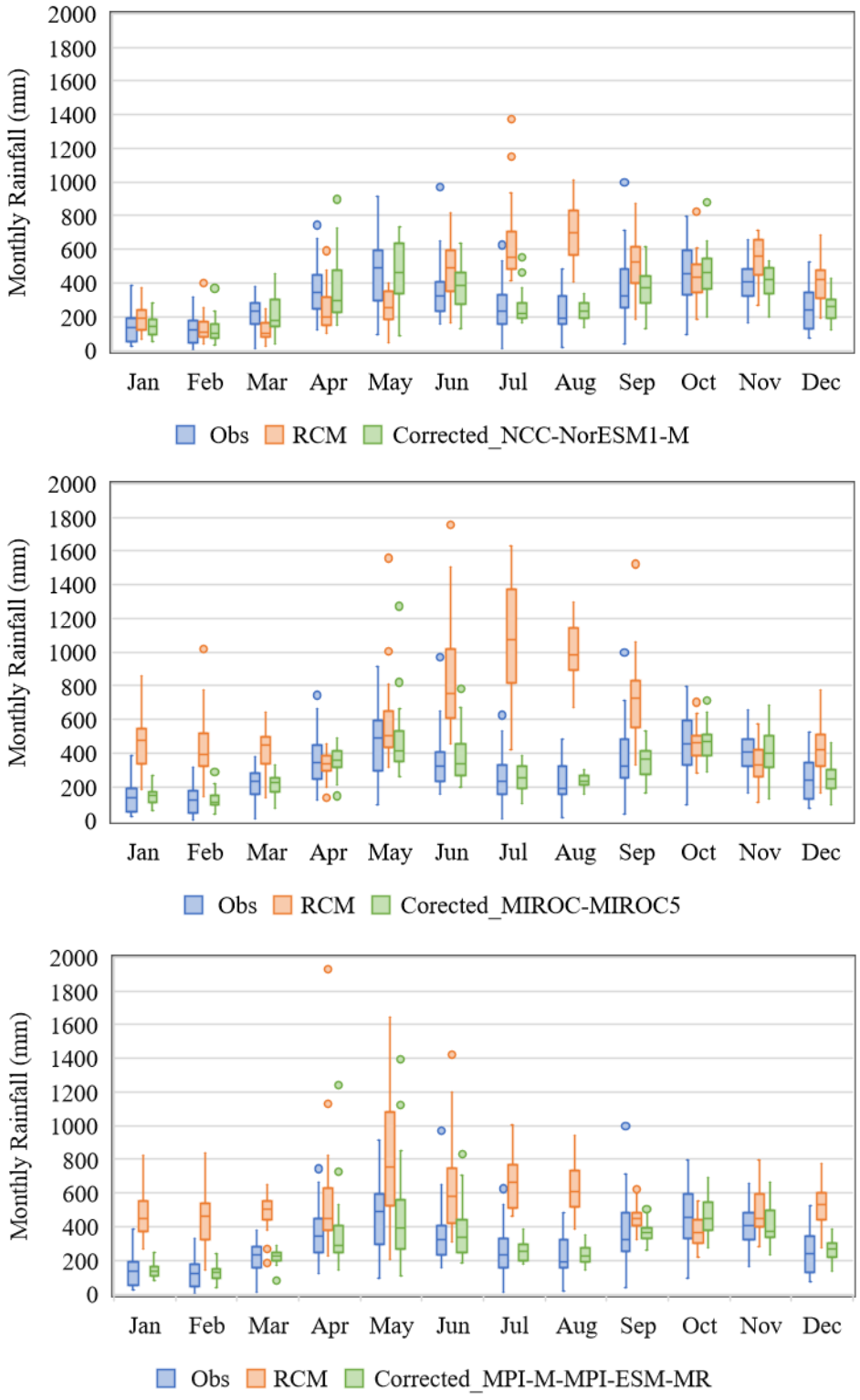

Figure 4-11: Variation of monthly observed rainfall, RCM rainfall, and bias-corrected RCM rainfall over 30 years (1976 to 2005)

4.6 Evaluation of Bias-Corrected RCM Precipitation Data

Bias correction can bring the GCM/RCM model outputs values nearer to the observed values by eliminating the accompanied biases with them. The selected climate model's (i.e., NCC-NorESM1-M) bias-corrected data for the Millakanda watershed was evaluated for the period of 2001 to 2005 (Table 4-11 and Figure 4-12). It shows variations of the monthly means as well as the seasonal means of four rainfall seasons (i.e., South-West monsoon (SWM), North-East monsoon (NEM), First Inter monsoon (1st IM), and Second Inter monsoon (2nd IM)) of observed rainfall, RCM precipitation, and bias-corrected RCM precipitation.

Table 4-11: Monthly and seasonal means of observed rainfall, RCM rainfall, and bias-corrected RCM rainfall for Millakanda watershed over evaluation period (2001 to 2005)

Type	Month	Precipitation (mm)			% Bias
		Observed	RCM raw data	Bias corrected RCM data	
Monthly Means	October	528	445	475	-10.0
	November	368	522	392	6.6
	December	292	463	290	-0.8
	January	205	191	143	-30.1
	February	131	137	126	-4.0
	March	251	129	234	-6.5
	April	403	213	323	-19.8
	May	451	203	371	-17.8
	June	285	463	362	27.0
	July	279	609	244	-12.5
	August	159	726	244	54.2
	September	342	524	372	8.8
Seasonal Means	SWM	1,515	2,525	1,593	5.1
	NEM	629	790	560	-11.0
	1st IM	654	341	558	-14.7
	2nd IM	896	968	867	-3.2

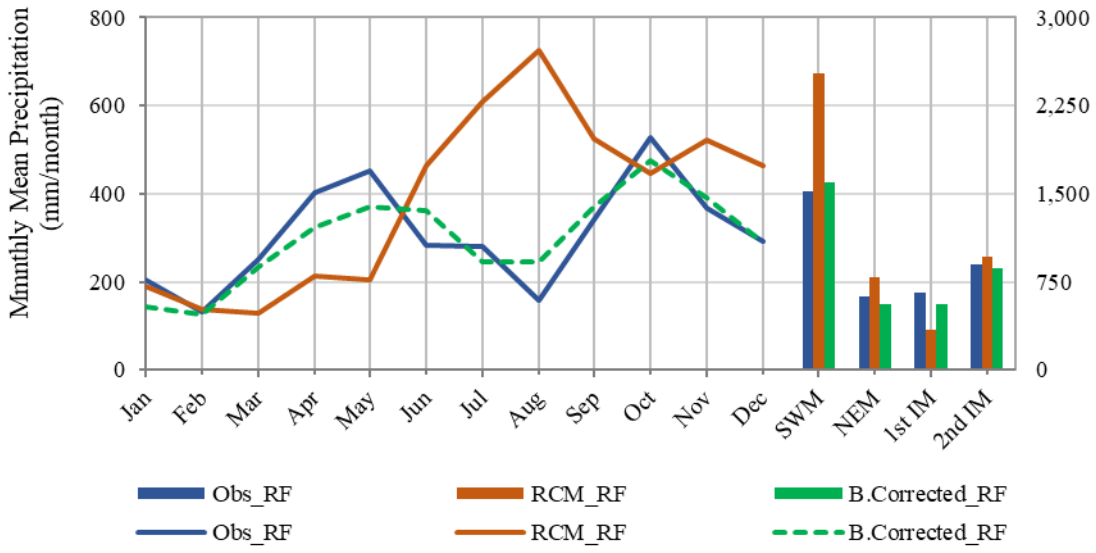

Figure 4-12: Variation of Monthly and seasonal means of observed rainfall, RCM rainfall, and bias-corrected RCM rainfall over evaluation period (2001 to 2005)

The same evaluation was performed for the six sub-basins of the hydrological model, comparing basin-wise Thiessen average rainfall with RCM data at four grided hindcast Thiessen average precipitation. The data tables and figures related to sub-basin-wise analysis are illustrated in the ANNEXURE IV.

4.6.1 Evaluate bias-corrected precipitation with drought analysis

Several dry spell characteristics were compared between bias-corrected RCM data and observed precipitation data. The reference evapotranspiration (ET_o) was selected as the threshold (Table 4-12) to determine dry spells, following the literature study mentioned in Section 2.8. Average monthly ET_o of Agalawatta and Ratnapura were used to derive the daily mean ET_o of the Millakanda sub-basin for each month.

Table 4-12: The reference evapotranspiration (ET_o) for each month

Month	Agalawatte (mm)	Ratnapura (mm)	Average (mm)	Mean Daily ET_o (mm)
October	97	100	98.5	3.2
November	103	108	105.5	3.8
December	120	128	124.0	4.0
January	111	118	114.5	3.8
February	108	115	111.5	3.6
March	99	107	103.0	3.4
April	106	111	108.5	3.5
May	111	115	113.0	3.6
June	109	107	108.0	3.6
July	104	104	104.0	3.4
August	90	89	89.5	3.0
September	87	89	88.0	2.8

Source: Hydrology Division (ID) (2019)*; Irrigation Department*

Dry spell characteristics, namely: i. Average dry spell length, ii. Max dry spell length, iii. The standard deviation of dry spell length, iv. 90^{th} percentile dry spell length, v. 95^{th} percentile dry spell length, and vi. 99^{th} percentile dry spell lengths were used to evaluate the response of the bias-coerced RCM precipitation data with the observed precipitation data, particularly during the dry months of the 1976-2005 period. The analysis results are illustrated in Figure 4-13 and tables in ANNEXURE III (Table III-1, Table III-2, Table III-3, Table III-4, Table III-5, and Table III-6).

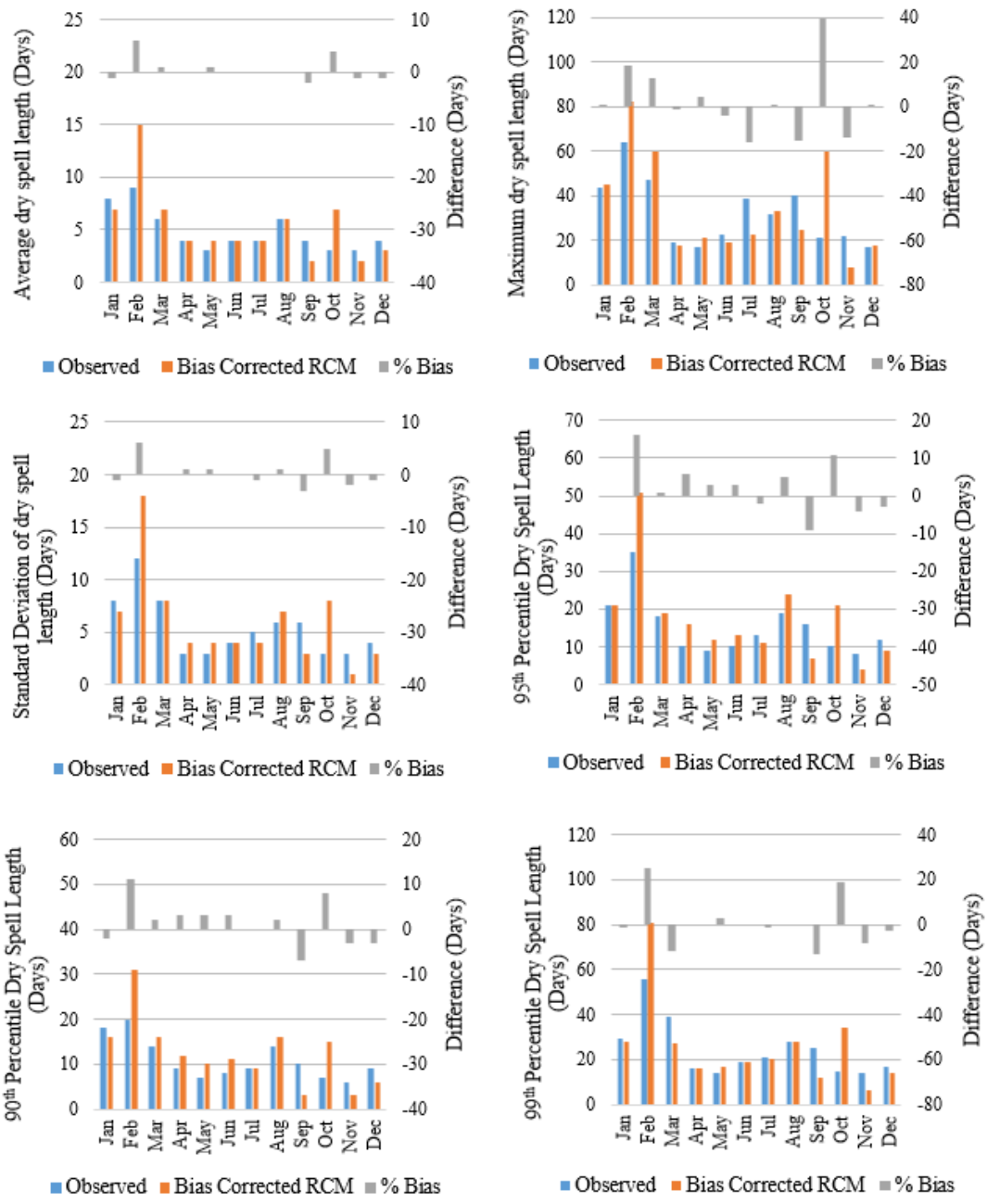

Figure 4-13: Comparison of the monthly variation of the dry spell characteristics of RCM precipitation data with the observed precipitation data over 30 years (1976 to 2005)

4.7 Variation of Projected Precipitation Relative to the Base Period (1976 to 2005)

Projections of precipitation data were analysed under RCP 2.6 and 8.5 compared to the 30-year base period (1976 to 2005). Thiessen average rainfall of the Millakanda watershed was used for the analysis. The exact monthly factors were used to bias correct the precipitation projections under two future scenarios, RCP 2.6 and 8.5 (as per equation [2-13]). The average annual rainfall of the projected precipitation for the next design horizon was compared relative to the base period under both scenarios. The projected average annual rainfall increases under both scenarios considered (Table 4-13). Also, the average monthly and seasonal precipitation variation graphs (Figure 4-14) illustrate the average monthly and seasonal variation of precipitation over the next design horizon. Figure 4-15 and Figure 4-16 show the decade-wise variation of monthly mean rainfall under RCP 2.6 and 8.5 scenarios.

Table 4-13: Average annual rainfall variation

	Average Annual Rainfall (mm)	% Variation from base
Base Period (1976 - 2005)	3,657	
RCP 2.6	3,820	4.5
RCP 8.5	3,992	9.2

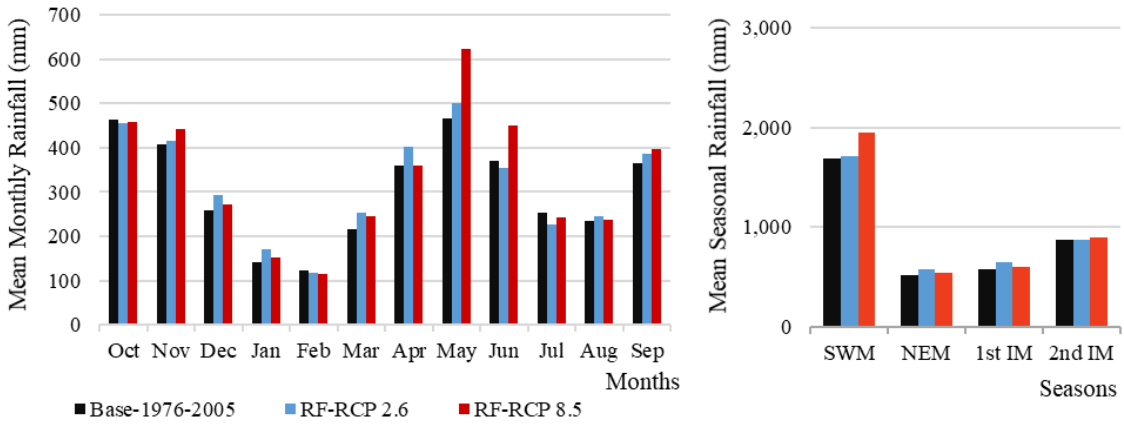

Figure 4-14: Average monthly and seasonal variation of precipitation compared to the historical base period (1976 to 2005) under RCP 2.6 and 8.5 scenarios

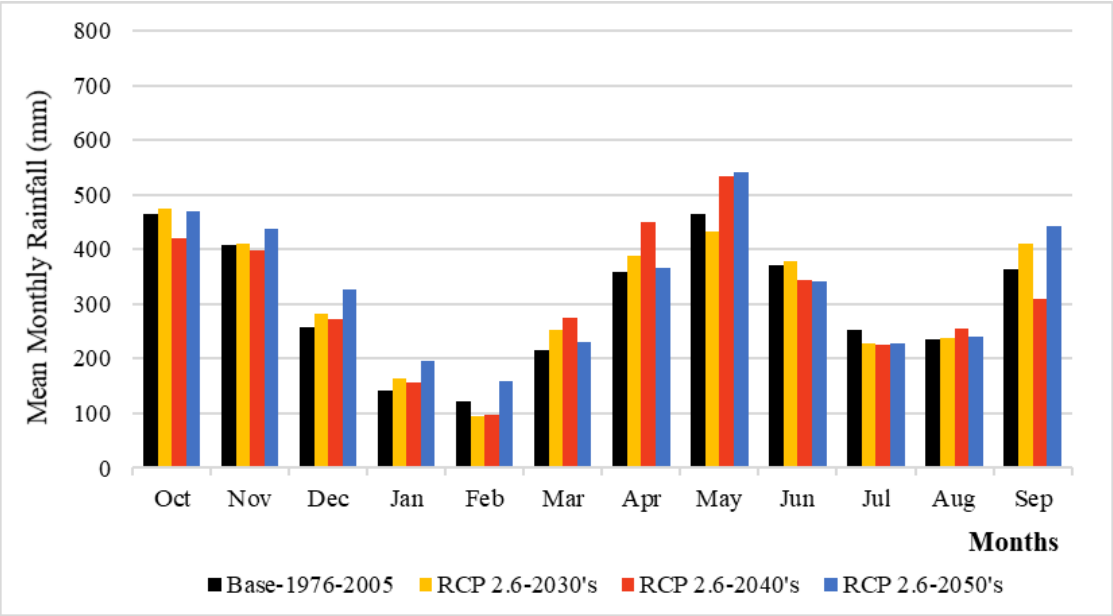

Figure 4-15: Average monthly variation of precipitation in three decades over the design period comparatively to the historical base period (1976 to 2005) under RCP 2.6

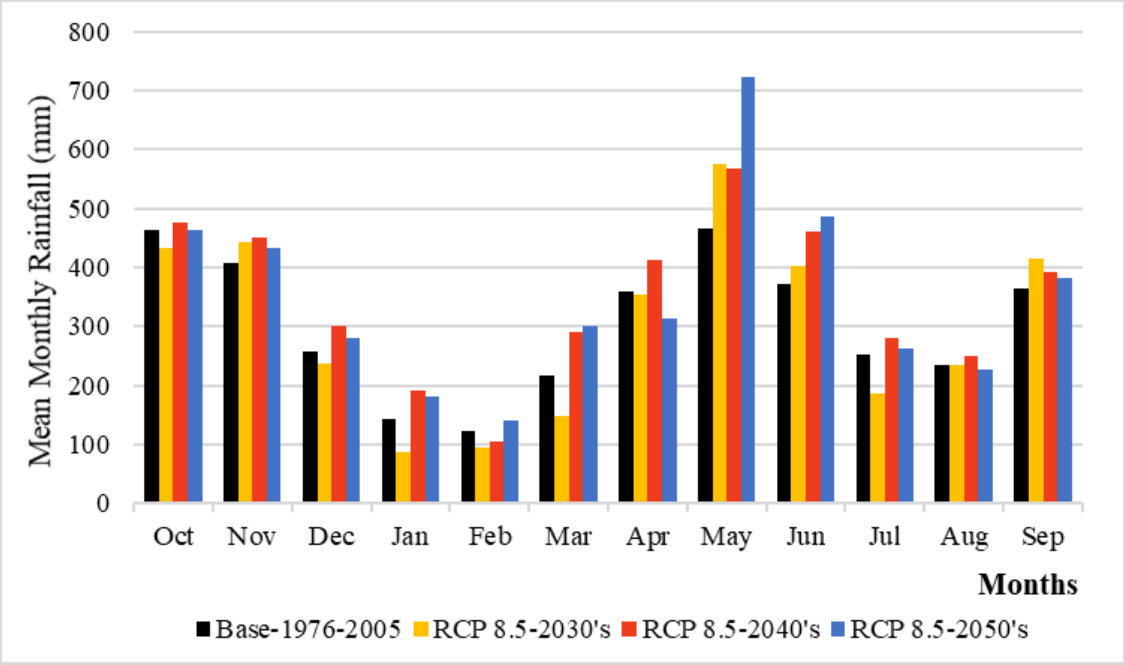

Figure 4-16: Average monthly variation of precipitation in three decades over the design period comparatively to the historical base period (1976 to 2005) under RCP 8.5

CHAPTER 5

5 MODEL DEVELOPMENT AND APPLICATIONS

5.1 Model Selection

HEC HMS model was selected as the hydrological model for this study based on the criteria described in the literature review Sections 2.3.1 and 2.5.

5.2 HEC HMS Model Development

This study required to estimate extraction capacity in Kuda Ganga at the Koleimodara water intake, to which it is necessary to obtain a runoff time series at the location. Since there is no observed flow series at the location, the streamflow flow records of the Millakanda river gauging station, which is located 4.8 km upstream of Kuda Ganga was used for the calibration and validation of the HEC HMS hydrological model. This study utilised the HEC HMS 4.7.1 version which was developed by the United States Army Corps of Engineers to model the rainfall-runoff system of dendritic catchments.

5.2.1 Development of the basin model

Basin model was developed considering the Main outlet at the Koleimodara intake location with a total of six sub-basins and five sub-basins upstream of the Millakanda river gauging station as shown in Figure 5-1. The GIS tools integrated with HEC HMS were used to delineate the sub-watersheds and reach elements with the terrain dataset fed for the basin model and it allows to assign coordinate system for the basin model. The watershed and reach physical characteristics also could be calculated from HEC HMS using the GIS data which were used to calculate parameters related to different model elements. Reach-2 and reach-3 were not delineated properly by the terrain; therefore, that data was manually calculated in Arc GIS 10.3.1 version (developed by ESRI Inc., USA) and fed for the model elements.

The Basin model requires several model components as and no of parameters to estimate the outflow from the precipitation. Table 5-1 summarises the basin model components and methods of estimating the model parameters.

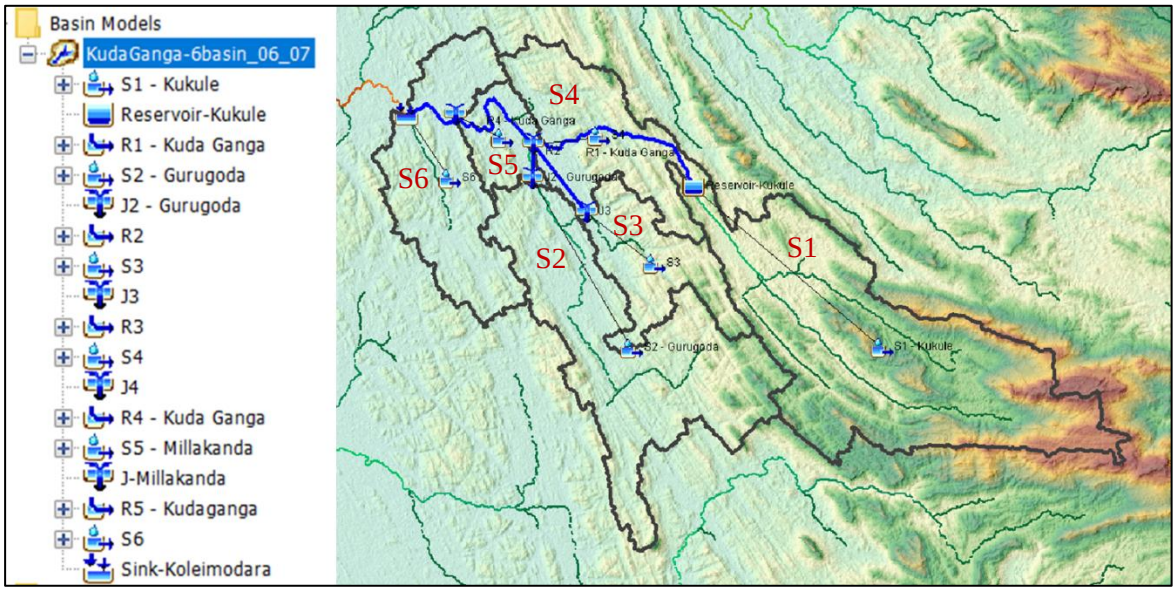

Figure 5-1: Six sub-basins and reach elements delineated by the GIS tools and terrain data and other basin elements of HEC HMS hydrological model

5.2.1.1 Estimation of canopy storage parameter

Canopy storage is the precipitation intercepted by vegetation during a rainfall event. Precipitation falls onto the ground surface after filling the canopy storage. Canopy storage values used by other researchers based on the vegetation type were used for this study as described in Section 2.5.2. The vegetation type was identified by the land use map and the canopy storage map was produced based on the land use and values given in Table 2-3. Canopy storage value for each sub-basin was calculated using the Arc GIS tools. Sample calculation of canopy storage for Kukule Ganga sub-basin is illustrated in the Sample calculation of canopy storage for Kukule Ganga sub-basin (S1) is shown in Table V-1of ANNEXURE V and the canopy storage map of the study area is illustrated in Figure 5-2. The estimated canopy storage value for each sub-basin is summarized in Table V-2.

Table 5-1: Basin model components, parameters, and methods of estimation

Component	Parameter	Unit	Method of estimation
Canopy (Simple Canopy)	Initial storage	%	Calibration
	Canopy max storage	mm	Landuse database
	Crop coefficient	-	Default
Surface (Simple Surface)	Initial storage	%	Calibration
	Surface max storage	mm	Landuse map
Loss (deficit and Constant)	Initial Deficit	mm	Calibration
	Maximum Deficit	mm	Soil Map Literature and calibration
	Constant Rate	mm/hr	Soil Map Literature and calibration
Transform (Snyder UH)	Standard Lag	hr	Snyder UH Method (C_t)
	Peaking Coefficient	-	C_p (ID Technical Guideline)
Baseflow (Linear Reservoir)	GW 1 Fraction	-	Calibration
	GW 1 Coefficient	hr	Calibration and basin Characteristics
	GW 1 Initial Discharge	$m^3/s/km^2$	Calibration
	GW 2 Fraction	-	Calibration
	GW 2 Coefficient	hr	Calibration and basin Characteristics
	GW 2 Initial Discharge	$m^3/s/km^2$	Calibration
Muskingum Routing	K	hr	Calibration
	X	-	Calibration

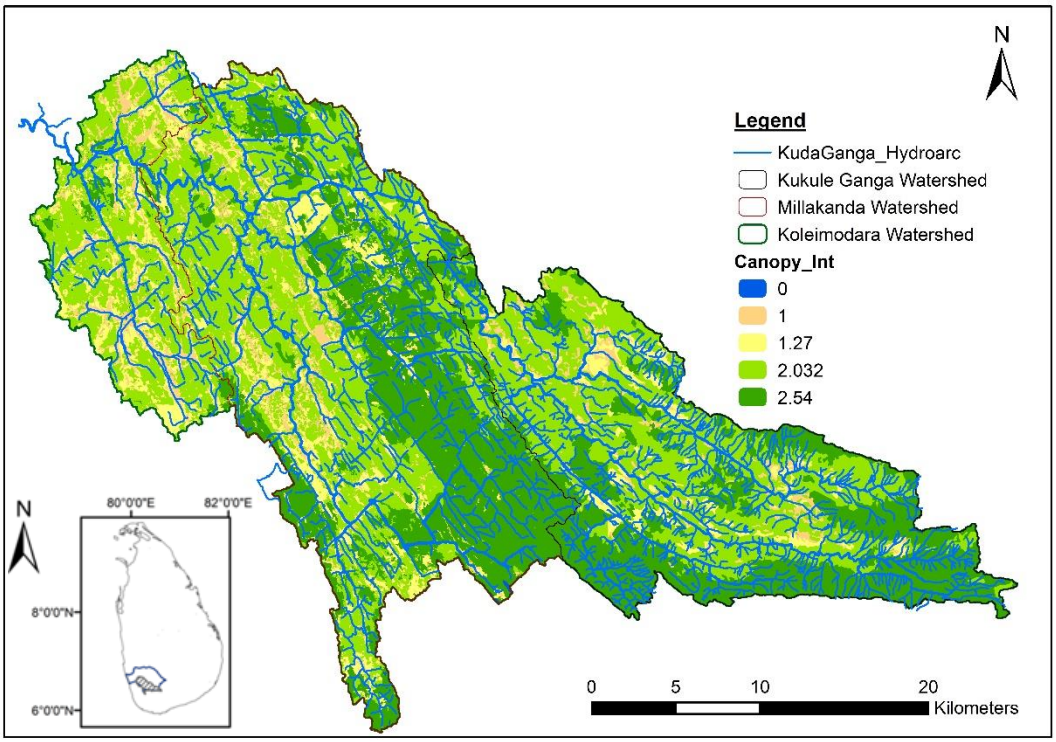

Figure 5-2: Canopy storage map of the Koleimodara watershed

5.2.1.2 Estimation of surface storage parameter

The surface storage component interprets the ground surface storage, in which water accumulates in surface depression storage during a rainfall event. After the canopy storage is filled, the rainwater falls onto the ground and fills the surface storage, and the balance water is captured by the loss method as illustrated in Figure 2-4. Surface depression values can be categorized according to the slope of the watershed as described in the Section 2.5.2. A slope raster of the Koleimodara watershed was prepared using the terrain data (30 m DEM). The surface storage values for each sub-basin were obtained using the Arc GIS raster calculation tools by referring to the values mentioned in Table 2-4. Calculation of the average surface storage of each basin is presented in the Table V-3 of ANNEXURE V.

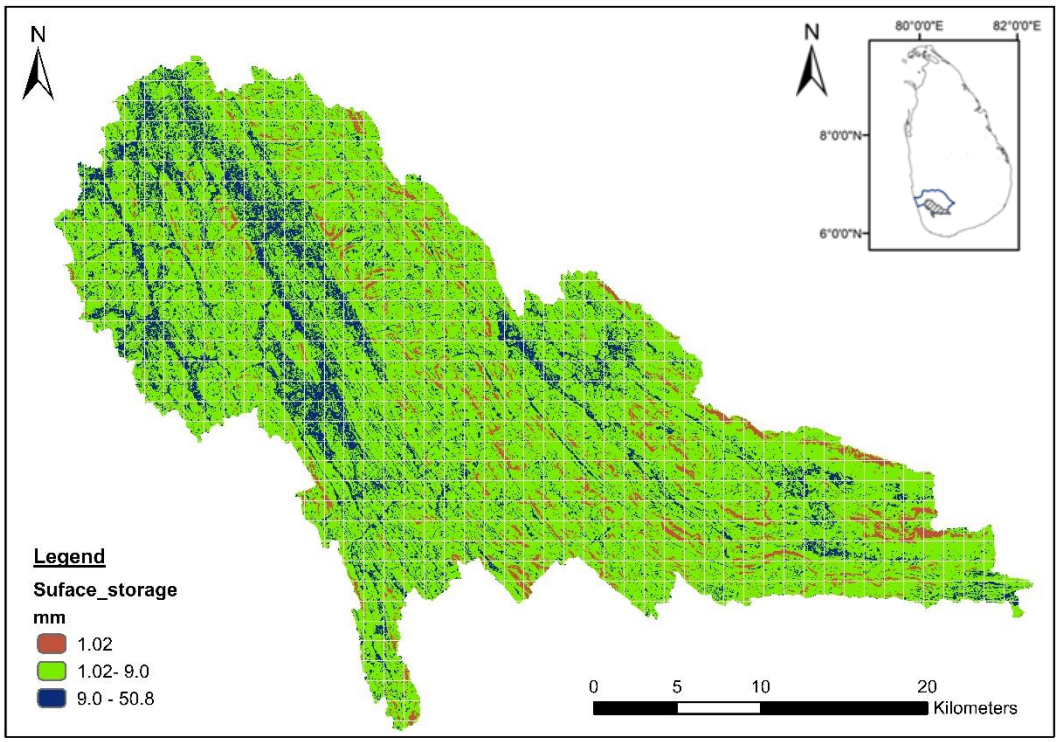

Figure 5-3: Surface storage map of the Koleimodara watershed

5.2.1.3 Estimation of deficit and constant loss method parameters

The deficit and constant loss method require initial deficit, maximum storage, constant rate, and impervious percentage of the basin. The initial deficit was assumed as 25 mm considering 3 to 5 no rainfall days before the start of each simulation event. The constant rate and the maximum deficit were calculated as described in Section 2.5.2, and a sample calculation for the Kukule Ganga sub-watershed is presented in Table V-4 in ANNEXURE V. The soil layer was assumed as 24 inches for the calculation. The percentage impervious of the basin is calculated based on the land use, and the impervious percentage of each land use type was obtained according to Prisloe et al. (2000). Calculation of percentage impervious for Kukule Ganga sub-basin is demonstrated in Table V-5, and the summary of estimated basin average deficit and constant parameters are listed in the Table V-6 of ANNEXURE V.

5.2.2 Development of the transform model

The Snyder UH method was selected as the transform method considering the findings described in the literature review Section 2.5.3 and the description of parameters also

mentioned in the same section. The parameters used to calculate the lag time of each basin and the peaking coefficient are presented in Table 5-2.

Table 5-2: Calculation of lag time and the peaking coefficient for sub-basins

Sub Basin	Lc		L		C_t	C_p	Lag time T_p
	(km)	(mile)	(km)	(mile)			(hr)
S1	22.11	13.74	48.31	30.02	5	0.47	30.45
S2	24.32	15.11	43.39	26.96	5	0.47	30.34
S3	8.44	5.24	21.00	13.05	5	0.47	17.76
S4	6.33	3.93	22.52	13.99	5	0.47	16.64
S5	10.75	6.68	17.51	10.88	5	0.40	18.09
S6	6.45	4.01	21.22	13.19	5	0.40	16.44

5.2.3 Development of the baseflow model

The linear reservoir baseflow method was selected with two reservoirs for this study (as described in Section 2.5.4). The linear reservoir method involves three parameters for each groundwater (GW) component, namely: (1) GW initial, (2) GW fraction, and (3) GW coefficient. The initial condition was selected as “Discharge Per Area”. All model runs were started when having initial streamflow of around 20 m^3/s of Millakanda observed streamflow after no rainfall events continuously for a few days. The GW fraction was initially set as 0.5 for each component of GW1 fraction and GW2 fraction. The GW 1 represents the interflow portion of the streamflow which is the fast-responding component typically that leaves a watershed soon after a flood event. The GW 2 represents the base flow portion which is the slow responding component of the streamflow (or hydrograph) typically streamflow between the rainfall events is maintained by the base flow component. In most modelling applications the initial condition is selected where GW 2 component can be matched with the observed flow. The HEC HMS guideline tutorials recommend setting the GW 1 Coefficient 3 times larger than the Clark Storage Coefficient and the GW 2 Coefficient 10 times larger than the Clark Storage Coefficient. The basin storage coefficient (R) is an index of the temporary storage of precipitation excess in the

watershed because it drains to the outlet point. It, too, can be estimated via calibration if gaged precipitation and streamflow data are available. Though R has units of time, there is only a qualitative meaning for it in the physical sense. Clark (1945) indicated that R could be computed as the ratio between flow at the inflection point on the falling limb of the hydrograph and the time derivative of flow (USACE, 2000). Clark Storage Coefficient can be estimated by the Equation [5-1](Ponrajah, 1989).

$$\frac{R}{R+T_c} = 0.65 \quad [5\text{-}1]$$

In the above equation, T_c is the time of concentration, estimated according to Ponrajah (1989), which is more suitable for Sri Lankan catchments (Equation [5-2]).

$$T_c \text{ in minutes} = \frac{L}{V \times 60} + 15 \text{ mins.} \quad [5\text{-}2]$$

where L is the length of the longest stream in miles and V is the average velocity in ft/s according to the river slope derived from Ponrajah, (1984).

All parameters related to each sub-basins' baseflow are indicated in Table 5-3.

Table 5-3: Calculation of parameters of each sub basin for linear reservoir baseflow

Sub-Basin	L		10-85 flow path slope	Average V (Ponrajah, 1984)	T_c	R	GW1 Coeff.	GW2 Coeff.
	(km)	(mile)		(ft/s)	(hr)	(hr)	(hr)	(hr)
S1	48.31	30.02	0.0212	2.0	22.26	41.34	124.03	413.42
S2	43.39	26.96	0.0074	1.5	26.61	49.42	148.27	494.23
S3	21.00	13.05	0.0153	2.0	9.82	18.24	54.71	182.37
S4	22.52	13.99	0.0154	2.0	10.51	19.52	58.57	195.22
S5	17.51	10.88	0.0013	1.5	10.89	20.22	60.67	202.23
S6	21.22	13.19	0.0009	1.5	13.14	24.41	73.22	244.07

5.2.4 Development of the routing model

Muskingum routing method was used for this study based on the number of parameters, channel slope, flood plain storage, and channel geometry. Muskingum K is essentially the travel time through the reach, and it can be estimated by dividing the reach length by the average velocity of the river. The average velocity of the reaches

was taken according to published literature (Ponrajah, 1984). The sub-reaches were derived by dividing the K by simulation time step (24 hours). Estimated Muskingum routing parameters are listed in Table 5-4.

Table 5-4: Calculation of parameters for Muskingum routing model for each reach element

Reach	Reach Length	slope	Average Velocity		Muskingum K	Simulation time (Δt)	Number of Sub-Reaches
	(km)		(ft/s)	(km/hr)	(hr)	(hr)	(K/Δt)
R1	17.3	0.0108	2.0	2.2	7.9	24	0.33
R2	2.2	0.0032	1.5	1.6	1.4	24	0.06
R3	8.1	0.0009	1.5	1.6	4.9	24	0.20
R4	10.2	0.0007	1.5	1.6	6.2	24	0.26
R5	6.1	0.0008	1.5	1.6	3.7	24	0.15

The number of sub-reaches was taken as 1 for each reach element as it is the smallest possible value. The Muskingum X is the weighting between inflow and outflow influence, ranging from 0.0 up to 0.5. The value of 0.0 refers to the maximum attenuation, whereas 0.5 results in no attenuation. The model calibrations were started with 0.25 for each reach element.

5.2.5 Reservoir routing method

Kukule Ganga run-off-the river powerplant operations were also considered for this study as its operations would be critical during low flow periods. The reservoir element was introduced downstream of the Kukule Ganga sub-basin. Since the same hydrological model is used for future projections, the capacity discharge relationship was selected based on the normal operating procedures connected with the reservoir water level. Therefore, the outflow curve routing method, which requires elevation - storage – discharge relationship data, was selected as the routing method and the relevant as illustrated in Figure 5-4.

Storage – Discharge function and the Elevation – Storage function were fed into the model as paired data. Elevation-Area-Capacity data and other relevant data related to the Kukule Ganga power plant weir and turbine operations are listed in Table 5-5 and

Table 5-6. The data were collected from the Deputy General Manager (Samanala Complex) office, Ceylon Electricity Board in Ratnapura.

Table 5-5: Kukule Ganga run-off-the river powerplant data for the study

Data Type	Unit	Value
Full Supply Level (FSL)	m	206
Minimum Operating Level (MOL)	m	204
Weir bed level	m	197
Capacity at FSL	Mm^3	1.63
1,000 year return period flood	m^3/s	2,000
Maximum release for power generation	m^3/s	47.5
Environmental Flow release	m^3/s	0.5

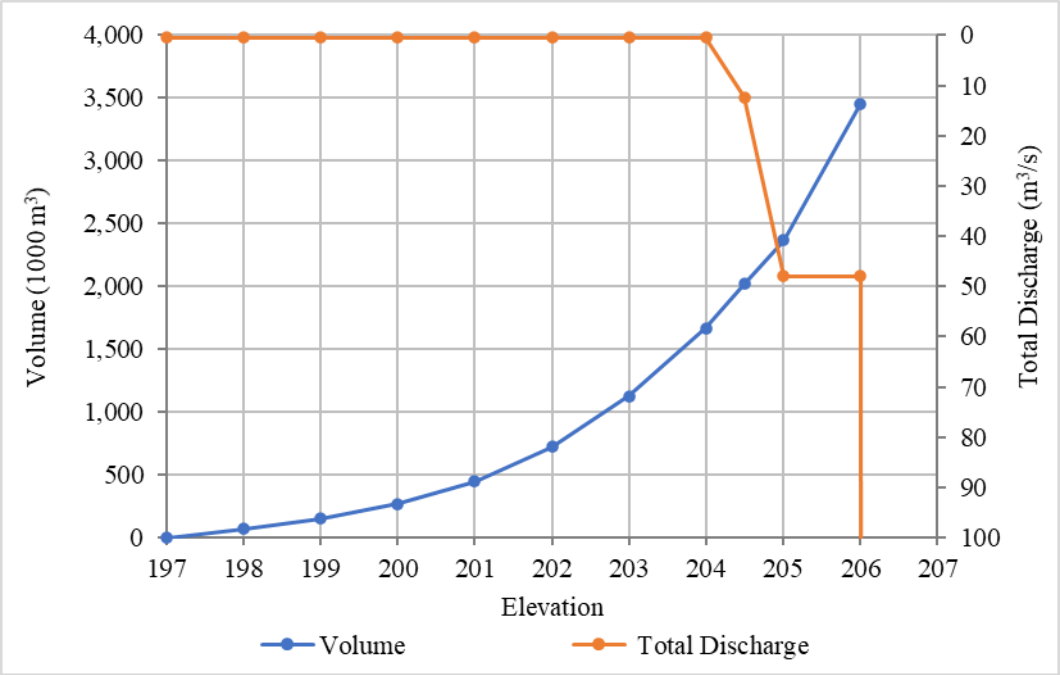

Figure 5-4: Elevation – capacity – discharge chart of Kukule Ganga weir

Table 5-6: Elevation - storage - discharge relationship data of Kukule Ganga run-off-the river powerplant

	Elevation	Volume	Discharge through turbines	Environmental release	Total Discharge
	(masl)	(1000 m^3)	(m^3/s)	(m^3/s)	(m^3/s)
HFL	206.1	3,467.0		0.5	2,000.00
FSL	206.0	3,458.0	47.500	0.5	48.00
	205.0	2,368.0	47.500	0.5	48.00
	204.5	2,021.0	11.875	0.5	12.38
MOL	204.0	1,666.0		0.5	0.50
	203.0	1,125.0		0.5	0.50
	202.0	724.0		0.5	0.50
	201.0	450.0		0.5	0.50
	200.0	267.0		0.5	0.50
	199.0	151.0		0.5	0.50
	198.0	68.0		0.5	0.50
Weir Bed Level	197.0	0.0		0.5	0.50

Until the reservoir level reaches 205 m elevation, the turbine runs at its full capacity, and they shut down when the water level reaches Minimum Operating Level (MOL). The environmental flow of 0.5 m^3/s releases downstream the weir location.

5.2.6 Precipitation model and time-series data

Precipitation is fed into each sub-basin by means of Thiessen average weights as gauge weights of selected rainfall stations. Evaporation data is fed as monthly averages. Thissen weights calculated for each sub-basin which were entered as gauge weight related to surrounding rainfall stations are listed in Table 5-7.

Table 5-7: Thissen weights calculated for each sub-basin for rainfall stations

Name of the sub-basin	Thiessen weights			
	Galatura Estate	Rakwana	Sirikandura	Usk Valley
S1		0.84		0.16
S2		0.07	0.20	0.73
S3				1.00
S4		0.31		0.69
S5				1.00
S6	0.08		0.48	0.45

Daily rainfall and discharge data are saved as DSS files using HEC DSSVue software and fed into the HEC HMS model. Time series data from 01/10/2004 to 31/09/2020 were saved in the DSS files. RCM precipitation data projected for the next design horizon period of the Koleimodara intake (2030-2060) also fed into the model as Thiessen rainfall of each sub-basin for both scenarios. Thissen weights of RCM grid points over each sub-basin are listed in Table 5-8.

Table 5-8: Thissen weights calculated for each sub-basin for RCM grid points

Name of the sub-basin	Thiessen weights			
	(260,141)	(261,141)	(260,140)	(261,140)
S1	0.02	0.44		0.55
S2	0.40	0.02	0.40	0.18
S3	0.81	0.16	0.03	
S4	1.00			
S5	1.00			
S6	1.00			

5.2.7 Control specification

Each model simulation requires a start and end date for the calibration and validation events, and these are entered and defined as different events under the control specifications.

5.2.8 Model simulation

Each calibration and validation run is defined under model simulation by selecting the relevant basin and meteorological models and control specifications.

5.3 HEC HMS Model Calibration

Since this study mainly focuses on the river discharge's low flow period, it was decided to calibrate the HEC HMS model with water cycles having longer dry periods. Hydrological model calibration period selected after 2005 as the Kukule Ganga run-off-the rivet powerplant came into operation without interruptions. Data after 2015 was not used due to the inconsistencies described in Section 4.2.4.

5.3.1 Event selection for model calibration and validation

Water cycles having longer deficit durations related to the probability exceedance flow of 90^{th} percent (Q_{90}) were selected as calibration and validation events during October/2005 to October/2015. The observed streamflow's seven-day moving average time series was used to obtain deficit durations to avoid dividing a lengthy deficit period into short time durations as described in Section 2.1.2. Figure 5-5 illustrates the number of flow deficit events and the durations in each water cycle of the study period.

Calibration and validation events always start with no rainfall events for more than three days and observed flow at Millakanda is around 20 m^3/s to match initial conditions. Details of the events selected for calibration and validation are listed in Table 5-9. Two events were selected for calibration, whereas validation was done concerning three selected events. Other than the event-based validation, the model was further validated for continuous simulation over 01/10/2005 to 31/09/2020 period.

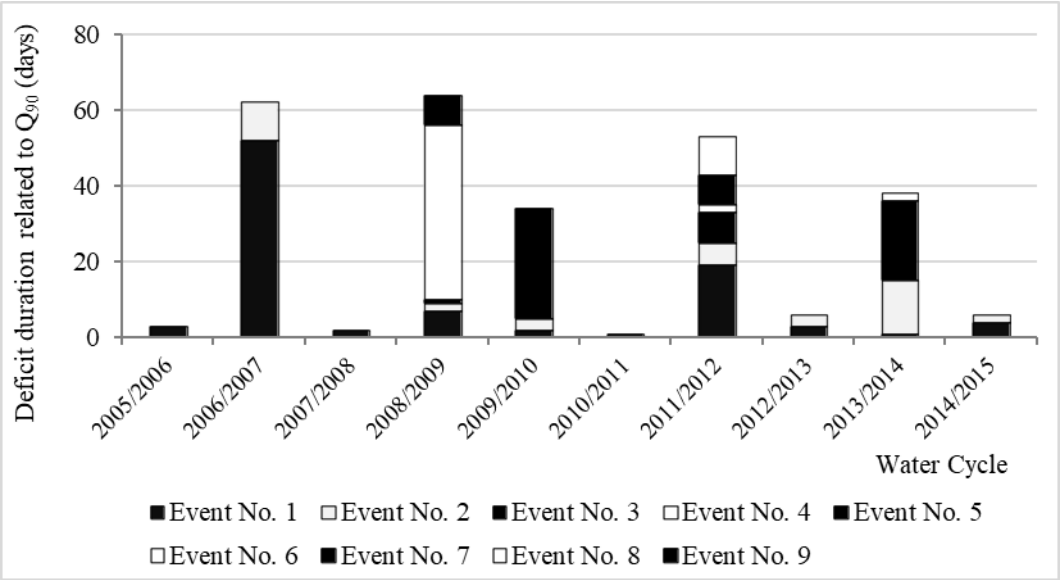

Figure 5-5: Number of dry spells and lengths relative to the probability exceedance flow of 90th percent (Q_{90})

Table 5-9: Details of the events selected for calibration and validation

	The water cycle period considered	Remarks on water cycle selection
Calibration	01/10/2006 – 30/09/2007	-
	10/05/2011 – 09/05/2012	Water cycle period shifted to avoid unrealistic high flow at the beginning of Jun 2012 which does not match with the RF and Kukule reservoir discharge pattern (Refer Figure I-7).
Validation	01/10/2008 – 30/09/2009	-
	14/09/2009 - 13/09/2010	Water cycle period shifted to avoid unrealistic high flow at the end of Sep 2010 which does not match with the RF and Kukule reservoir discharge pattern (Refer Figure 4-5).
	01/10/2013 – 30/09/2014	-

5.3.2 Finalized objective functions for the study

The MRAE is used as a primary metric objective function in this study. Many researches have used this indicator widely in hydrologic modelling of Sri Lankan river basins (Dissanayaka, 2017; Dissanayake, 2017; Herath & Wijesekera, 2021; Jayadeera & Wijesekera, 2019b; Perera & Wijesekera, 2011; Wijesekera & Abeynayake, 2003). This objective function is also suggested by the World Meteorological Organization (WMO, 1975). Additionally, NSE_{rel}, RMSE, and PBIAS objective functions were used to determine the model performances.

The NSE_{rel} proved to be a suitable objective function for low flow conditions even though with the disadvantages of low performance for peak-flow conditions and requirement of adjustment for data including zero flow observations (Althoff & Rodrigues, 2021; Krause et al., 2005b). Since this study emphasizes the low flow situations at the Koleimodara intake, and also there are no recorded zero streamflow records (and will not be in the future being a river basin in the wet zone) NSE_{rel} was selected as a fair, objective function for checking model performance (model Calibration and Validation) together with PBIAS and RMSE.

CHAPTER 6

6 RESULTS ANALYSIS

6.1 Model Calibration and Validation Results

The hydrological model was calibrated by matching the observed flow at Millakanda river gauging station data with the simulated flow at the junction Millakanda in the distributed model. The results of the parameters used to calibrate the model are listed in the

Table V-7 in ANNEXURE V. The calibrated model results are evaluated via flow duration curves, outflow hydrographs, and finally, the objective function for calibration and validation event and continuous model simulation validation. The monthly observed and simulated flow mass balance and dry spell lengths of 7-day moving average flow related to Q_{90} of the observed flow during 2005-2015 were evaluated in the ten-year continuous flow validation run.

6.1.1 Outflow hydrographs

Observed and simulated hydrographs for calibration (Figure 6-1 and Figure 6-2) and validation (Figure 6-3 and Figure 6-4) are illustrated in normal and semi-log scales. The hydrographs of continuous model simulation for the 2005 to 2010 period are presented in normal and semi-log scales (Figure 6-5).

The calibration hydrographs show that the model captures the high flow and low flow events (Figure 6-1 and Figure 6-2). The 2006/2007 water cycle possesses a longer dry period compared to the 2011/2012 water cycle. The simulated flow gets underestimated when the dry period gets longer and less in quantity as in the 2006/2007 and overestimated when the dry period is comparatively short as in 2011/2012.

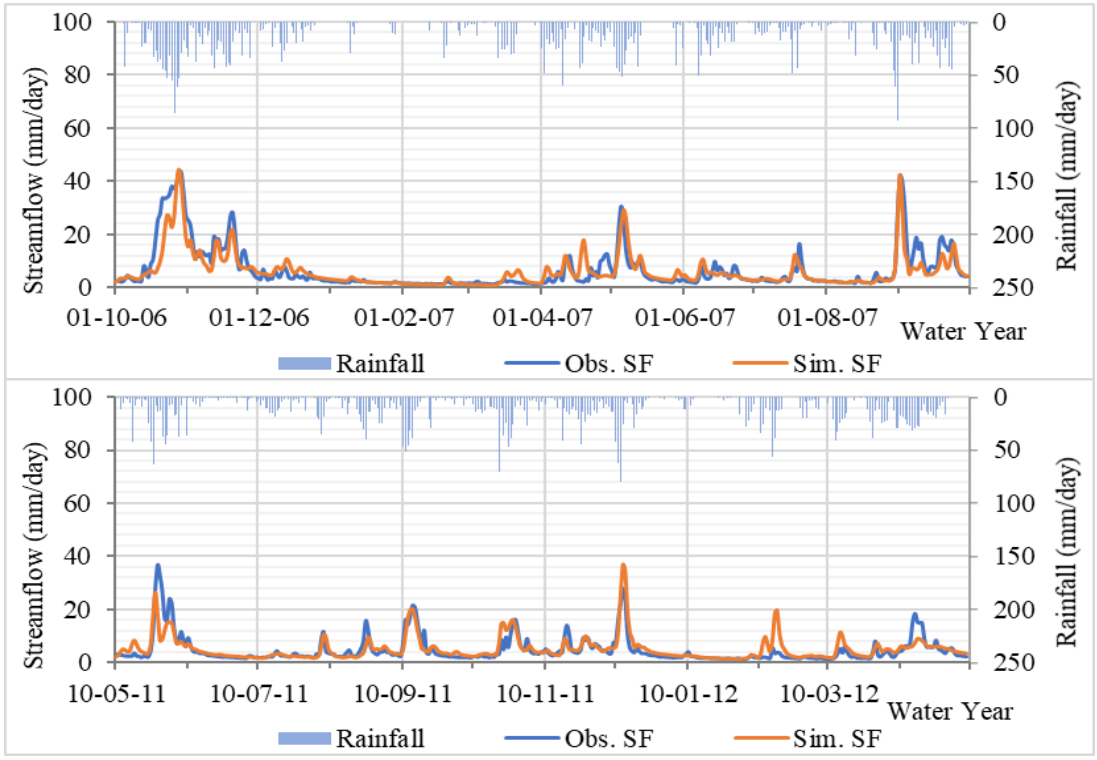

Figure 6-1: Hydrographs for the calibration events 2006/2007 and 2011/2012 water cycles

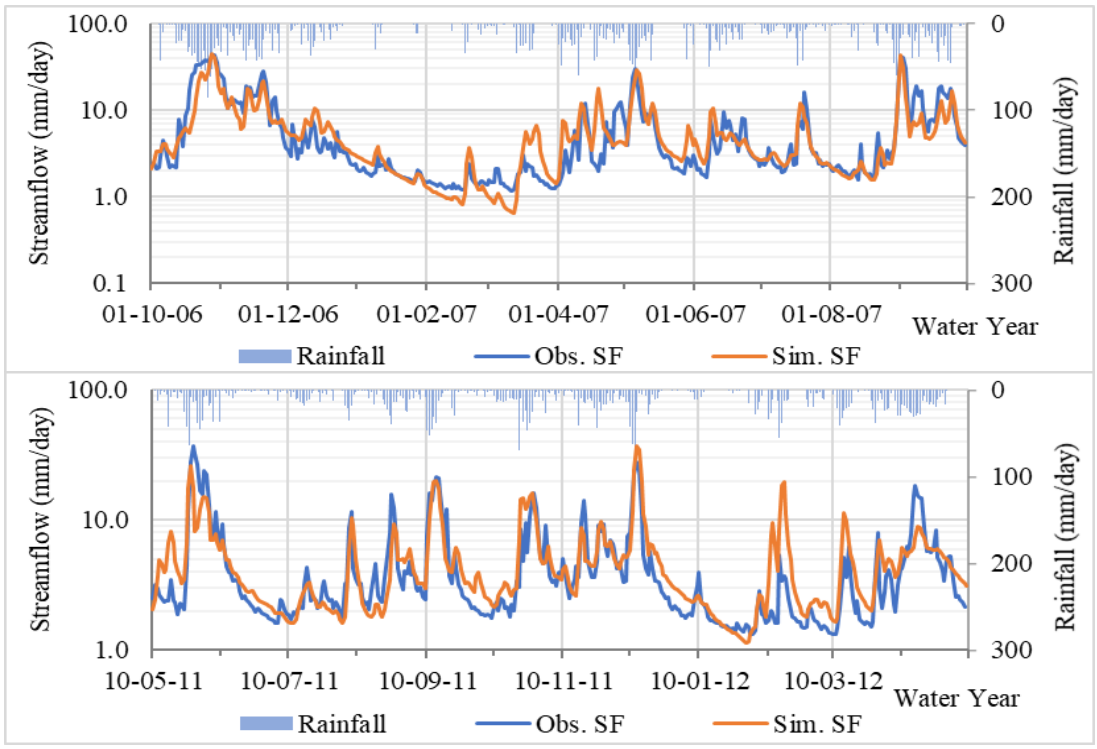

Figure 6-2: Hydrographs for the calibration events2006/2007 and 2011/2012 water cycles (semi-log scale)

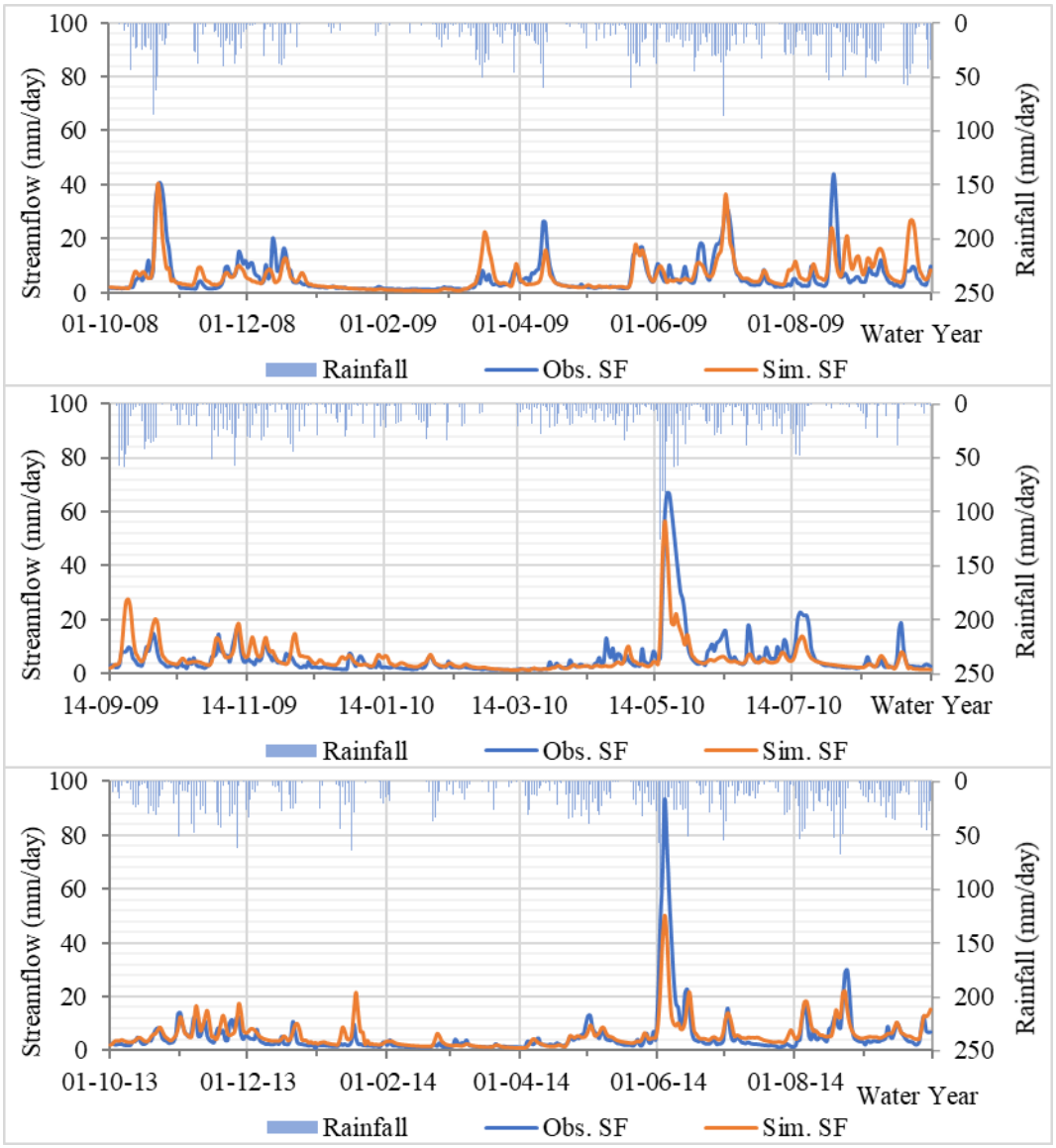

Figure 6-3: Hydrographs for the validation events 2008/2009, 2009/2010 and 2013/2014

The validation event also confirms that the model has the ability to capture the high flow and low flow events (Figure 6-3 and Figure 6-4). When considering the validation events, the longer dry period water cycle 2008/2009 simulated flow get underestimated. Over estimation of low flow can be observed in 2013/2014 water cycle and with the comparatively short span of low flow periods.

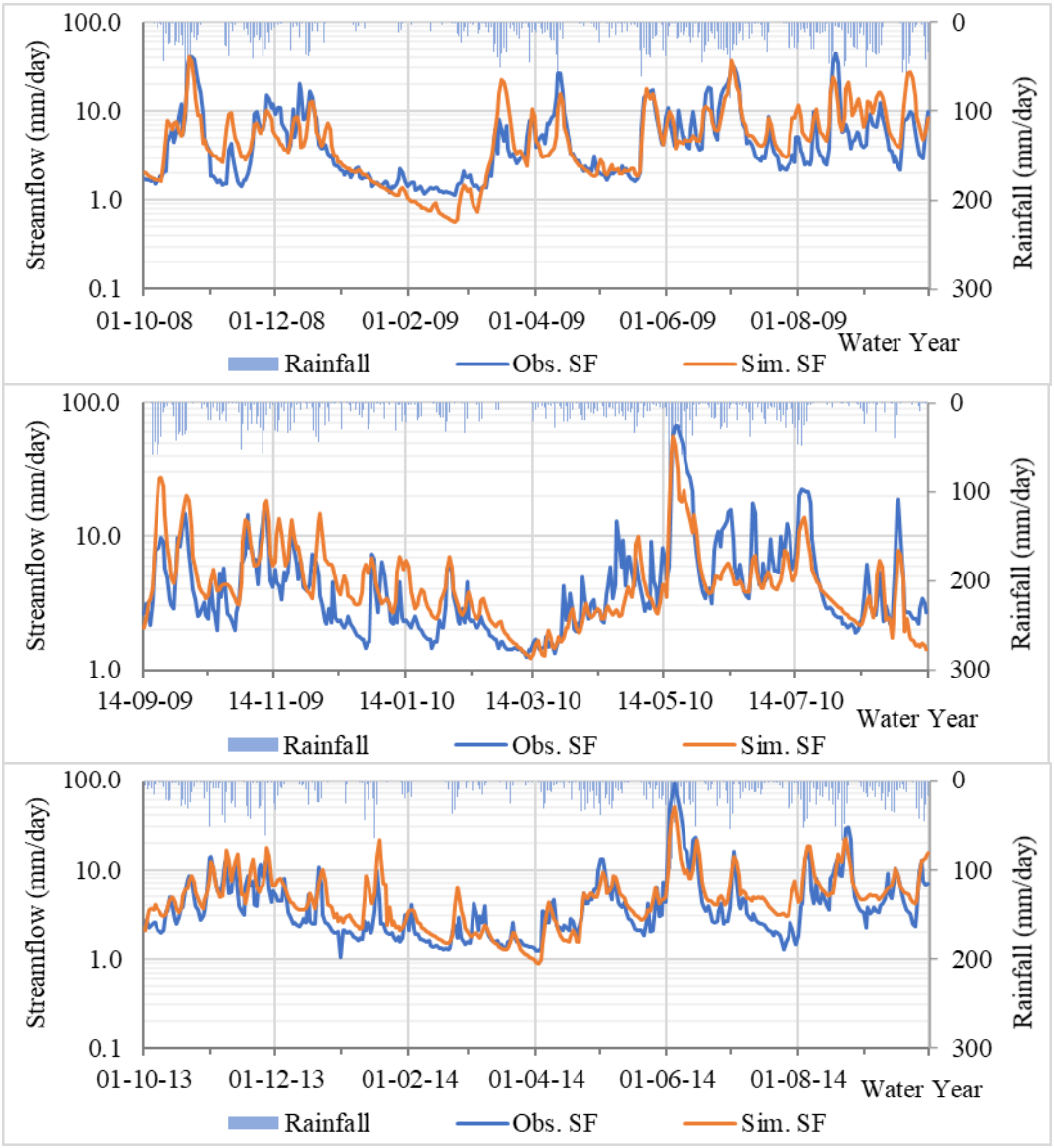

Figure 6-4: Hydrographs for the validation events 2008/2009, 2009/2010, and 2013/2014 water cycles (semi-log scale)

Continuous simulation hydrographs from October/2005 to September/2015 (10-years) also indicate that the model captures the low flow and high flow events considerably well except for the flood event on 02/06/2012 which does not comply with rainfall (Figure 6-5). The model underestimates the flood peaks as it is more emphasised for capturing low flow events.

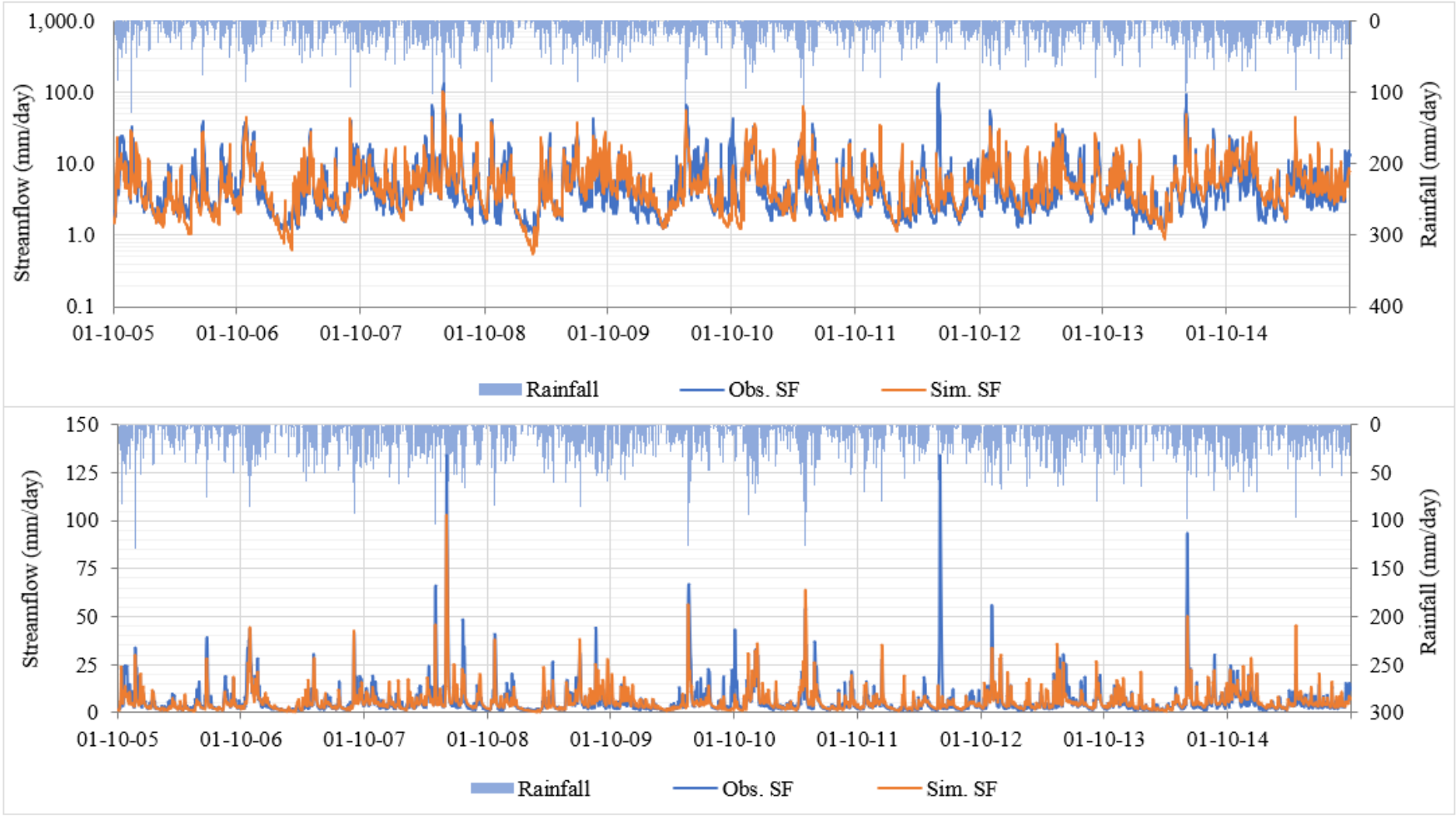

Figure 6-5: Hydrographs for the continuous model validation simulation 2005-2015 in normal and semi-log scale

6.1.2 Flow duration curves

Flow duration curves (FDC) were plotted for all calibration and validation events comparing observed FDC with the simulated flows on the same day. FDCs were plotted in both normal and semi-log scales and presented in Figure 6-6 for calibration and Figure 6-7 and Figure 6-8 for validation events.

When considering the calibration water cycles (Figure 6-6), it was observed that the model slightly underestimates the low flow below Q_{90} of the 2006/2007 flow duration curve, whereas model output slightly overestimates the low flows during 2011/2012. When trying to match the shorter low flow periods in the 2011/2012 water cycle, the 2006/2007 longer low flow period flows are further underestimated. The model underestimates the high flows and overestimates the intermediate flows according to the FDC.

The model's tendency of underestimation high flow and overestimation of intermediate flow can be observed in the validation events as well (Figure 6-7 and Figure 6-8). When considering the low flow region of FDC. Similarly, as in the calibration events the model underestimates low flow below Q_{90} in the 2008/2009 water cycle and overestimates in the water cycle 2009/2010 (from Q_{80} to Q_{95}) which has longer and comparatively shorter low flow periods respectively.

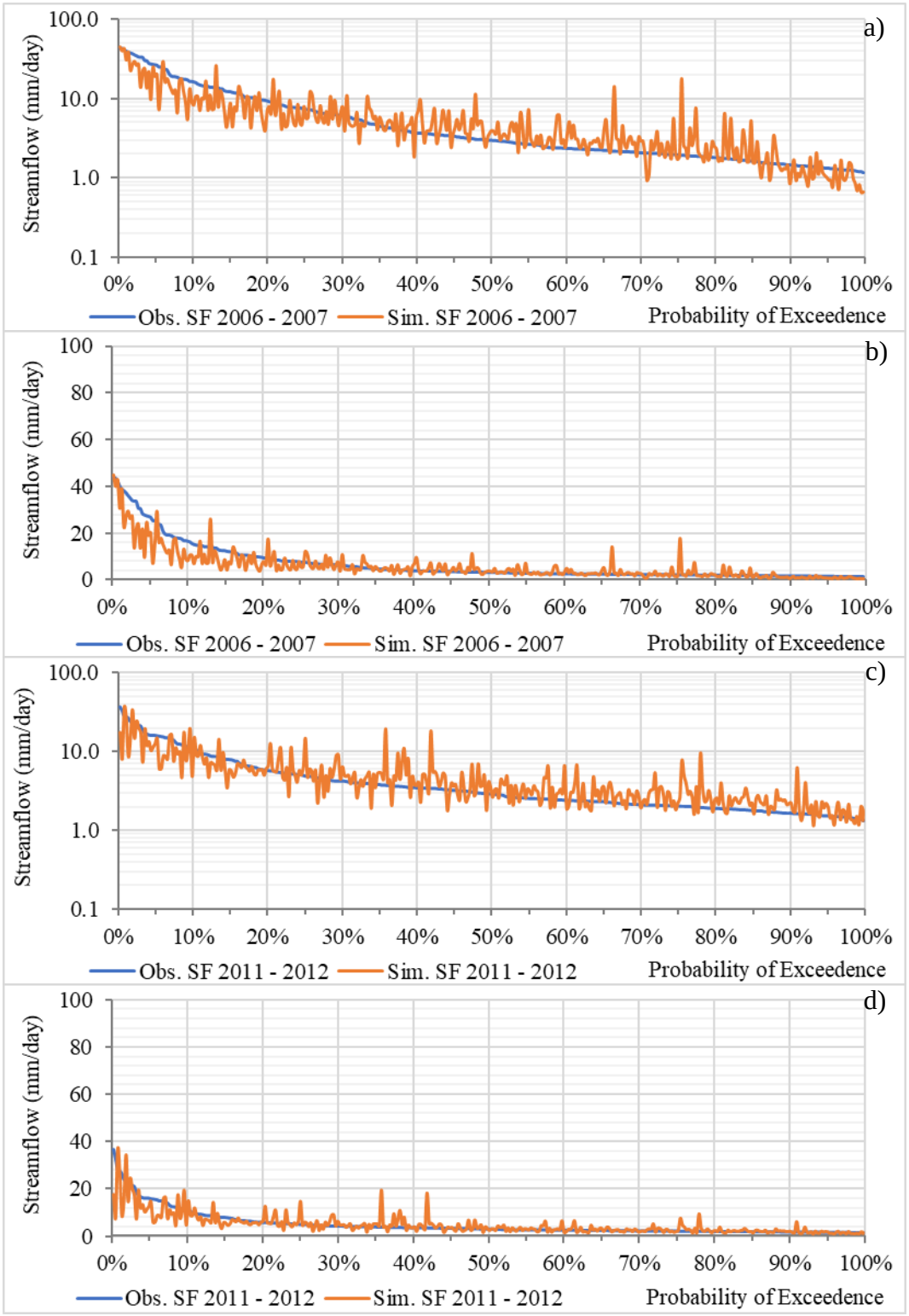

Figure 6-6: Flow duration curve for the calibration event water cycles; 2006/2007(a, b), 2011/2012 (c, d)

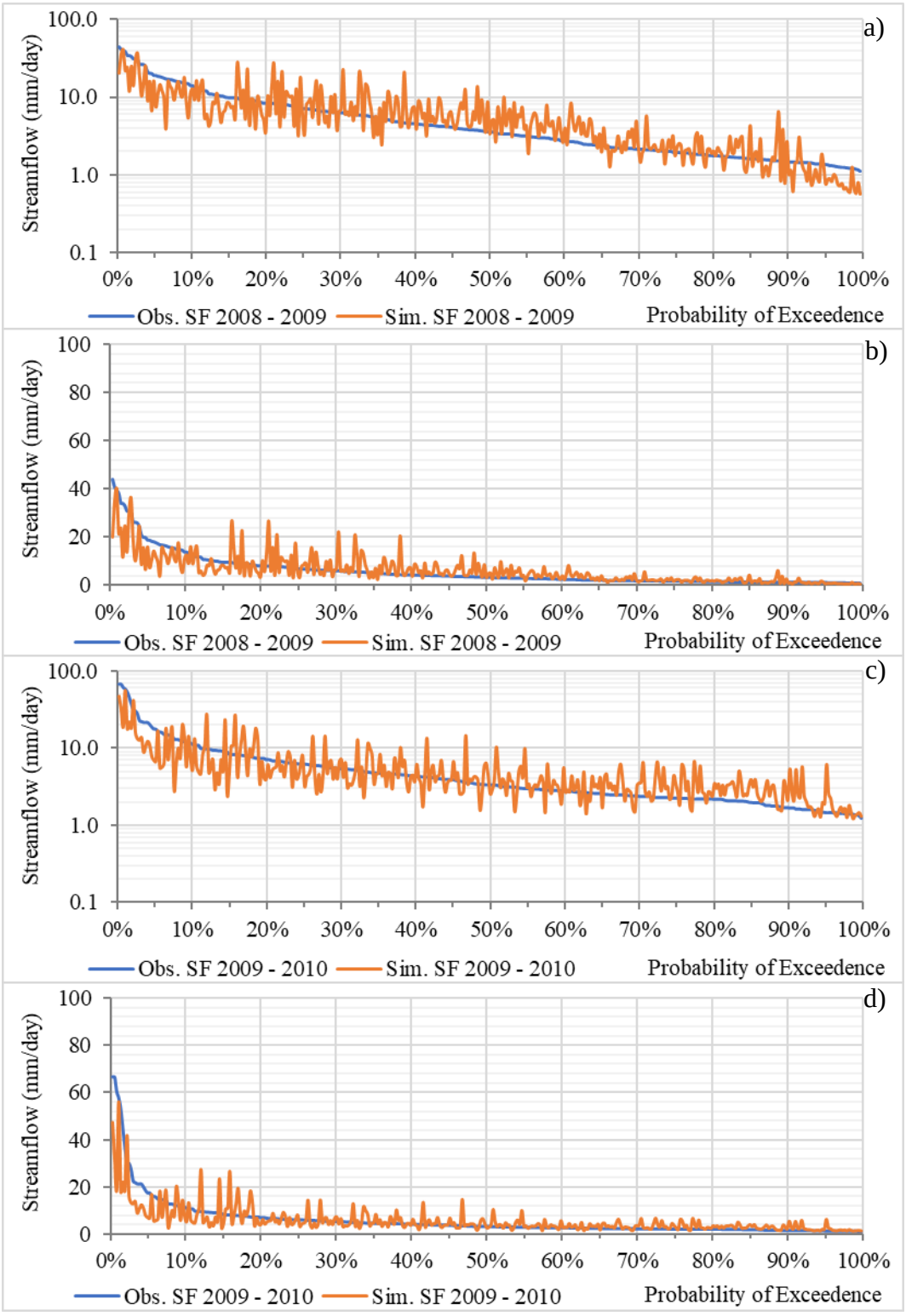

Figure 6-7: Flow duration curve for the validation event water cycles; 2008/2009 (a, b), 2009/2010 (c, d)

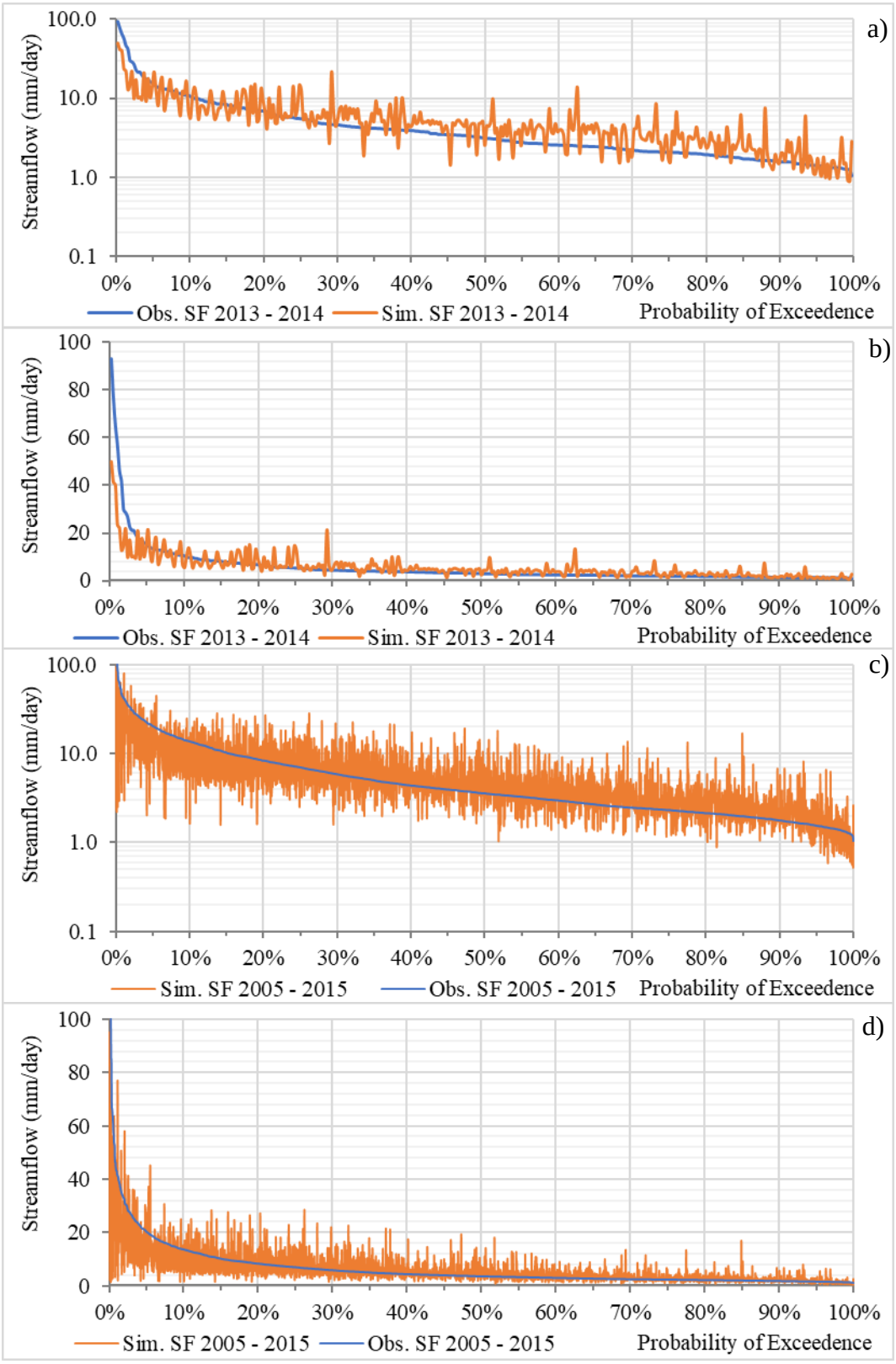

Figure 6-8: Flow duration curve for the validation event water cycle; 2013/2014 (a, b), continuous model run 2005 to 2015 (c, d)

6.1.3 Model performance

The model performance was evaluated with NSE_{rel}, MRAE, PBIAS, and RMSE for the complete calibration and verification periods. The results are presented in Table 6-1.

Table 6-1: Model performance of calibration and validation

	Period	NSE_{rel}	MRAE	PBIAS (%)	RMSE
Calibration	01/10/2006 – 30/09/2007	0.85	0.15	-8.63	34.5
	10/05/2011 – 09/05/2012	0.67	0.24	5.74	29.7
Validation	01/10/2008 – 30/09/2009	0.84	0.21	3.05	40.7
	14/09/2009 - 13/09/2010	0.77	0.20	-5.67	48.2
	01/10/2013 – 30/09/2014	0.74	0.35	5.09	46.3
Validation 10 years continuous simulation	01/10/2005 – 30/09/2015	0.81	0.20	-3.86	55.1

Continuous model performance from 01/10/2005 to 30/09/2015 was further evaluated based on the length of deficit duration and the number of deficit days related to the 90% probability exceedance value (Q_{90} = 15.8 m^3/s) of the same duration. This step has been followed to check the model performance to identify dry spells. The drought analysis threshold was taken as Q_{90} (as described in low flow deficit analysis in Section 2.1.2) of the continuous simulation period (2005-2015). The most prolonged deficit duration of the observed and the simulated drought events percentage errors were also evaluated. The relevant results are presented in Table 6-2.

Table 6-2: Summary of deficit durations of drought events during the period 2005-2015

Water cycles with drought events	Longest deficit duration (days)		
	Simulated flow	Observed flow	Difference
2006/2007	32	52	-20
2011/2012	17	20	-03
2008/2009	55	46	09
2009/2010	23	29	-06
2013/2014	23	21	02
		No of Deficit days	
	Simulated flow	Observed flow	% Bias
2005 –2015	257	272	-5.51

6.2 Assessment Future Projections of Precipitation of Kuda Ganga Basin

Future water extraction capacities of the Koleimodara intake were assessed based on the simulated runoff from the hydrological model from the bias-corrected precipitation projections from two RCP scenarios (RCP 2.6 and 8.5) of the NCC-NorESM1-M model (details described in Sections 4.5 and 4.6).

The standard precipitation index (SPI) was used to assess the historical, present, and future precipitation projection. One month SPI (SPI-1) was used for this study as it is possible to detect shorter drought periods within the month, which may not be detected by the longer time scale SPI. Also, a longer dry period with less rain followed by a high rainfall event (which is more likely to the situation of the study area) cannot be identified by a longer time scale SPI. The SPI-1 was calculated considering the Thiessen average rainfall of the Millakanda watershed from October 1992 to September 2020 (27 years). The Gamma probability distribution function was used to calculate SPI (Mckee et al., 1993). The futuristic SPI-1 was calculated using the same precipitation time series generated under RCP 2.6 and RCP 8.5 for 2030 to 2060 (30-years) using the Thiessen average precipitation of four grid points (as described under Section 4.5). The futuristic SPI-1 was calculated based on the rainfall distribution of the historical period (1993-2020) (i.e., the historical mean and standard deviation were based to calculate futuristic SPI-1) (Huang et al., 2016). This method has been followed by expecting to present a more comprehensive way, how far the deviation of the rainfall will move relative to the present situations. Variation of SPI-1 between 2030 and 2060 under RCP 2.6 and PCP 8.5 (relative to the historical base period) is illustrated in Figure 6-9 and Figure 6-10, respectively.

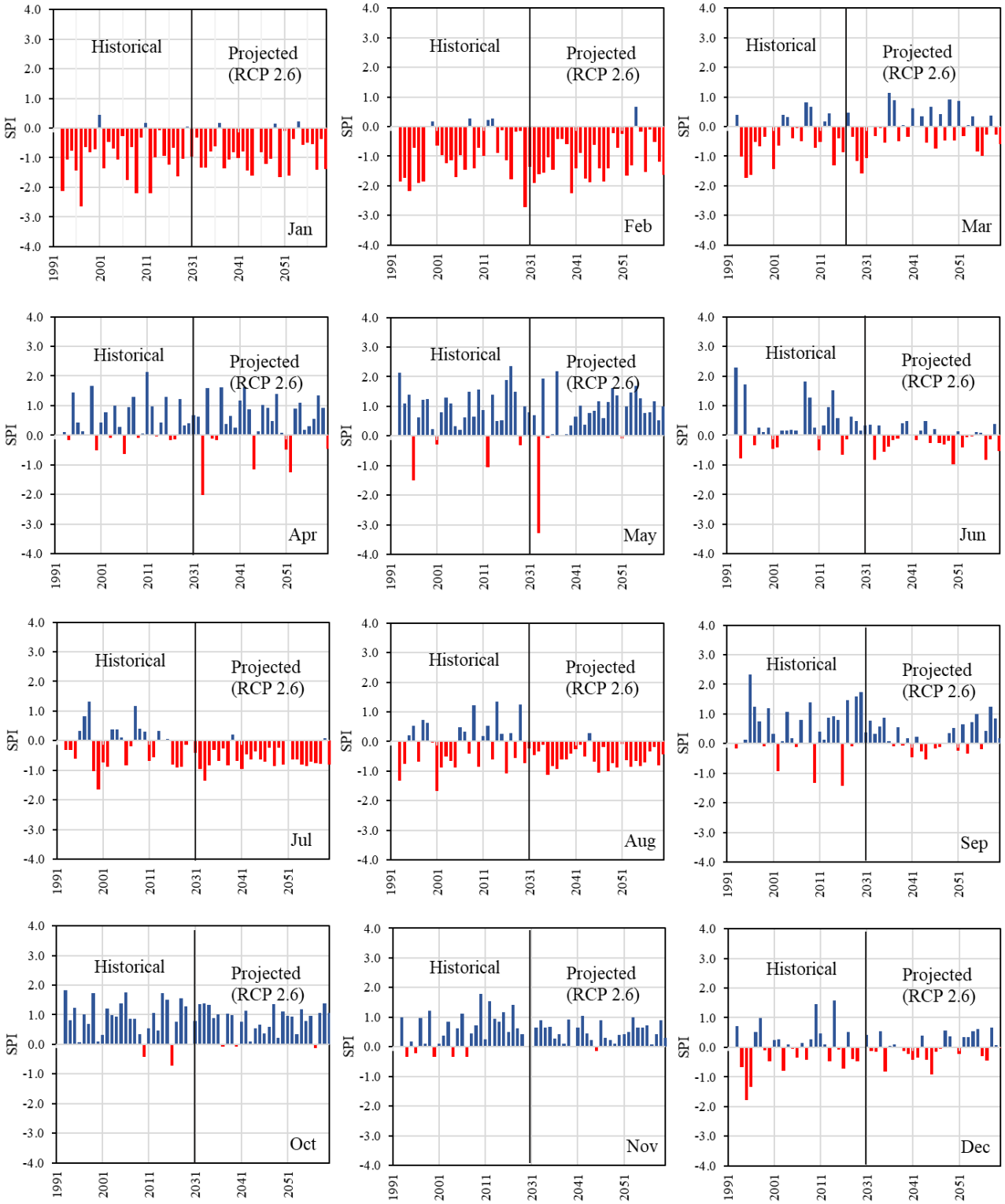

Figure 6-9: Monthly variation of SPI-1 until 2060 comparatively to the historical base period (1992 to 2020) under RCP 2.6 scenario.

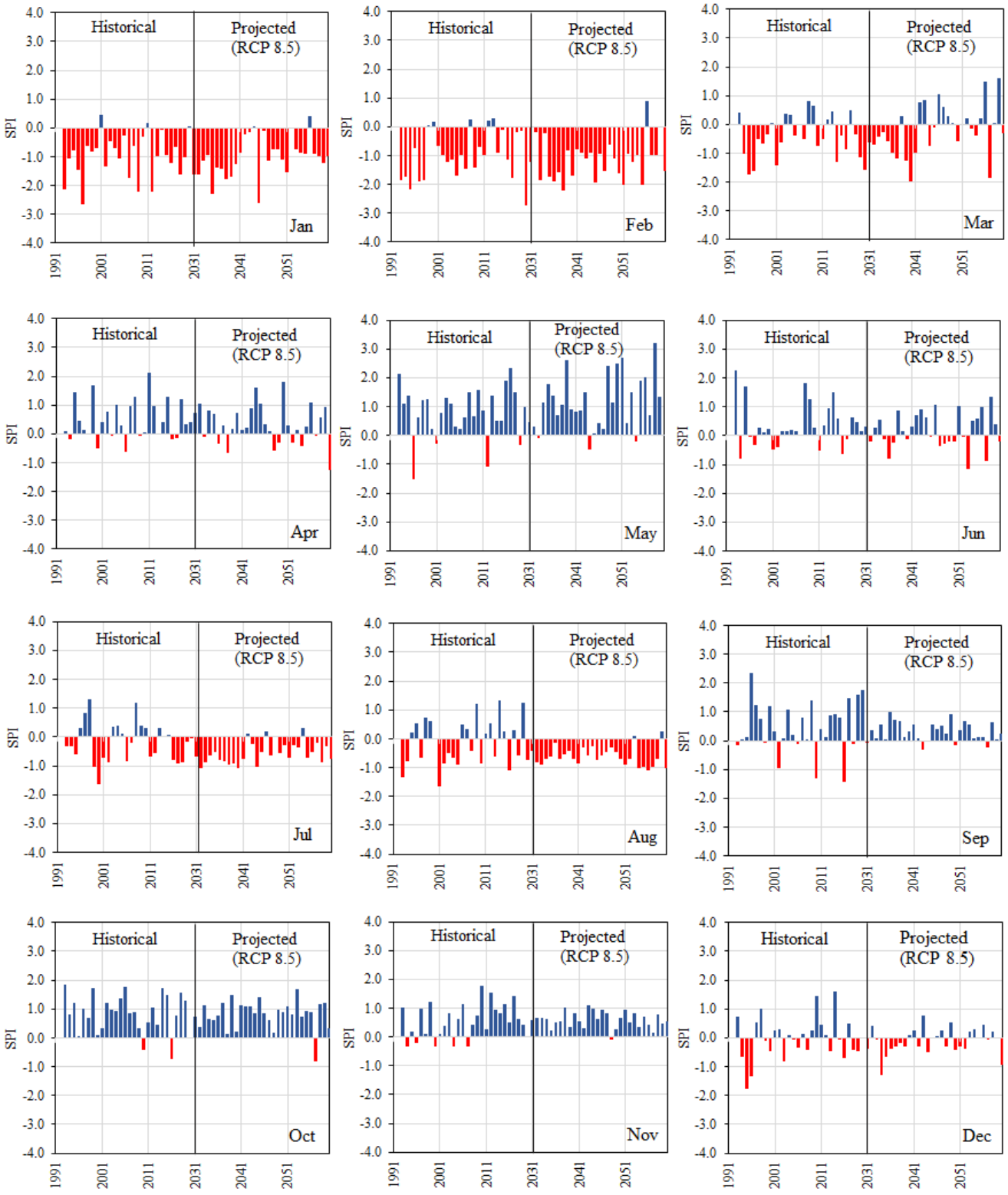

Figure 6-10: Monthly variation of SPI-1 until 2060 comparatively to the historical base period (1992 to 2020) under RCP 8.5 scenario.

6.3 Assessment of Future Projections of Streamflow at Koleimodara Intake

The hydrological model includes the operation of the Kukule Ganga powerplant, which came into operation consistently after 2004, and the hindcasted RCM data is available up to 2005. Therefore, the hydrological model could not run for historical bias-corrected precipitation data of the selected RCM model (NCC-NorESM1-M), which is a limitation of this research. Bias corrected projected precipitation data were used as the input to the HEC- HMS hydrological model to obtain simulated streamflow at Koleimodara intake for the next design horizon period of 2030 to 2060 (30-years) under two future scenarios, RCP 2.6 and 8.5.

Since the study's main objective is to assess and predict low flow conditions of the Kuda Ganga using projected climate change scenarios, several low flow indices (as mentioned in the following paragraph) were used to investigate the low flows. Low flow indices were calculated for simulated future streamflow projections under RCP 2.6 and 8.5. The relative differences of the low flow indices were analysed relative to the model simulations of the base period (i.e., from 2005 to 2020, 15 years). Since no RCM data is available for this period, the observed precipitation was used to simulate the base period's streamflow series.

The selected low flow indices are Q_{50} or the median discharge, and Q_{90} or the 90% exceeded discharge during the selected period, 7-day mean annual minima (MAM7), 30-day mean annual minima (MAM30), and Baseflow index (BFI). Those indices were used by Sapač et al. (2019) in their study to investigate low flow conditions concerning the climate change projections. Further the low flow deficit analysis parameters such as deficit duration, deficit volume or the severity, and intensity were also used.

6.3.1 Probability exceedance flow of 90th percent (Q_{90}) and 50th percent (Q_{50})

The probability of exceedance of low flow threshold Q_{90} and median flow (Q_{50}) during design period 2030 to 2060 were evaluated relative to the base period (2005-2020) under both projection scenarios. The analysis results are shown in Table 6-3 and Figure 6-11.

Table 6-3: Probability exceedance of flow indices Q_{90} and Q_{50} and variation relative to the base period 2005-2020 under RCP 2.6 and 8.5

	RCP 2.6		RCP 8.5	
Period of Time	Probability exceeding flow (m^3/s)	% Change	Probability exceeding flow (m^3/s)	% Change
Q_{90} - Base	15.8		15.8	
Q_{50} - Base	52.6		52.6	
Q_{90} - 2030's	10.2	-35.4	7.1	-55.1
Q_{90} - 2040's	12.7	-19.6	16.3	3.2
Q_{90} - 2050's	15.2	-3.8	14.7	-7.0
Q_{50} - 2030's	44.9	-14.6	44.9	-14.6
Q_{50} - 2040's	46.9	-10.8	52.3	-0.6
Q_{50} - 2050's	49.6	-5.7	50.5	-4.0

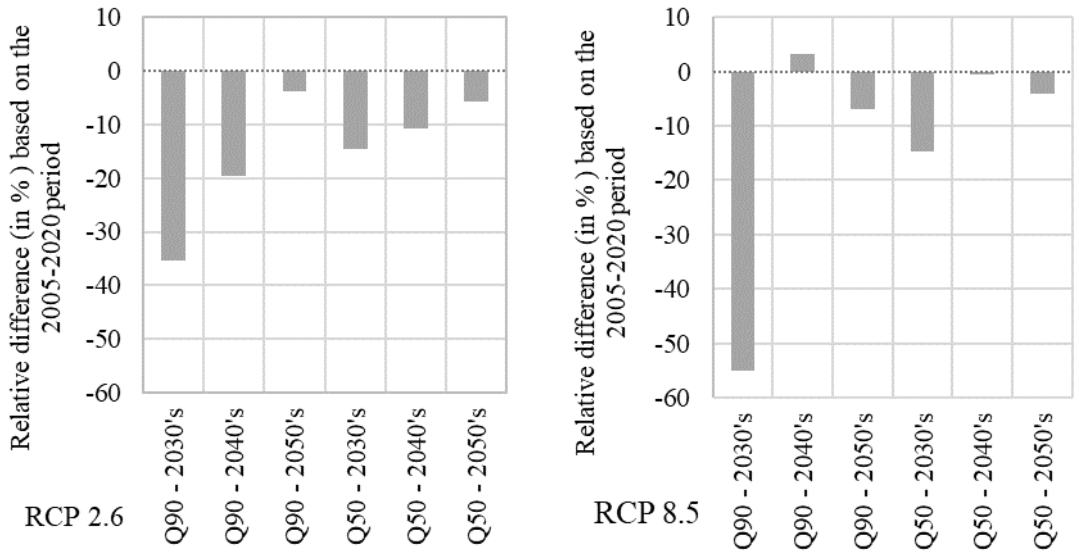

Figure 6-11: Variation of probability exceedance of flow indices Q_{90} and Q_{50} relative to the historical base period (2005 to 2020) under RCP 2.6 and 8.5 scenarios

6.3.2 Mean n-day annual minima (MAMn)

The MAMn values were obtained for each annual water cycle and four seasons (SWM, NEM, 1st IM, and 2nd IM) for the baseline period and for the 2030-2060 period under RCP 2.6 and 8.5. The MAM was calculated by taking the minimum of *n* day as a moving average. The minimum value is *n* day minima of that particular year. Seasonal minima of the same duration were also calculated to evaluate the seasonal variations. MAM1 is the mean annual minimum flow, which is not suitable for low-flow analysis because of possible measurement error or day-to-day variations (Smakhtin, (2001) and Bormann & Pinter, (2017)). Therefore, MAM7 and MAM30 were used for this study. The percentage-wise relative differences of these indices are illustrated in Figure 6-12 and the relevant data tables (Table VI-1to Table VI-4) are given in ANNEXURE VI.

6.3.3 Baseflow index (BFI)

The variation of BFI in the Koleimodara intake watershed was analysed for the projected streamflow under seasonal and annual scales. The Baseflow component of each sub-basin was obtained by the HEC HMS hydrological model simulation results, and the BSI was calculated according to equation [6-1]. The results of the BFI are presented in annexure tables Table VI-5 and Table VI-6 and Figure 6-13.

$$\mathrm{BFI} = \frac{Baseflow}{Streamflow} \qquad [6\text{-}1]$$

In this study, variation of BFI is only correlated with the change of precipitations because the modeling framework does not account for the other factors affecting the baseflow. Factors such as temperature, land-use change or vegetation, terrestrial water storage, potential evapotranspiration, and humidity index can influence baseflow and BFI (Tan et al., 2020). Even though the lithological, topographical, and basin factors like slope, soil, and aquifer characteristics do not change significantly under natural conditions, they can also influence baseflow and BFI.

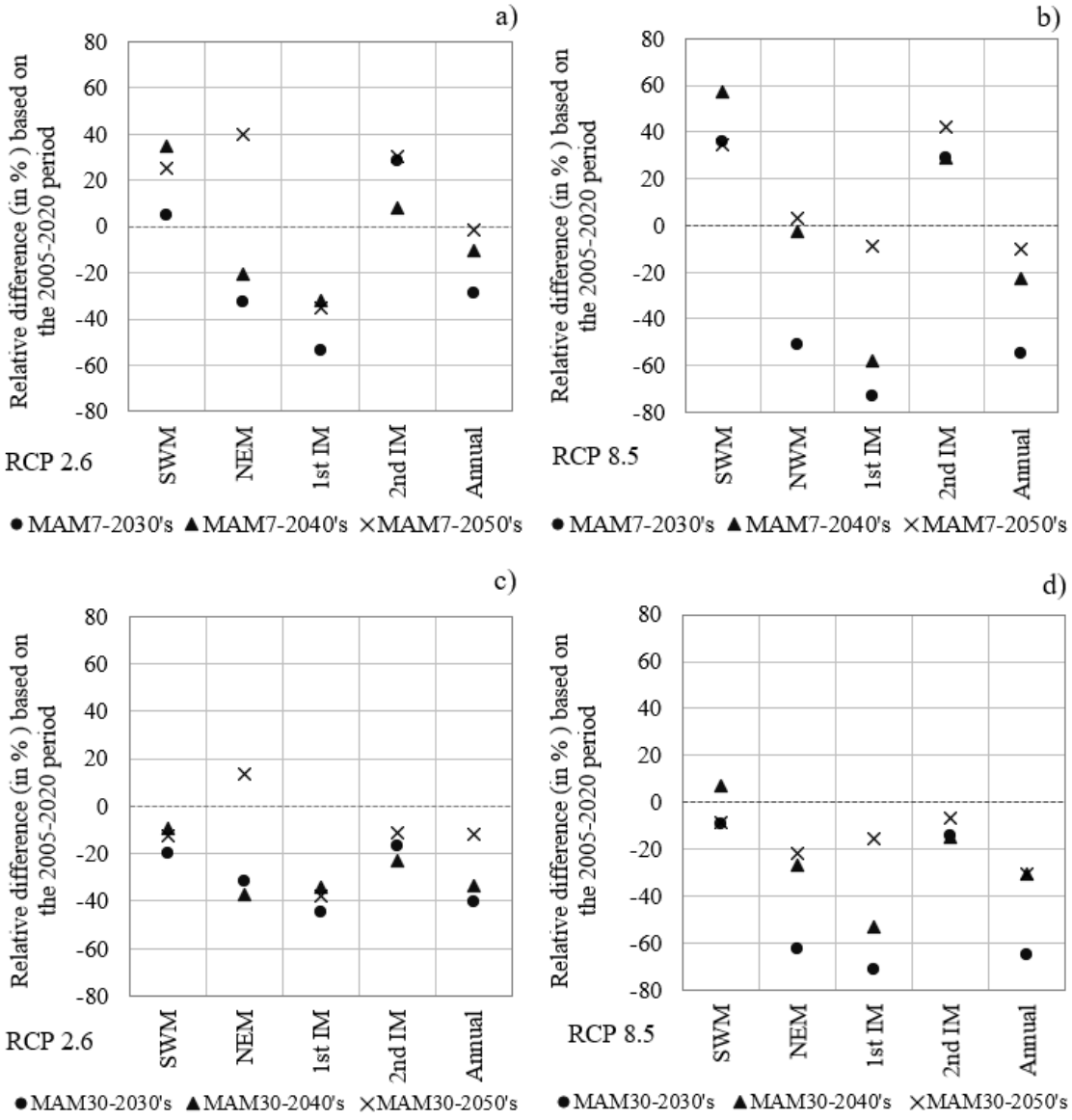

Figure 6-12: Percentage difference of MAM7 under RCP 2.6 and RCP 8.5 (a, b) and the MAM30 under RCP 2.6 and RCP 8.5 (c, d) relative to the base period 2005-2020

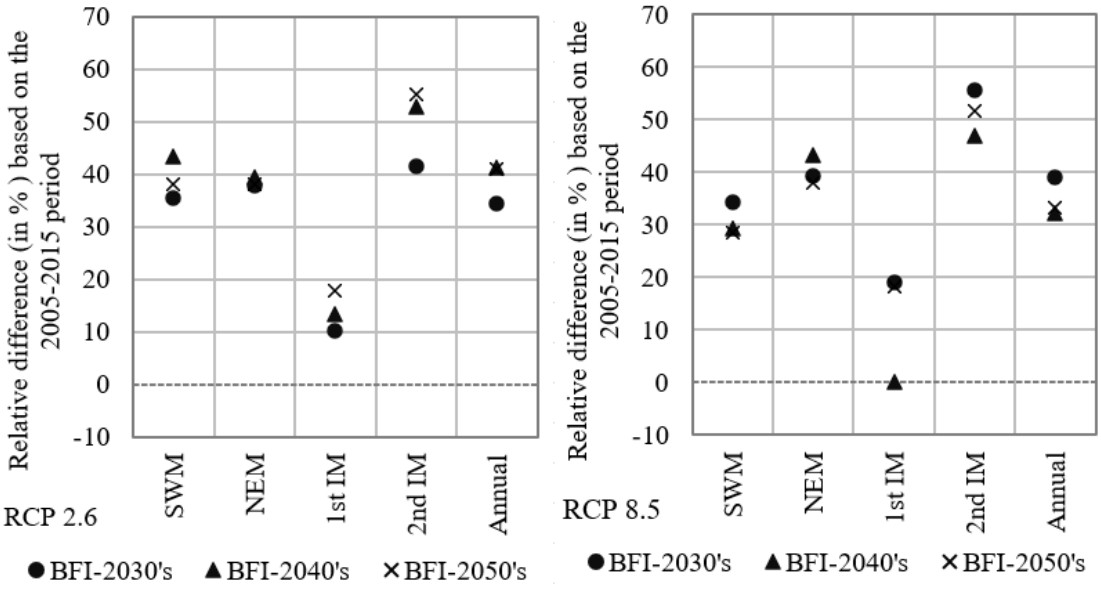

Figure 6-13: Average annual and seasonal baseflow index (BFI) variation and percentage change relative to the base period 2005-2015 under RCP 2.6 and 8.5

6.3.4 Continuous low flow and deficit volume

Continuous low flow and deficit volume analysis were performed to compare deficit duration, deficit volume or the severity, and intensity by taking the flow threshold as 3.0 m^3/s while accounting for water extraction and environmental flow requirement (as described in Section 4.3). When the flow is less than the low flow threshold value of 3 m^3/s, the deficit water volume per day to fulfil the water extraction of 1.5 m^3/s was estimated after allowing the rest of the flow as the environmental flow. Duration of deficit was taken as the number of days where the projected flow is less than the threshold of 3 m^3/s. The intensity was calculated by dividing the deficit volume by the duration. Deficit parameter calculations were performed for observed precipitation simulated flow series from 2005 to 2020 as the base historical period and for projected flow series under both RCP 2.6 and 8.5 scenarios. Analysis results are summarised in Table 6-4 and illustrated in Figure 6-14 and Figure 6-15.

Table 6-4: Calculation results of deficit duration, deficit volume, and intensity for water extraction of 1.5 m^3/s of the base period 2005-2020 and during the design period 2030-2060 under RCP 2.6 and 8.5 scenarios

Period	Nos	Year	Season	No of Deficit Days	Event Deficit Volume (1000 m^3)	Deficit Intensity (1000 m^3/day)
Historical (2005-2020)	1	2009	NEM	8	289	36
	2	2020	1st IM	8	54	7
RCP 2.6 (2030-2060)	1	2031	1st IM	10	289	29
	2	2031	1st IM	3	54	18
	3	2033	NEM/1st IM	12	453	38
	4	2033	1st IM/SWM	47	4,945	105
	5	2033	SWM	11	1,081	98
	6	2034	NEM/1st IM	15	970	65
	7	2040	NEM/1st IM	2	20	10
	8	2040	1st IM	5	247	49
	9	2043	NEM	5	138	28
	10	2044	NEM	7	233	33
	11	2052	NEM	4	59	15
	12	2060	NEM	6	80	13
RCP 8.5 (2030-2060)	1	2035	NEM/1st IM	42	4,409	105
	2	2036	NEM/1st IM	43	3,223	75
	3	2037	1st IM	25	2,021	81
	4	2038	NEM/1st IM	13	734	56
	5	2040	1st IM	35	3,234	92
	6	2045	NEM	18	1,440	80
	7	2051	NEM/1st IM	24	1,471	61
	8	2053	1st IM	1	1	1
	9	2057	1st IM	6	206	34

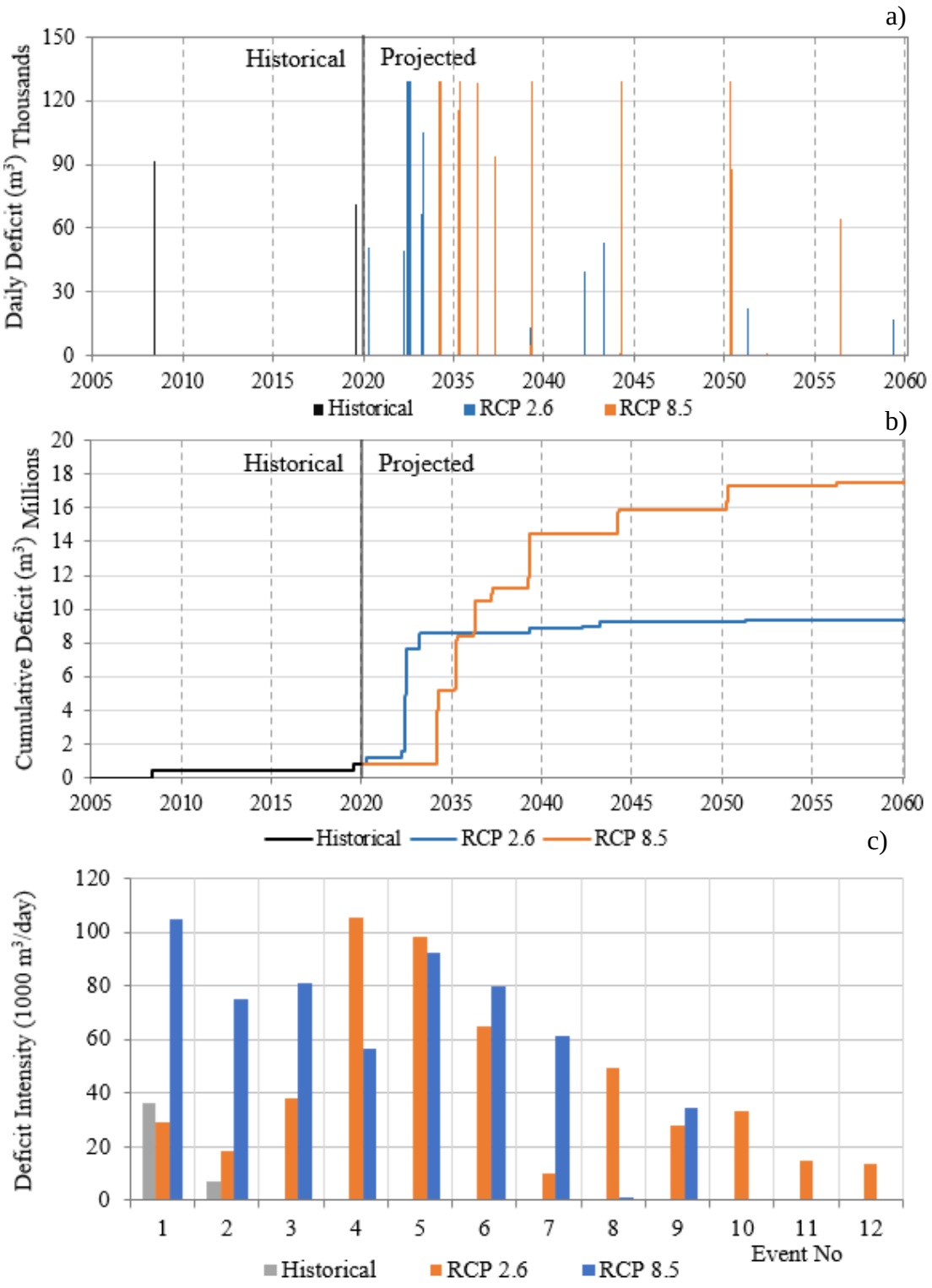

Figure 6-14: Variation of deficit characteristics; daily deficit (a), the cumulative deficit (b) over historical and projected time scales, and the deficit intensity of the events (c) for water extraction of 1.5 m^3/s during the base period 2005-2020 and the design period 2030-2060 under RCP 2.6 and 8.5 scenarios

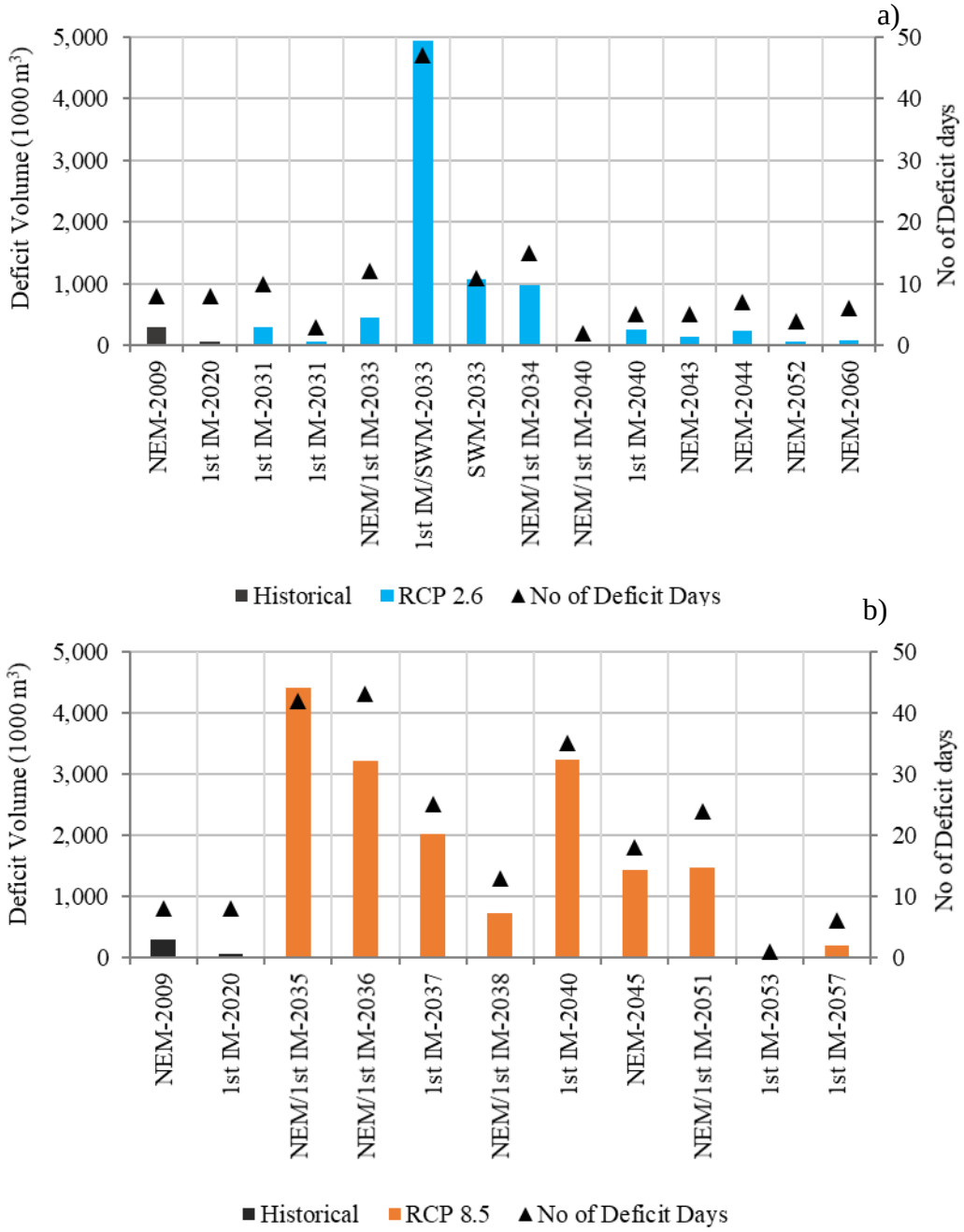

Figure 6-15: Deficit volume and the number of days of the events for water extraction of 1.5 m^3/s during the base period (2005-2020) and the design period 2030-2060 under RCP 2.6 (a) and RCP 8.5 (b) scenarios

CHAPTER 7

7 DISCUSSION

7.1 Selection of Data Period for Analysis

The starting period of the hydraulic model simulation was based on the operation of the Kukule Ganga run-off-the river power plant. Since this study mainly focuses on the river's low flow conditions, the powerplant's low flow discharges during those periods needed to be captured. Therefore, the data period of the water cycle starting from October 2005 to September 2015 was selected for model simulations. Since the observed streamflow data from 2015 to 2020 are unreliable (as described in Section 4.2.4), it was excluded from model calibration and validation. Model water cycle-wise calibration and validation events were also selected by avoiding the inconsistent rainfall and streamflow events as presented in Table 5-9.

7.2 HEC HMS Model Performance

7.2.1 Model performance in calibration

Two calibration water cycles were selected from the beginning and the end of the data period. Events were selected based on criteria related to the most prolonged deficit duration of the water cycles (as described in Section 5.3.1). The model was calibrated to achieve the optimum match between the observed and simulated low flow conditions while maintaining the water-mass balance at an acceptable level. As indicated in the Section 6.1.1 (referring to the hydrographs) and Section 6.1.2 (referring to the flow duration curves), underestimation and overestimation of low flow events occur in calibration events 2006/2007 and 2011/2012, respectively. When trying to match the shorter low flow periods in the 2011/2012 water cycle, the 2006/2007 longer low flow period flows are further underestimated. Therefore, calibration was carried out to balance the underestimation and overestimation of these

two events. Also, a minor variation between simulated and observed flows can be observed during the low flow beyond the 90th percentile (compared to intermediate and high flows) (Figure 6-6). The same result can be observed from separate FDCs of simulated and observed flows (Figure 7-1). When inspecting the hydrographs (Figure 6-1 and Figure 6-2), it can be seen that the underestimation of the low flow occurs when its duration is high (e.g., 2006/2006 water cycles). The model tends to overestimate the low flows when the relevant events are of a shorter duration.

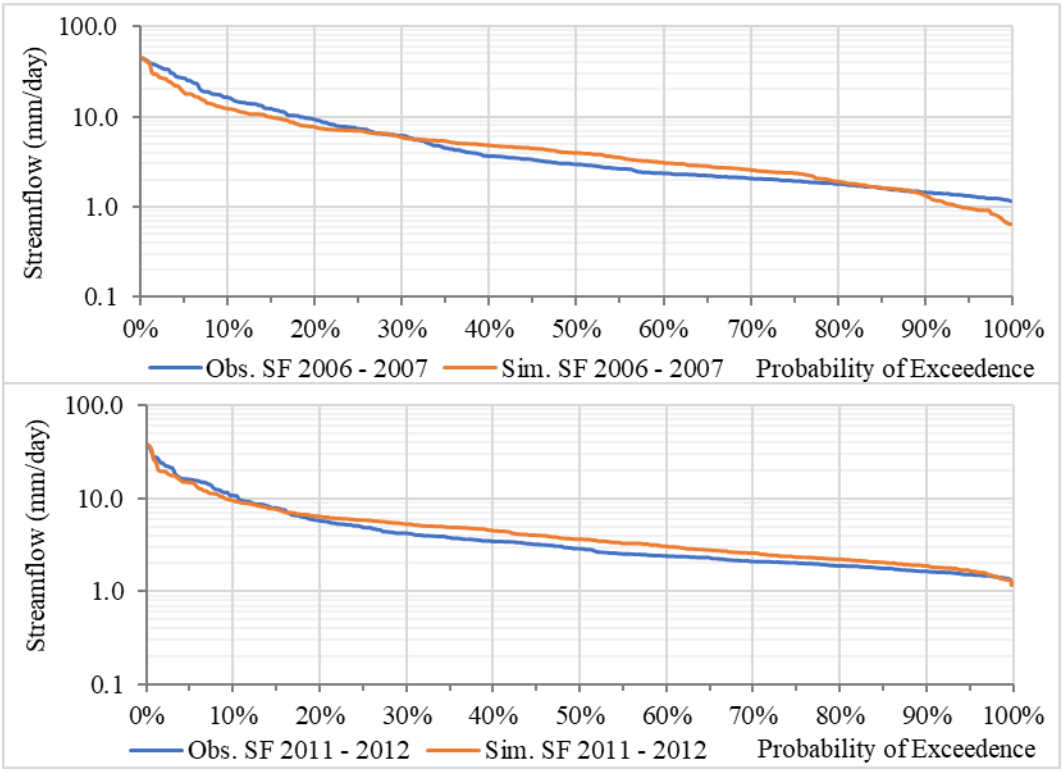

Figure 7-1: Flow duration curves for the calibration period

When comparing the objective function results, out of all the calibration and validation events, the highest NSE_{rel} (0.85) and the lowest MRAE (0.15) has occurred in 2006/2007 (Table 6-1). That is explained by the good agreement between Q_{78} (16.7 m^3/s) and Q_{90} (13.1 m^3/s) low flows observed during the same period. The highest PBIAS (-8.63%) has occurred in 2006/2007 may be due to the model underestimating the more extended high flow event during October and November in 2006. Out of the two calibration events, the lowest PBIAS (-5.74%) and RMSE (29.7) has occurred in the 2011/2012 water cycle (Table 6-1). Nevertheless, the NSE_{rel} value (0.67) is the

lowest of all the calibration and validation events, possibly due to the overestimation of the low flows.

7.2.2 Model performance during validations

Three water cycles with more extended dry periods (2008/2009, 2009/2010 and 2013/2014) were selected for the event-wise water cycle validation (Table 5-9). The 2008/2009 water cycle underestimated the low flow below Q_{90} (13.1 m^3/s), possibly due to the prolonged dry period similar to the 2006/2007 event. The 2008/2009 event shows good results in performance indicators such as 0.84 in NSE_{rel}, 0.21 in MRAE, 3.05% in PBIAS (which is the lowest of all calibration and validation events), and 40.7 in RMSE. Those results may have occurred because the simulated low flows between Q_{70} (19.1 m^3/s) to Q_{90} (13.1 m^3/s) show minimal variations (compared to the observed streamflow). According to the flow duration and hydrograph of the 2009/2010 water cycle, the model slightly overestimates the low flow from Q_{80} to Q_{95} (Figure 6-7). However, according to simulated and observed sorted FDC in Figure 7-2, low flows beyond Q_{90} (13.3-10.8 m^3/s) show a good match with the observed streamflow. The performance indicators of the 2009/2010 event are 0.77 in NSE_{rel}, 0.20 in MRAE, -5.67% in PBIAS, and 48.2 in RMSE. The higher value in RMSE may be due to the overestimation of short-duration low flow events as illustrated in hydrographs (Figure 6-3, Figure 6-4). The 2013/2014 water cycle shows the best performance indicator results as 0.74 in NSE_{rel}, 0.35 in MRAE, 5.09% in PBIAS, and 46.3 in RMSE. This water cycle has the highest MRAE of all five events, possibly because the model could not match the high flood event in June 2014.

Besides the event-wise validation, model performance throughout the continuous period of 01/10/2005 to 31/09/2015 (ten-year period) was also used to verify its performances. The continuous simulation also indicated better results in performance as 0.81 in NSE_{rel}, 0.20 in MRAE, -3.86% in PBIAS, and 55.1 in RMSE. Hydrographs of the continuous model simulations (Figure 6-5) show that the model identifies the peaks and low flow depressions of the observed flow well, although it underestimates the low flows during prolonged dry periods. Even though the model could identify the

flood events, it could not match the peaks as the calibration was focused on matching the low flow conditions.

Further, the model performance of the continuous stimulation was evaluated for low flow assessment by comparing the most prolonged deficit durations of drought events by taking 7-day moving average flow and Q_{90} of observed flow during 2005-2015 as the threshold. According to the results presented in Table 6-2, 2006/2007 and 2008/2009 water cycles have the most prolonged drought events. The 2006/2007 event underestimated the deficit duration (32 and 52 days for the simulated and observed flows, respectively), whereas the 2008/2009 event overestimated with 55 and 46 days respectively for the simulated and observed flows. Other events show good agreement between simulated and observed events with three, six, and two days differences during 2011/2012, 2009/2010, and 2013/2014, respectively. Further, the number of deficit days comparison shows less bias (-5.51%) with respect to the observed flow when comparing the total data period (Table 6-2).

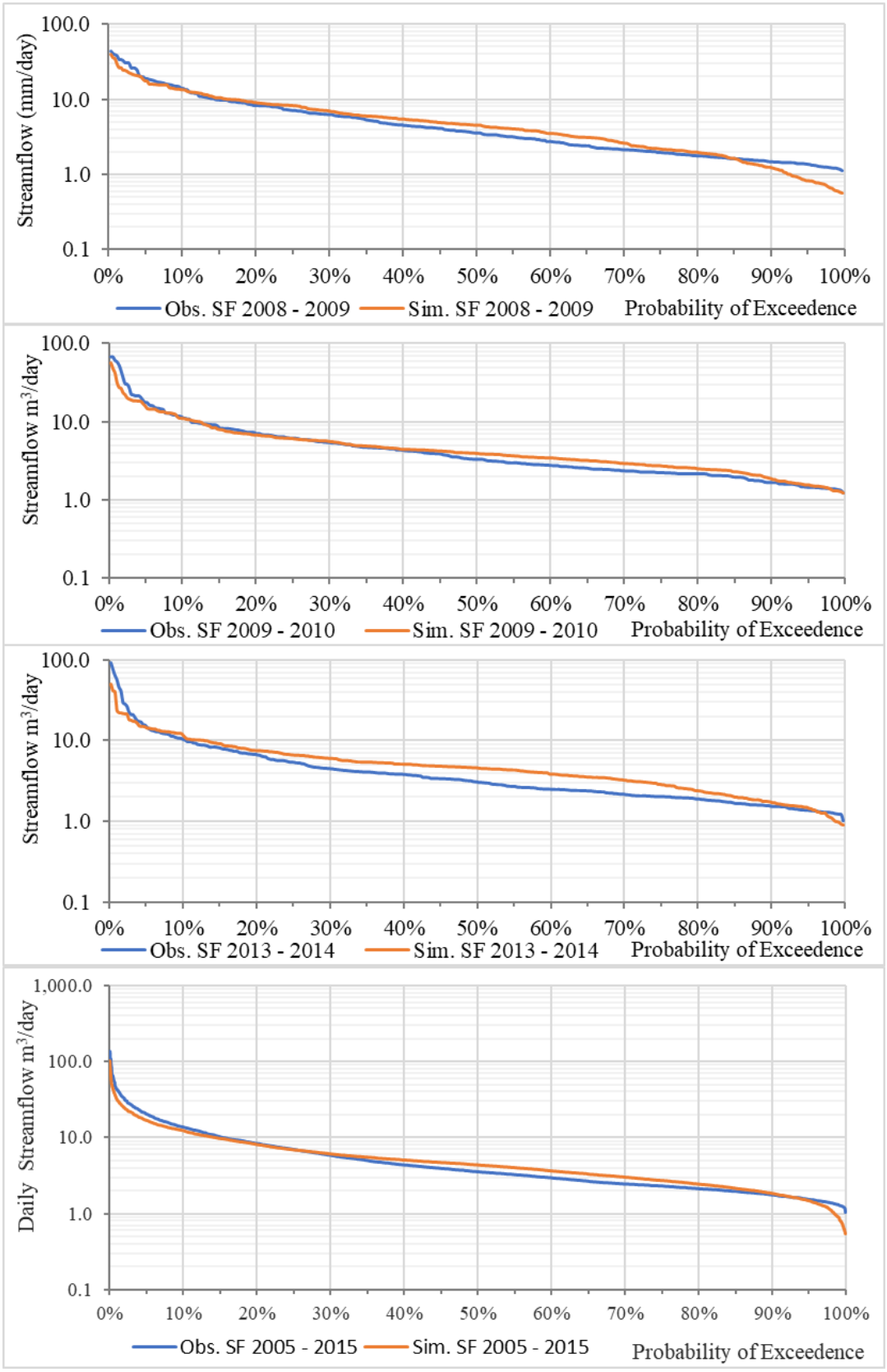

Figure 7-2: Flow duration curves for the validation period

7.3 Future Projections of Precipitation

7.3.1 Evaluation of bias-corrected precipitation

Future precipitation was derived from NCC-NorESM1-M model projections based on the ICTP-RegCM4-7 (as described in Sections 4.2.3) and bias-corrected with the mean-based method (as described in Sections 2.7 and 4.5). Bias-corrected hindcasted precipitation data was compared with the observed precipitation as Thiessen average rainfall for Millakanda watershed by considering 2001-2005 as an evaluation period. According to the monthly and seasonal means (Table 4-11), November, December, February, March, and September contain less than ±10 % biases compared to the observed precipitation. Out of the low flow months, January and August contain -30.1% and 54% biases, respectively. When considering seasonal-wise result SWM, NEM, 1st IM and 2nd IM contain 5.1%, -11%, -14.7%, and -3.2% biases, respectively.

Bias-corrected historical data were further analysed with dry spell characteristics of (i) Average dry spell length over a 30-year data period (1976-2005), (ii) Max dry spell length, (iii) The standard deviation of dry spell length, (iv) 90th percentile dry spell length, (v) 95th percentile dry spell length, and (vi) 99th percentile dry spell length (Figure 4-13) (definitions of the dry spell characteristics are described in Section 4.6.1).

February and October show an overestimation of dry spell signatures under all indices. February and October overestimated the average dry spell length by six days and four days respectively. The average dry spell length of all the other months shows a reasonably good correlation with observed data (two days difference in September and within ±one days or none in other months). The maximum dry spell length of February, March, and October is overestimated by 18, 13, and 39 (the maximum value) days, respectively, while July, September, and November are underestimated by 16, 15, and 14 (the minimum value) days. The standard deviation of dry spell length of February (+six days) and October (+five days) shows higher variation and +one to -three days variation in the other months. All the months show minor deviations over 90th percentile dry spell length except for February and October, with 11- and 9-days overestimations, respectively, and a 7-day underestimation in September (± three days

variation in other months). A similar deviation was observed in the other two indices (i.e., 95th and 99th percentile dry spell lengths) with a -9 to +16-day difference and -13 to +25-day difference.

7.3.2 Evaluation of future climate projections of precipitation

Future climate projections were evaluated based on the projection scenarios (as described in Section 4.7) over the next design horizon of the Koleimodara intake (30 years from 2030 to 2060). The average annual rainfall of the base period (1976-2005) is 3,657 mm, which is projected to increase by 4.5 % (3,820 mm) and by 9.2 % (3,992 mm) under RCP 2.6 and RCP 8.5, respectively. When comparing the monthly plots (Figure 4-14), projected monthly rainfall tends to increase under RCP 8.5 (by 0.01 % to 33.5% (in May) relative to the base period) during all months except October, February, April, July, and August (decreased by 1.4% to 6.7% relative to base period). Except for October, February, April, June, and July, projected monthly rainfall may also increase under RCP 2.6 (by 1.7% to 20.9% relative to the base period).

When comparing decade-wise precipitation projections under both scenarios (Figure 4-15 and Figure 4-16) the first decade of the design period (2030-2040) may become drier except for the months May, June, August, September, and November (by -39.4% to -1.7%) under RCP 8.5 and during the months of February, May and July (by -21.6% to -7.3%) under RCP 2.6, compared to the base period (1976 to 2005). During the other two decades, precipitation is projected to be increasing. During the 2040-2050 decade the monthly precipitation is projected as increasing during all the months even greater than the base period (by 2.9% to 34.4%) except for February under RCP 8.5 while under the RCP 2.6 shows mix variation (by -19.5% to 27.3%) compared to the base period. During the final decade of the design period, the monthly mean precipitation relative to the base period varies between -13.0% to 55.2% and -9.8% to 30.6% under RCP 8.5 and 2.6, respectively.

7.3.3 Standardized Precipitation Index (SPI)

One-month Standardized Precipitation Index (SPI-1) was used to analyse the projected precipitation variations and drought conditions. Figure 6-9 and

Figure 6-10 illustrate the monthly-wise SPI-1 variation during the base and design periods (2030-2060). Observed precipitation from 1991 to 2020 (30-years) was considered as the baseline precipitation. Analysis revealed that under RCP 2.6, June, July, and August months would become drier towards the end of the design period, while the prevailing dry conditions projected to continue in January and February.

Under RCP 8.5, July and August are likely to become drier towards the end of the design period. Even though September does not seem to be a dry month, precipitation may reduce (SPI-1 becomes less than one) compared to the baseline period (during which SPI-1 increased beyond one in eight years). Further, prevailing dry conditions of January and February are projected to continue, while May would receive more precipitation with high rainfall events.

Both Scenarios indicate that the first decade of the design period would be drier than the subsequent decades of the design period (i.e., 2040-2060).

7.4 Future Projections of Streamflow

Future streamflow was obtained by forcing the calibrated and validated hydrological model with the bias-corrected precipitation projections under RCP 2.6 and 8.5. The hydrological model results are valid for the observed data after 2005 as Kukule Ganga run-off-the river powerplant came to full operations after 2005. Its operations are included in the model, which was needed to capture the discharge of environmental flow (0.5 m^3/s) during dry periods.

The hindcast precipitation data is only available until 2005. Hence, the model could not be forced with RCM based precipitation as historical base period. Therefore, the base period streamflow was obtained by forcing the observed precipitation from 2005 to 2020 (15 years). Since the study's main objective is to assess and predict the low flow conditions of Kuda Ganga, analysis of the river's low flow behaviour would assist in deciding the conclusions with future projections. Several indices were used to capture and study the low flow behaviour of the river.

7.4.1 Probability exceedance flow of 90th percent (Q_{90}) and 50th percent (Q_{50})

According to the results presented (Figure 6-11 in section 6.3.1), Q_{90} and Q_{50} are projected to decrease under both scenarios (compared to baseline conditions). The Q_{90} is projected to decrease by 35% and 55% under RCP 2.6 and 8.5, respectively, during the first decade of the design period. The Q_{90} is projected to decrease at a higher rate than Q_{50}, which is about 15% under both scenarios. It indicates that the low flows are further declining than the mean flows.

The first decade of the design period is likely to be the driest period in both scenarios. The projected streamflow improves under RCP 2.6 during 2050-2060 (but Q_{90} and Q_{50} are still less than the base period, 2005-2020), with the same pattern being observed with the SPI analysis (Figure 6-9). The flow drastically improves under RCP 8.5, with Q_{90} increasing by 3.2% more and Q_{50} up to -0.6% during 2040-2050 and again dropped to -7.0% and -4.0%, respectively during 2050-2060 (relative to the base period).

7.4.2 Mean 7-day annual minima (MAM7) and Mean 30-day annual minima (MAM30)

Average yearly minima and seasonal minima of 7-day and 30-day moving average flow were evaluated in MAM7 and MAM30 analysis. Projected MAM7 results indicate that the low flow values would improve during the wet seasons of the basin; i.e., SWM increase by 4.87 to 34.7% and 34.8 to 57.0%, 2nd IM increase by 4.87 to 34.7% and 34.8 to 57.0% respectively, under RCP 2.6 and 8.5, (when higher rainfall events occur), while the low flows might even further reduce during dry seasons i.e., NEM decreased by 20.8 to 32.7% and 2.7 to 51.2%, 1st IM decreased by 31.9 to 53.8% and 9.1 to 72.4% respectively, under RCP 2.6 and 8.5, during the design period (2030-2060) relative to the base period (2005-2020) (Figure 6-12 and Table VI-1and Table VI-3). Contrarily, MAM7 of NEM would be increased by 40.1% and 3.3% respectively, under RCP 2.6 and 8.5 during the last decade (2050-2060) relative to the base period value (11.07 m^3/s).

However, the annual minima results show that the low flows may reduce up to 30% under RCP 2.6 and 10% to 55% under RCP 8.5 during the total design period. Projected low flows would increase up to 8.73 m^3/s and up to 7.95 m^3/s under RCP 2.6

and 8.5, respectively during the 2050-2060 period but remain less than the baseline period values (8.85 m^3/s) (Table VI-1 and Table VI-3). Under RCP 2.6, low flows are projected to improve than the base period during the NEM of the last decade (i.e., 2050-2060).

When considering MAM30, low flows are projected to reduce during all four seasons under both scenarios (Figure 6-12). The annual minimal values of MAM30 also show a reduction in projected values under RCP 2.6 (by 12.0 to 40.5%) and RCP 8.5 (by 10.1% to 54.6%) during the design horizon (2030-2060) relative to the base value of 16.56 m^3/s (Table VI-2 and Table VI-4).

The seasonal-wise variation and the annual variation of MAM7 and MAM30 relative to the base period (2005-2020) under RCP 2.6 and 8.5 are summarised in Table VI-1, Table VI-2, Table VI-3, and Table VI-4. In both scenarios, the lowest deviation is likely to occur during the last decade. It shows that the longer period averages have reduced compared to the base period, which may be due to the prolonged dry periods projected during the design horizon.

7.4.3 Baseflow index (BFI)

The projected BFI has increased during all four seasons and under both scenarios (compared with the base period, 2005-2020) (Figure 6-13), indicating that the base flow component might significantly influence the streamflow. The BFI has shown as getting increased by 30 to 45% in the SWM, NEM and by 40 to 55% in the 2nd IM seasons, whereas BFI in the 1st IM has increased by ~20% during the design horizon (2030-2060) under both scenarios relative to the base period. This can be correlated with the decrease of MAM30 (compared to MAM7 and base period), possibly due to prolonged dry periods projected (compared to the base period).

7.4.4 Continuous low flow and deficit volume

According to the base period simulations (2005-2020), only two events are recorded with an eight-day duration and deficit intensity of 36,000 and 7,000 m^3/day. Nine and twelve such events are projected under RCP 2.6 and 8.5, respectively, when considering the future streamflow. All those events are projected to occur during the

NEM or 1st IM period. Most of the high severity events (~50%) are projected to occur during the first decade of the design period, and the severity gets reduced towards the end of the design period. The maximum deficit events related to the future projections have occurred during the first decade under both scenarios with a total deficit volume of 4,945 thousand m^3/day (over 47 days) and 4,409 thousand m^3/day (over 42 days) respectively, under RCP 2.6 and 8.5.

No of events, durations, and intensities related to the drought events are likely to get reduced towards the last decade of the design horizon (2050-2060) under both scenarios, i.e., two events (with deficit durations of four and six days with respective intensities of 15 and 13 thousand m^3/day) under RCP 2.6 and two events (with deficit durations 1 and 6-days with respective intensities of 1 and 34 thousand m^3/day) under RCP 8.5. Other low flow indices; Q_{90}, MAM7, and MAM30 also indicated a possible improvement of low flow conditions towards the last decade of design horizon under RCP 2.6 and still less than the base period (2005-2020) values. A similar pattern was observed under RCP 8.5 also regarding the MAM7 and MAM30 nevertheless, Q_{90} tends to get reduced during the last decade than the 2040-2050 decade. Other researchers have also concluded that the Kalu Ganga Basin would become warmer and wetter with increased discharges during the SWM periods of the late 21st century (Sirisena et al., 2021). A decade-wise study from the 2030 to 2060 period could not be found for the basin area or for Sri Lanka. This study's results can be relatable to the findings presented by Nyunt et al. (2012). They have used an ensemble of nine GCMs from the 4th IPCC assessment report and concluded that more intense rainfalls might occur during the monsoon seasons while longer dry spells are expected over the 2046-2065 period.

CHAPTER 8

8 CONCLUSIONS AND RECOMMENDATIONS

8.1 Conclusions

- The HEC HMS hydrological model captured the low flow conditions of the Kuda Ganga catchment at Koleimodara (with performance indices NSE_{rel}: 0.67 to 0.85, MRAE: 0.15 to 0.35, PBIAS: -8.63% to 3.05% and RMSE: 29.7 to 55.1 for all calibration and validation events) which is the most concern of the study.
- Calibration and validation results showed that the model underestimates the dry weather flow, specifically the discharges less than 13 m^3/s. Therefore, the low flow estimations would be conservative and safe side.
- These results are fair enough to identify the future trends of precipitation and low flow characteristics of Kuda Ganga with the knowledge of data and model uncertainties.
- The annual rainfall in the basin is projected to increase, but dry months like January, February, July, and August continue to become drier while wet months like May, June, September, and October continue to become wetter with more precipitation.
- The first decade (2030-2040) of the design period would be more critical as the river discharges are projected to decrease, especially during the 1st IM (March, April) and NEM (December to February).
- Koleimodara intake would fail to supply the required demand during 2030-2040 under the RCP 2.6 with a maximum deficit volume of 4.945 MCM for 47 days with 105,000 m^3/day intensity.

- Similarly, the deficit event indicates under RCP 8.5 has a deficit volume of 4.409 MCM for 42 days with the intensity of 105,000 m^3/day over the 2030-2040 period.
- Hence, NWSDB would require maintaining storage of about 4.9 MCM to remain on the safe side for providing an uninterrupted water supply in the low flow period during the next design horizon (2030 – 2060).

8.2 Recommendations

- Since the Koleimodara location has the potential to fail in providing water extraction during the next design horizon it is recommended to search for another alternative water source.
- This study did not account for the future temperature variation-related parameters such as potential evapotranspiration for the future projections. Future possible land-use changes also would affect the hydrological parameters of the model. Therefore, it is recommended to further perform future climate-related studies in the area accounting for these factors as well.
- Several RCM/GCM models can be studied other than studying a single model and assembled to get a more generalised fair result even though a single RCM model has been studied in this study due to the time limitations.
- The hydrological model could not be forced with the historical hindcasted precipitation data from the climate model as the historical hindcast data are only available up to 2005. Therefore, this study can be further improved with the recently released IPCC AR6 climate data projections with more recent historical data and updated future projections

BIBLIOGRAPHY

Ali, M., Khan, S. J., Aslam, I., & Khan, Z. (2011). Simulation of the impacts of land-use change on surface runoff of Lai Nullah Basin in Islamabad, Pakistan. *Landscape and Urban Planning*, *102*(4), 271–279. https://doi.org/https://doi.org/10.1016/j.landurbplan.2011.05.006

Allen, R., Pereira, L., Raes, D., & Smith, M. (1998). Crop evapotranspiration, guidelines for computing crop water requirements. In *Irrigation and drain, Paper No. 56, FAO*.

Althoff, D., & Rodrigues, L. N. (2021). Goodness-of-fit criteria for hydrological models: Model calibration and performance assessment. *Journal of Hydrology*, *600*. https://doi.org/10.1016/j.jhydrol.2021.126674

Ampitiyawatta, A. D., & Guo, S. (2010). Precipitation trends in the Kalu Ganga basin in Sri Lanka. *Journal of Agricultural Sciences – Sri Lanka*, *4*(1), 10. https://doi.org/10.4038/JAS.V4I1.1641

Anderson, M. L., Z.-Q., C., Kavvas, M. L., & Arlen, F. (2002). Coupling HEC-HMS with Atmospheric Models for Prediction of Watershed Runoff. *Journal of Hydrologic Engineering*, *7*(4), 312–318. https://doi.org/10.1061/(ASCE)1084-0699(2002)7:4(312)

Azmat, M., Choi, M., Kim, T.-W., & Liaqat, U. W. (2016). Hydrological modeling to simulate streamflow under changing climate in a scarcely gauged cryosphere catchment. *Environmental Earth Sciences*, *75*(3), 186. https://doi.org/10.1007/s12665-015-5059-2

Azmat, M., Qamar, M. U., Ahmed, S., Hussain, E., & Umair, M. (2017). Application of HEC-HMS for the event and continuous simulation in high-altitude scarcely-gauged catchment under changing climate. In *European Water* (Vol. 57).

Bai, Y., Zhang, Z., & Zhao, W. (2019). Assessing the Impact of Climate Change on Flood Events Using HEC-HMS and CMIP5. *Water, Air, and Soil Pollution*, *230*(6). https://doi.org/10.1007/s11270-019-4159-0

Bardsley, W. E. (1994). Against objective statistical analysis of hydrological extremes. *Journal of Hydrology*, *162*(3–4), 429–431. https://doi.org/10.1016/0022-1694(94)90240-2

Barnston, A. G. (1992). Correspondence among the Correlation, RMSE, and Heidke Forecast Verification Measures; Refinement of the Heidke Score. *Weather and Forecasting*, *7*(4), 699–709. https://doi.org/https://doi.org/10.1175/1520-0434(1992)007<0699:CATCRA>2.0.CO;2

Basnayake, B. R. S. B., & Vithanage, J. C. (2004). Future climate scenarios of rainfall and temperature for Sri Lanka. *Proceedings of the 60th Annual Session of Sri Lanka Association for the Advancement of Science (SLASS), Section E1*, 222.

Bennett, T. H., & Peters, J. C. (2004). Continuous Soil Moisture Accounting in the Hydrologic Engineering Center Hydrologic Modeling System (HEC-HMS). *Joint Conference on Water Resource Engineering and Water Resources Planning and Management 2000: Building Partnerships*, *104*, 1–10. https://doi.org/10.1061/40517(2000)149

Bong, C. H. J., & Richard, J. (2020). Drought and climate change assessment using Standardized Precipitation Index (SPI) for Sarawak River Basin. *Journal of Water and Climate Change*, *11*(4), 956–965. https://doi.org/10.2166/WCC.2019.036

Bormann, H., & Pinter, N. (2017). Trends in low flows of German rivers since 1950: Comparability of different low-flow indicators and their spatial patterns. *River Research and Applications*, *33*(7), 1191–1204. https://doi.org/10.1002/RRA.3152

Brauer, T., & Fleming, M. (2017). Period of Record Simulation of the Russian River Watershed with the Hydrologic Modeling System (HEC-HMS). *World Environmental and Water Resources Congress 2017: Watershed Management, Irrigation and Drainage, and Water Resources Planning and Management -*

Selected Papers from the World Environmental and Water Resources Congress 2017, 12–21. https://doi.org/10.1061/9780784480601.002

Caloiero, T., Coscarelli, R., Ferrari, E., & Sirangelo, B. (2015). Analysis of Dry Spells in Southern Italy (Calabria). In *Water* (Vol. 7, Issue 6). https://doi.org/10.3390/w7063009

CEA. (2018). *Guidelines for Determination of Environmental Flows (e-flows) for Development Projects that Result in Impounding of Water in Streams/ Rivers Central*. http://203.115.26.10/2018/EIA_PUB/e-flow.pdf

Chandrapala, L. (1996, March 7). Calculation of areal precipitation of Sri Lanka on district basis using Voronoi Tessalation Method. *Proceedings of National Symposium on Climate Change*.

Chemeda, D. (2013). Dry and Wet Spell Analysis of the Two Rainy Seasons for Decision Support in Agricultural Water Management for Crop production in the Central Highlands of Ethiopia. *Journal of Biology, Agriculture and Healthcare*, *3*(11). www.iiste.org

Chen, G., & Costa, G. D. (2017). Climate change impacts on water resources case of Sri Lanka. *Nvironment and Ecology Research*, *5*(5), 347–356. https://scholar.google.com/scholar?hl=en&as_sdt=0%2C5&q=G.+Chen+and+G.+D.+Costa%2C+%E2%80%9CClimate+change+impacts+on+water+resources+case+of+Sri+Lanka%2C%E2%80%9D+Environment+and+Ecology+Research%2C+vol.+5%2C+no.+5%2C+pp.+347%E2%80%93356%2C+2017.&btnG=

Chen, J., Brissette, F. P., Zhang, X. J., Chen, H., Guo, S., & Zhao, Y. (2019). Bias correcting climate model multi-member ensembles to assess climate change impacts on hydrology. *Climatic Change 2019 153:3*, *153*(3), 361–377. https://doi.org/10.1007/S10584-019-02393-X

Chow, V. T., Maidment, D. R., & Mays, L. W. (1988). *Applied Hydrology* . McGraw-Hill Book Company. https://books.google.lk/books?id=RRwidSsBJrEC&printsec=copyright&source=gbs_pub_info_r#v=onepage&q&f=false

Coffey, M. E., Workman, S. R., Taraba, J. L., Fogle, A. W., Coffey, M. E. ;, Workman, S. R. ;, & Taraba, J. L. ; (2004). *Statistical Procedures for Evaluating Daily and Monthly Hydrologic Model Predictions Repository Citation*. https://doi.org/10.13031/2013.15870

CSIP. (2019). *Report on Water Demand Projections Comprehensive Strategic Investment Program (CSIP) for the Water Supply and Sanitation Sector and NWSDB Master Plan*.

Cunderlik, J. (2003). *Hydrologic model selection for the CFCAS project: assessment of water resources risk and vulnerability to changing climatic conditions*.

Cunderlik, J., & Simonovic, S. (2004). Calibration, Verification and Sensitivity Analysis of the HEC-HMS Hydrologic Model. *Water Resources Research Report*. https://ir.lib.uwo.ca/wrrr/11

Dasgupta, S., Akhter, F., Zahirul, K., Khan, H., Choudhury, S., The, A. N., & Bank, W. (2014). *River Salinity and Climate Change Evidence from Coastal Bangladesh*. http://econ.worldbank.org.

de Silva, M. M. G. T., Weerakoon, S. B., & Herath, S. (2014). Modeling of Event and Continuous Flow Hydrographs with HEC–HMS: Case Study in the Kelani River Basin, Sri Lanka. *Journal of Hydrologic Engineering*, *19*(4), 800–806. https://doi.org/10.1061/(asce)he.1943-5584.0000846

Demuth, S. Heinrich, B. (1997). Temporal and spatial behaviour of drought in south Germany. *FRIEND'97 – Regional Hydrology: Concepts and Models for Sustainable Water Resource Management, IAHS Publication*, *246*, 151–157.

Devia, G. K., Ganasri, B. P., & Dwarakish, G. S. (2015). A Review on Hydrological Models. *Aquatic Procedia*, *4*, 1001–1007. https://doi.org/10.1016/j.aqpro.2015.02.126

di Bucchianico, A. (2008). Coefficient of Determination (R2). In *Encyclopedia of Statistics in Quality and Reliability*. American Cancer Society. https://doi.org/https://doi.org/10.1002/9780470061572.eqr173

Ding, T., & Ke, Z. (2013). A comparison of statistical approaches for seasonal precipitation prediction in Pakistan. *Weather and Forecasting*, *28*(5), 1116–1132. https://doi.org/10.1175/WAF-D-12-00112.1

Dissanayaka, K. D. C. R. (2017). *Climate Extremes and Precipitation Trends in Kelani River Basin, Sri Lanka and Impact on Streamflow Variability under Climate Change*.

Dissanayake, P. M. (2017). *Applicability of a two paramter water balance model to simulate daily rainfall-runoff a case study of Kalu and Gin river basins In Sri Lanka*. http://dl.lib.mrt.ac.lk/handle/123/13027

Durman, C. F., Gregory, J. M., Hassell, D. C., Jones, R. G., & Murphy, J. M. (2001). A comparison of extreme European daily precipitation simulated by a global and a regional climate model for present and future climates. *Quarterly Journal of the Royal Meteorological Society*, *127*(573), 1005–1015. https://doi.org/10.1002/QJ.49712757316

Eriyagama, N., & Smakhtin, V. (2015). *Uncorrected Proof The Sri Lanka environmental flow calculator : a science-based tool to support sustainable national water management*. *December*. https://doi.org/10.2166/wp.2015.158

Fan, M. (2015). *ASIAN DEVELOPMENT BANK Sri Lanka's Water Supply and Sanitation Sector Achievements and a Way Forward*. www.adb.org

Flato, G., Marotzke, J., Abiodun, B., Braconnot, P., Chou, S. C., Collins, W., Cox, P., Driouech, F., Emori, S., Eyring, V., Forest, C., Gleckler, P., Guilyardi, E., Jakob, C., Kattsov, V., Reason, C., & Rummukainen, M. (2013). Evaluation of climate models. In T. F. Stocker, D. Qin, G.-K. Plattner, M. Tignor, S. K. Allen, J. Doschung, A. Nauels, Y. Xia, V. Bex, & P. M. Midgley (Eds.), *Climate Change 2013: The Physical Science Basis. Contribution of Working Group I to the Fifth Assessment Report of the Intergovernmental Panel on Climate Change* (pp. 741–882). Cambridge University Press. https://doi.org/10.1017/CBO9781107415324.020

Fleming, M., & Neary, V. (2004). Continuous Hydrologic Modeling Study with the Hydrologic Modeling System. *Journal of Hydrologic Engineering*, *9*(3), 175–183. https://doi.org/10.1061/(ASCE)1084-0699(2004)9:3(175)

Frei, C., Christensen, J. H., Déqué, M., Jacob, D., Jones, R. G., & Vidale, P. L. (2003). Daily precipitation statistics in regional climate models: Evaluation and intercomparison for the European Alps. *Journal of Geophysical Research: Atmospheres*, *108*(D3), n/a–n/a. https://doi.org/10.1029/2002jd002287

Frich, P., Alexander, L. v, Della-Marta, P., Gleason, B., Haylock, M., Tank, A. M. G. K., & Peterson, T. (2002). Observed coherent changes in climatic extremes during the second half of the twentieth century. *Climate Research*, *19*(3), 193–212. https://www.int-res.com/abstracts/cr/v19/n3/p193-212/

Ghimire, U., Srinivasan, G., & Agarwal, A. (2019). Assessment of rainfall bias correction techniques for improved hydrological simulation. *International Journal of Climatology*, *39*(4), 2386–2399. https://doi.org/https://doi.org/10.1002/joc.5959

Giorgi, F., Coppola, E., Solmon, F., Mariotti, L., Sylla, M. B., Bi, X., Elguindi, N., Diro, G. T., Nair, V., Giuliani, G., Turuncoglu, U. U., Cozzini, S., Güttler, I., O'Brien, T. A., Tawfik, A. B., Shalaby, A., Zakey, A. S., Steiner, A. L., Stordal, F., … Brankovic, C. (2012). RegCM4: model description and preliminary tests over multiple CORDEX domains. *Climate Research*, *52*(1), 7–29. https://doi.org/10.3354/CR01018

Good, P., Bärring, L., Giannakopoulos, C., Holt, T., & Palutikof, J. (2006). Non-linear regional relationships between climate extremes and annual mean temperatures in model projections for 1961–2099 over Europe. *Climate Research*, *31*(1), 19–34. https://doi.org/10.3354/CR031019

Green, I. R. A., & Stephenson, D. (1986). Criteria for comparison of single event models. *Hydrological Sciences Journal*, *31*(3), 395–411. https://doi.org/10.1080/02626668609491056

Guo, S., Wang, J., Xiong, L., Ying, A., & Li, D. (2002). A macro-scale and semi-distributed monthly water balance model to predict climate change impacts in China. *Journal of Hydrology*, *268*, 1–15. www.paper.edu.cn

Gupta, H. V., Sorooshian, S., & Yapo, P. O. (1999). Status of Automatic Calibration for Hydrologic Models: Comparison with Multilevel Expert Calibration. *Journal of Hydrologic Engineering*, *4*(2), 135–143. https://doi.org/10.1061/(ASCE)1084-0699(1999)4:2(135)

Gupta, H. v., Kling, H., Yilmaz, K. K., & Martinez, G. F. (2009). Decomposition of the mean squared error and NSE performance criteria: Implications for improving hydrological modelling. *Journal of Hydrology*, *377*(1–2), 80–91. https://doi.org/10.1016/J.JHYDROL.2009.08.003

Gustard, A., Bullock, A., & Dixon, J. M. (1992). *Low flow estimation in the United Kingdom*. Institute of Hydrology, Report No 108.

Halwatura, D., & Najim, M. M. M. (2013). Application of the HEC-HMS model for runoff simulation in a tropical catchment. *Environmental Modelling and Software*, *46*, 155–162. https://doi.org/10.1016/j.envsoft.2013.03.006

HEC-HMS Tutorials and Guides. (n.d.). Retrieved November 4, 2021, from https://www.hec.usace.army.mil/confluence/hmsdocs/hmsguides/applying-loss-methods-within-hec-hms/applying-the-deficit-and-constant-loss-method

Herath, M. H. B. C. W., & Wijesekera, N. T. S. (2021). Evaluation of HEC-HMS Model for Water Resources Management in Maha Oya Basin in Sri Lanka. *Engineer: Journal of the Institution of Engineers, Sri Lanka*, *54*(2), 45. https://doi.org/10.4038/engineer.v54i2.7441

Herrera, S., Fita, L., Fernández, J., & Gutiérrez, J. M. (2010). Evaluation of the mean and extreme precipitation regimes from the ENSEMBLES regional climate multimodel simulations over Spain. *Journal of Geophysical Research: Atmospheres*, *115*(D21), 21117. https://doi.org/10.1029/2010JD013936

Huang, Y. F., Ang, J. T., Tiong, Y. J., Mirzaei, M., & Amin, M. Z. M. (2016). Drought Forecasting Using SPI and EDI under RCP-8.5 Climate Change Scenarios for

Langat River Basin, Malaysia. *Procedia Engineering*, *154*, 710–717. https://doi.org/10.1016/J.PROENG.2016.07.573

Hussain, F., Wu, R.-S., & Yu, K.-C. (2021). Application of Physically Based Semi-Distributed Hec-Hms Model for Flow Simulation in Tributary Catchments of Kaohsiung Area Taiwan. *Journal of Marine Science and Technology*, *29*(1). https://doi.org/10.51400/2709-6998.1003

Hydrology Division (ID). (2019). *IDF Curves 75% Probability Rainfall Evapotranspiration*.

Jain, S. K., & Singh, V. P. (2003). *Water resources systems planning and management.* (S. K. Jain & V. P. Singh, Eds.). Elsevier Science B.V. https://www.cabdirect.org/cabdirect/abstract/20043165716

Jajarmizadeh, M., Harun, S., & Salarpour, M. (2012). A Review on Theoretical Consideration and Types of Models in Hydrology Cite this paper. *Journal of Environmental Science and Technology*, 249–261.

Jayadeera, P. M., & Wijesekera, N. T. S. (2019a). A Diagnostic Application of HEC–HMS Model to Evaluate the Potential for Water Management in the Ratnapura Watershed of Kalu Ganga Sri Lanka. *Engineer: Journal of the Institution of Engineers, Sri Lanka*, *52*(3), 11. https://doi.org/10.4038/engineer.v52i3.7361

Jayadeera, P. M., & Wijesekera, N. T. S. (2019b). A Diagnostic Application of HEC–HMS Model to Evaluate the Potential for Water Management in the Ratnapura Watershed of Kalu Ganga Sri Lanka. *Engineer: Journal of the Institution of Engineers, Sri Lanka*, *52*(3), 11. https://doi.org/10.4038/engineer.v52i3.7361

Jayatillake, H. M., Chandrapala, L., Basnayake, B. R. S. B., & Dharmaratne, G. H. P. (2005). *Water resources and climate change. Proceedings of Workshop on Sri Lanka National Water Development Report* (N. T. S. Wijesekera, K. A. U. S. Imbulana, & B. Neupane, Eds.). France: World Water Assessment Programme (WWAP). www.unesco.org/water/wwap

Jones, G. (2002). Setting Environmental Flows to Sustain a Healthy Working River. *WaterShed*, *February*.

Kanchanamala, D. P. H. M., Herath, H. M. H. K., & Nandalal, K. D. W. (2016). Impact of Catchment Scale on Rainfall Runoff Modeling: Kalu Ganga River Catchment upto Ratnapura. *Engineer: Journal of the Institution of Engineers, Sri Lanka*, *49*(2), 1. https://doi.org/10.4038/engineer.v49i2.7003

Khandu, D. (2015). *monthly water balance model for evalution of climate change impacts on the streamflow of Gingaga and Kelani Ganga basins, Sri Lanka*. http://dl.lib.mrt.ac.lk/handle/123/12893

Klein Tank, A. M. G., & Können, G. P. (2003). Trends in Indices of Daily Temperature and Precipitation Extremes in Europe, 1946–99. *Journal of Climate*, *16*(22), 3665–3680.

Krause, P., Boyle, D. P., & Bäse, F. (2005a). Comparison of different efficiency criteria for hydrological model assessment. *Advances in Geosciences*, *5*, 89–97. https://doi.org/10.5194/ADGEO-5-89-2005

Krause, P., Boyle, D. P., & Bäse, F. (2005b). Comparison of different efficiency criteria for hydrological model assessment. *Advances in Geosciences*, *5*, 89–97.

Krause, P., Boyle, D. P., & Bäse, F. (2005c). Comparison of different efficiency criteria for hydrological model assessment. *Advances in Geosciences*, *5*, 89–97. https://hal.archives-ouvertes.fr/hal-00296842

Lafon, T., Dadson, S., Buys, G., & Prudhomme, C. (2013). Bias correction of daily precipitation simulated by a regional climate model: A comparison of methods. *International Journal of Climatology*, *33*(6), 1367–1381. https://doi.org/10.1002/joc.3518

Lana, X., Martínez, M. D., Burgueño, A., Serra, C., Martín-Vide, J., & Gómez, L. (2006). Distributions of long dry spells in the iberian peninsula, years 1951–1990. *International Journal of Climatology*, *26*(14), 1999–2021. https://doi.org/https://doi.org/10.1002/joc.1354

Lars, B., Tom, H., Maj -Lena, L., Maciej, R., Marco Moriondo, & Jean, P. P. (2006). CLIMATE RESEARCH Clim Res. *Climate Research*, *31*, 35–49. www.int-res.com

Legates, D. R., & McCabe, G. J. (1999). Evaluating the use of "goodness-of-fit" Measures in hydrologic and hydroclimatic model validation. *Water Resources Research*, *35*(1), 233–241. https://doi.org/10.1029/1998WR900018

Lenderink, G., Buishand, A., & van Deursen, W. (2007). Estimates of future discharges of the river Rhine using two scenario methodologies: direct versus delta approach. *Hydrology and Earth System Sciences*, *11*(3). www.hydrol-earth-syst-sci.net/11/1145/2007

Li, Z., Li, Y., Shi, X., & Li, J. (2017). The characteristics of wet and dry spells for the diverse climate in China. *Global and Planetary Change*, *149*, 14–19. https://doi.org/10.1016/j.gloplacha.2016.12.015

Luo, M., Liu, T., Meng, F., Duan, Y., Frankl, A., Bao, A., & de Maeyer, P. (2018). Comparing bias correction methods used in downscaling precipitation and temperature from regional climate models: A case study from the Kaidu River Basin in Western China. *Water (Switzerland)*, *10*(8). https://doi.org/10.3390/w10081046

Madsen, H., Wilson, G., & Ammentorp, H. C. (2002). Comparison of different automated strategies for calibration of rainfall-runoff models. *Journal of Hydrology*, *261*(1–4), 48–55. www.elsevier.com/locate/jhydrol

Mahmood, R., Jia, S., Tripathi, N. K., & Shrestha, S. (2018). Precipitation extended linear scaling method for correcting GCM precipitation and its evaluation and implication in the transboundary Jhelum River basin. *Atmosphere*, *9*(5). https://doi.org/10.3390/atmos9050160

Maracchi, G., Sirotenko, O., & Bindi, M. (2005). Impacts of Present and Future Climate Variability on Agriculture and Forestry in the Temperate Regions: Europe. *Climatic Change*, *70*(1), 117–135. https://doi.org/10.1007/s10584-005-5939-7

Marambe, B., Punyawardena, R., Silva, P., Premalal, S., Rathnabharathie, V., Kekulandala, B., Nidumolu, U., & Howden, M. (2015). Climate, Climate Risk, and Food Security in Sri Lanka: The Need for Strengthening Adaptation

Strategies. In *Handbook of Climate Change Adaptation* (pp. 1759–1789). Springer Berlin Heidelberg. https://doi.org/10.1007/978-3-642-38670-1_120

Mckee, T. B., Doesken, N. J., & Kleist, J. (1993). THE RELATIONSHIP OF DROUGHT FREQUENCY AND DURATION TO TIME SCALES. In *Eighth Conference on Applied Climatology*.

McMahon, T. A., Peel, M. C., Lowe, L., Srikanthan, R., & McVicar, T. R. (2013). Estimating actual, potential, reference crop and pan evaporation using standard meteorological data: a pragmatic synthesis. *Hydrology and Earth System Sciences*, *17*(4), 1331–1363. https://doi.org/10.5194/hess-17-1331-2013

Meenu, R., Rehana, S., & Mujumdar, P. P. (2013). Assessment of hydrologic impacts of climate change in Tunga-Bhadra river basin, India with HEC-HMS and SDSM. *Hydrological Processes*, *27*(11), 1572–1589. https://doi.org/10.1002/hyp.9220

Miller, M. P., Buto, S. G., Susong, D. D., & Rumsey, C. A. (2016). The importance of base flow in sustaining surface water flow in the Upper Colorado River Basin. *Water Resources Research*, *52*(5), 3547–3562. https://doi.org/10.1002/2015WR017963

Mishra, A. K., & Singh, V. P. (2010). A review of drought concepts. *Journal of Hydrology*, *391*(1), 202–216. https://doi.org/https://doi.org/10.1016/j.jhydrol.2010.07.012

Mizukami, N., Rakovec, O., Newman, A. J., Clark, M. P., Wood, A. W., Gupta, H. v., & Kumar, R. (2019). On the choice of calibration metrics for “high-flow” estimation using hydrologic models. *Hydrology and Earth System Sciences*, *23*(6), 2601–2614. https://doi.org/10.5194/HESS-23-2601-2019

Mngodo, R. J. (1997). Flow duration characteristics of Southern African rivers. *FRIEND’97 – Regional Hydrology: Concepts and Models for Sustainable Water Resource Management, IAHS Publication*, *246*, 49–63.

Moormakn, F. R., & Panabokke, C. R. (1961). *Soils of Ceylon*.

Moradkhani, H., & Sorooshian, Soroosh. (2008). General Review of Rainfall-Runoff Modeling: Model Calibration, Data Assimilation, and Uncertainty Analysis. *Hydrological Modeling and the Water Cycle.Springer*, *63*, 290.

Moriasi, D. N., Arnold, J. G., Liew, M. W. van, Bingner, R. L., Harmel, R. D., & Veith, T. L. (2007). MODEL EVALUATION GUIDELINES FOR SYSTEMATIC QUANTIFICATION OF ACCURACY IN WATERSHED SIMULATIONS. *Transactions of the American Society of Agricultural and Biological Engineers ASABE*, *50*(3).

Mukherjee, S., Mishra, A., & Trenberth, K. E. (2018). Climate Change and Drought: a Perspective on Drought Indices. *Current Climate Change Reports*, *4*(2), 145–163. https://doi.org/10.1007/s40641-018-0098-x

Nandalal, K. D. W. (2009). Use of a hydrodynamic model to forecast floods of Kalu River in Sri Lanka. *Journal of Flood Risk Management*, *2*(3), 151–158. https://doi.org/10.1111/J.1753-318X.2009.01032.X

Nyunt, T. C., Yamamoto, H., Yamamoto, A., Nemoto, T., Kitsuregawa, M., & Koike, T. (2012). A PPLICATION OF BIAS-CORRECTION AND DOWNSCALING METHOD TO KALU GANGA BASIN IN SRI LANKA. *Journal of Japan Society of Civil Engineers, JSCE*, *68*(4), 115–120.

Oleyiblo, J. O., & Li, Z. J. (2010). Application of HEC-HMS for flood forecasting in Misai and Wan'an catchments in China. *Water Science and Engineering*, *3*(1), 14–22. https://doi.org/10.3882/j.issn.1674-2370.2010.01.002

Osborn, T. J. (1997). Areal and point precipitation intensity changes: Implications for the application of climate models. *Geophysical Research Letters*, *24*(22), 2829–2832. https://doi.org/https://doi.org/10.1029/97GL02976

P1 Manual – Project Planning Feasibility (2nd Rev). (2019). National Water Supply and Drainage Board.

Pathirana, A., Herath, S., Yamada, T., & Swain, D. (2007). Impacts of absorbing aerosols on South Asian rainfall. *Climatic Change*, *85*(1), 103–118. https://doi.org/10.1007/s10584-006-9184-5

Perera, K. R. J., & Wijesekera, N. T. S. (2011). Identification of the Spatial Variability of Runoff Coefficients of Three Wet Zone Watersheds of Sri Lanka. *Engineer: Journal of the Institution of Engineers, Sri Lanka*, *44*(3), 1. https://doi.org/10.4038/ENGINEER.V44I3.6960

Peterson, T. C., Folland, C. K., Gruza, G., Hogg, W., Mokssit, A., & Plummer, N. (2001). *Report on the Activities of the Working Group on Climate Change Detection and Related Rapporteurs 1998-2001, Reports WCDMP-47, WMO-TD 1071*.

Petts, G. E. (2009). Instream Flow Science for Sustainable River Management. *Journal of the American Water Resources Association (JAWRA)*, *45*(5), 1071–1086. https://doi.org/10.1111/j.1752-1688.2009.00360.x

Ponrajah, A. J. P. (1984). *Design of Irrigation Systems for Small Catchments* (2nd ed.). Irrigation Department.

Ponrajah, A. J. P. (1989). *Technical Guidelines for Irrigation Works*. Irrigation Department., Sri Lanka.

Pre-feasibility Report - Aluthgama Mathugama Agalawatta Integrated Water Supply Project. (2011).

Premalal, K. H. M. S. (2009). *Weather and climate trends, climate controls & risks in Sri Lanka*. Department of Meteorology.

Prisloe, M., Educator, G., & Manager, G. (2000, September 10). Determining Impervious Surfaces for Watershed Modeling Applications. *National Nonpoint Source Monitoring Conference*.

Punyawardena, B. V. R., Mehmood, S., Hettiarachchi, A. K., Iqbal, M., de Silva, S. H. S. A., & Goheer, A. (2013). Future climate of Sri Lanka: an approach through dynamic downscaling of ECHAM4 General Circulation Model (GCM). *Tropical Agriculturist*, *161*, 35–52. https://www.cabdirect.org/cabdirect/abstract/20143293785

Ratna, S. B., Ratnam, J. v., Behera, S. K., Rautenbach, C. J. de W., Ndarana, T., Takahashi, K., & Yamagata, T. (2014). Performance assessment of three

convective parameterization schemes in WRF for downscaling summer rainfall over South Africa. *Climate Dynamics*, *42*(11–12), 2931–2953. https://doi.org/10.1007/S00382-013-1918-2

Rawls, W. J., Brakensiek, D. L., & Miller, N. (1983). Greenampt Infiltration Parameters from Soils Data. *Journal of Hydraulic Engineering*, *109*(1), 62–70. https://doi.org/10.1061/(ASCE)0733-9429(1983)109:1(62)

Raymond, F., Ullmann, A., Camberlin, P., Drobinski, P., & Chateau Smith, C. (2016). Extreme dry spell detection and climatology over the Mediterranean Basin during the wet season. Geophysical Research Letters Extreme dry spell detection and climatology over the Mediterranean Basin during the wet season. *Geophysical Research Letters*, *13*, 7196–7204. https://doi.org/10.1002/2016GL069758ï

Rivoire, P., Tramblay, Y., Neppel, L., Hertig, E., & Vicente-Serrano, S. M. (2019). Impact of the dry-day definition on Mediterranean extreme dry-spell analysis. *Natural Hazards and Earth System Sciences*, *19*(8), 1629–1638. https://doi.org/10.5194/nhess-19-1629-2019

Rosenberg, D. M., McCully, P., & Pringle, C. M. (2000). Global-scale environmental effects of hydrological alterations: introduction. *Bio Science*, *50*(9), 746–751.

Sampath, D. S., Weerakoon, S. B., & Herath, S. (2015). HEC-HMS Model for Runoff Simulation in a Tropical Catchment with Intra-Basin Diversions-Case Study of the Deduru Oya River Basin, Sri Lanka. *Engineer: Journal of the Institution of Engineers, Sri Lanka*, *XLVIII*(01), 1–9. http://iesl.nsf.ac.lk/bitstream/handle/1/1846/Engineer-2015-48%281%29_1.pdf?sequence=2&isAllowed=y

Sanjay, J., Ramarao, M. V. S., Mahesh, R., Ingle, S., Singh, B., & Krishnan, R. (2012). *Regional Climate Change Datasets for South Asia*. http://cccr.tropmet.res.in/home/reports.jsp

Sapač, K., Medved, A., Rusjan, S., & Bezak, N. (2019). Investigation of low- and high-flow characteristics of karst catchments under climate change. *Water (Switzerland)*, *11*(5). https://doi.org/10.3390/w11050925

Scharffenberg, B., Bartles, M., Brauer, T., Fleming, M., & Karlovits, G. (2018). *Hydrologic Modeling System HEC-HMS User's Manual CPD-74A* (4.3). United States Army Corps of Engineers, Hydrologic Engineering Centre.

Schulz, L., & Kingston, D. G. (2017). GCM-related uncertainty in river flow projections at the threshold for "dangerous" climate change: the Kalu Ganga river, Sri Lanka. *Hydrological Sciences Journal*, *62*(14), 2369–2380. https://doi.org/10.1080/02626667.2017.1381965

Semenov, V., & Bengtsson, L. (2002). Secular trends in daily precipitation characteristics: greenhouse gas simulation with a coupled AOGCM. *Climate Dynamics*, *19*(2), 123–140. https://doi.org/10.1007/s00382-001-0218-4

Sharifi, M. (2015). *Calibration and verificaion of a-two paramter montly water balance model and Its application potential for evalution of water resourcesa case study of Kalu and Mahaweli rivers of Sri Lanka*. http://dl.lib.mrt.ac.lk/handle/123/12954

Sharma, D., Gupta, A. das, & Babel, M. S. (2007). Spatial disaggregation of bias-corrected GCM precipitation for improved hydrologic simulation: Ping River Basin, Thailand. *Hydrology and Earth System Sciences*, *11*(4), 1373–1390. https://doi.org/10.5194/HESS-11-1373-2007

Shrestha, S., & Deb, P. (n.d.). *HYDROLOGY: MEASUREMENT AND ANALYSIS*. Asian Institute of Technology (AIT).

Singh Thakuri Pratik. (2016). *Suitability of a Selected Hydrological Model and Objective Function for Rural Watershed Management in Sri Lanka*.

Sirisena, T. A. J. G., Maskey, S., Bamunawala, J., Coppola, E., & Ranasinghe, R. (2021). Projected Streamflow and Sediment Supply under Changing Climate to the Coast of the Kalu River Basin in Tropical Sri Lanka over the 21st Century. *Water*, *13*(21), 3031. https://doi.org/10.3390/w13213031

Smakhtin, V., & Anputhas, M. (2006). An Assessment of Environmental Flow Requirements of Indian River Basins. *IWMI Research Report 107*, *107*, 37. http://dx.doi.org/10.3910/2009.106

Smakhtin, V. U. (2001). Low flow hydrology: A review. *Journal of Hydrology*, *240*(3–4), 147–186. https://doi.org/10.1016/S0022-1694(00)00340-1

Solberg, S. (2004). Summer drought: a driver for crown condition and mortality of Norway spruce in Norway. *Forest Pathology*, *34*(2), 93–104. https://doi.org/10.1111/J.1439-0329.2004.00351.X

Sonoda, H. (2007). *Kukule Ganga Hydroelectric Power Project (Field Survey: November 2007)*. https://www.jica.go.jp/english/our_work/evaluation/oda_loan/post/2008/pdf/e_project07_full.pdf

Sorooshian, S. (2008). *Hydrological modelling and the water cycle : coupling the atmospheric and hydrological models*. Springer.

Tan, X., Liu, B., & Tan, X. (2020). Global Changes in Baseflow Under the Impacts of Changing Climate and Vegetation. *Water Resources Research*, *56*(9). https://doi.org/10.1029/2020WR027349

Taylor, K. E., Stouffer, R. J., & Meehl, G. A. (2012). An overview of CMIP5 and the experiment design. In *Bulletin of the American Meteorological Society* (Vol. 93, Issue 4, pp. 485–498). https://doi.org/10.1175/BAMS-D-11-00094.1

Tennant, D. L. (1976). Instream Flow Regimens for Fish, Wildlife, Recreation and Related Environmental Resources. *Fisheries*, *1*(4), 6–10. https://doi.org/10.1577/1548-8446(1976)001<0006:IFRFFW>2.0.CO;2

Thapa, B., Danegulu, A., Suwal, N., Upadhyay, S., Manandhar, B., & Prajapati, R. (2020). RAINFALL-RUNOFF MODELLING OF THE WEST RAPTI BASIN, NEPAL. *Issue 1 TECHNICAL JOURNAL TECHNICAL JOURNAL*, *2*(1). http://dhm.gov.np/

The Program for Climate Model Diagnosis and Intercomparison. (2014). https://pcmdi.llnl.gov/about.html

Todd Howard Bennett. (1998). *Development and application of a continuous soil moisture accounting algorithm for the Hydrologic Engineering Center Hydrologic Modeling System (HEC-HMS) (Book, 1998) [WorldCat.org]* [M.S.

University of California]. https://www.worldcat.org/title/development-and-application-of-a-continuous-soil-moisture-accounting-algorithm-for-the-hydrologic-engineering-center-hydrologic-modeling-system-hec-hms/oclc/42712111

USACE. (n.d.). *Hydrologic Modeling System HEC-HMS User's Manual - Version 4.7.1*. United States Army Corps of Engineers, Hydrologic Engineering Centre. Retrieved November 4, 2021, from https://www.hec.usace.army.mil/confluence/hmsdocs/hmsum/4.7.1

USACE. (2000). *Hydrologic Modeling System HEC-HMS Technical Reference Manual* (A. D. Feldman, Ed.; 4.3). United States Army Corps of Engineers, Hydrologic Engineering Centre.

Vicente-Serrano, S. M., & Beguería-Portugués, S. (2003). Estimating extreme dry-spell risk in the middle Ebro valley (northeastern Spain): a comparative analysis of partial duration series with a general Pareto distribution and annual maxima series with a Gumbel distribution. *International Journal of Climatology*, *23*(9), 1103–1118. https://doi.org/https://doi.org/10.1002/joc.934

Vogel, R. M., & Fennessey, N. M. (1994). Flow duration curves. I. A new interpretation and confidence intervals. *J. Water Resour. Plan. Manag*, *120*(4), 485–504.

Wang, M., Zhang, L., & Baddoo, T. D. (2016). Hydrological Modeling in A Semi-Arid Region Using HEC-HMS. *Journal of Water Resource and Hydraulic Engineering*, *5*(3), 105–115. https://doi.org/10.5963/jwrhe0503004

Wijesekera, N. T. S., & Abeynayake, J. C. (2003). Watershed similarity conditions for peak flow transition. A study of river basins in the wet zone of Sri Lanka. *Engineer, Journal of the Institution of Engineers Sri Lanka*.

Willmott, C. J., & Matsuura, K. (2005). Advantages of the mean absolute error (MAE) over the root mean square error (RMSE) in assessing average model performance. *Undefined*, *30*(1), 79–82. https://doi.org/10.3354/CR030079

(WMO). (2009). Manual on Low-flow Estimation and Prediction. Operational Hydrology Report No. 50. WMO-No. 1029. In A. Gustard & S. Demuth (Eds.), *Operational Hydrology Report: Vol. No*, *50* (Issue 1029). World Meteorological Organization.

Wood, A. W., Leung, L. R., Sridhar, V., & Lettenmaier, D. P. (2004). Hydrologic implications of dynamical and statistical approaches to downscaling climate model outputs. *Climatic Change* , *62*, 189–216. https://cig.uw.edu/publications/hydrologic-implications-of-dynamical-and-statistical-approaches-to-downscaling-climate-model-outputs/

Xuefeng, C., & Alan, S. (2009). Event and Continuous Hydrologic Modeling with HEC-HMS. *Journal of Irrigation and Drainage Engineering*, *135*(1), 119–124. https://doi.org/10.1061/(ASCE)0733-9437(2009)135:1(119)

ANNEXURE I

I. STREAMFLOW RESPONSE WITH RAINFALL

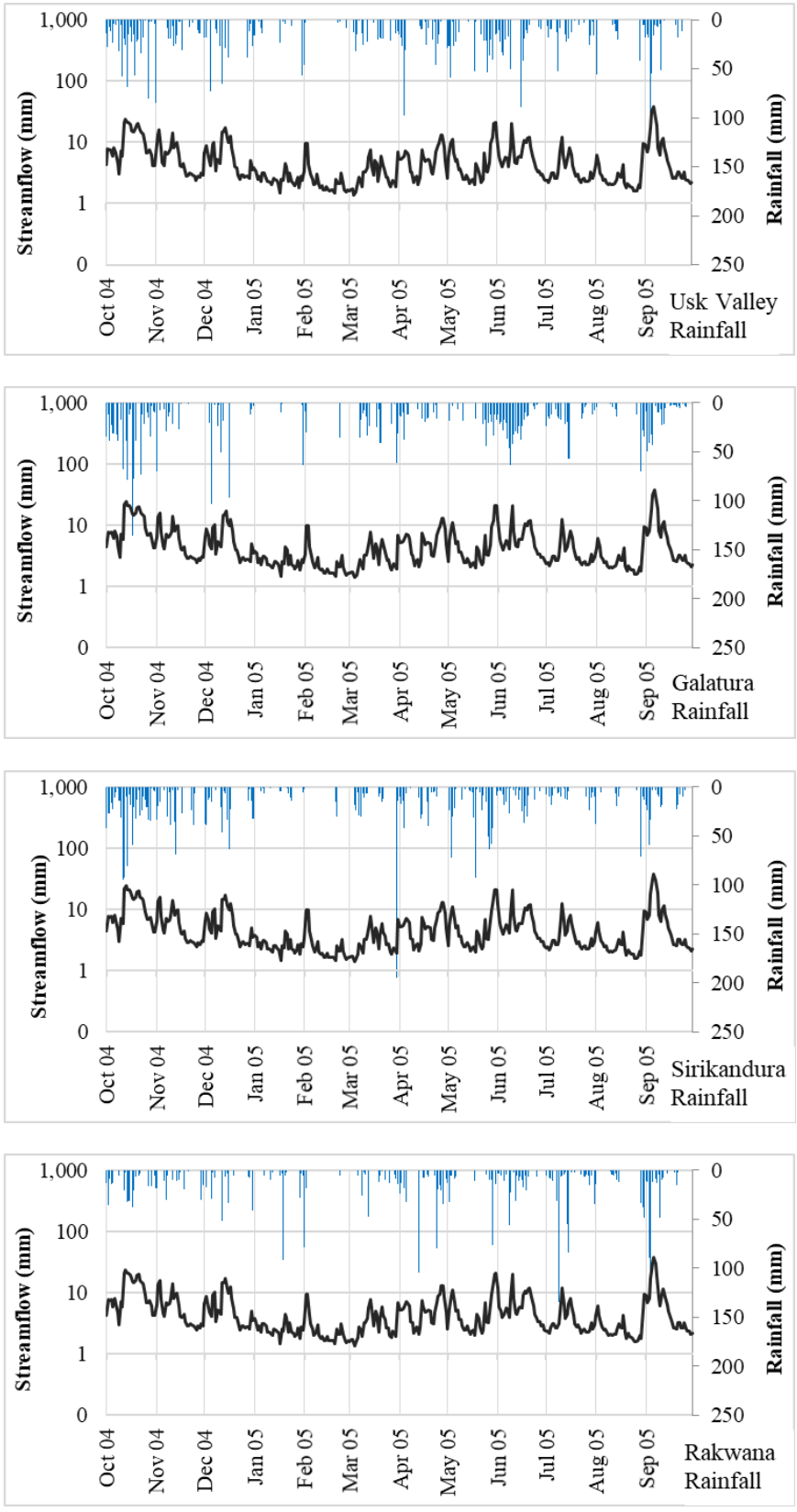

Figure I-1: Streamflow response to rainfall in Millakanda watershed in 2004/2005

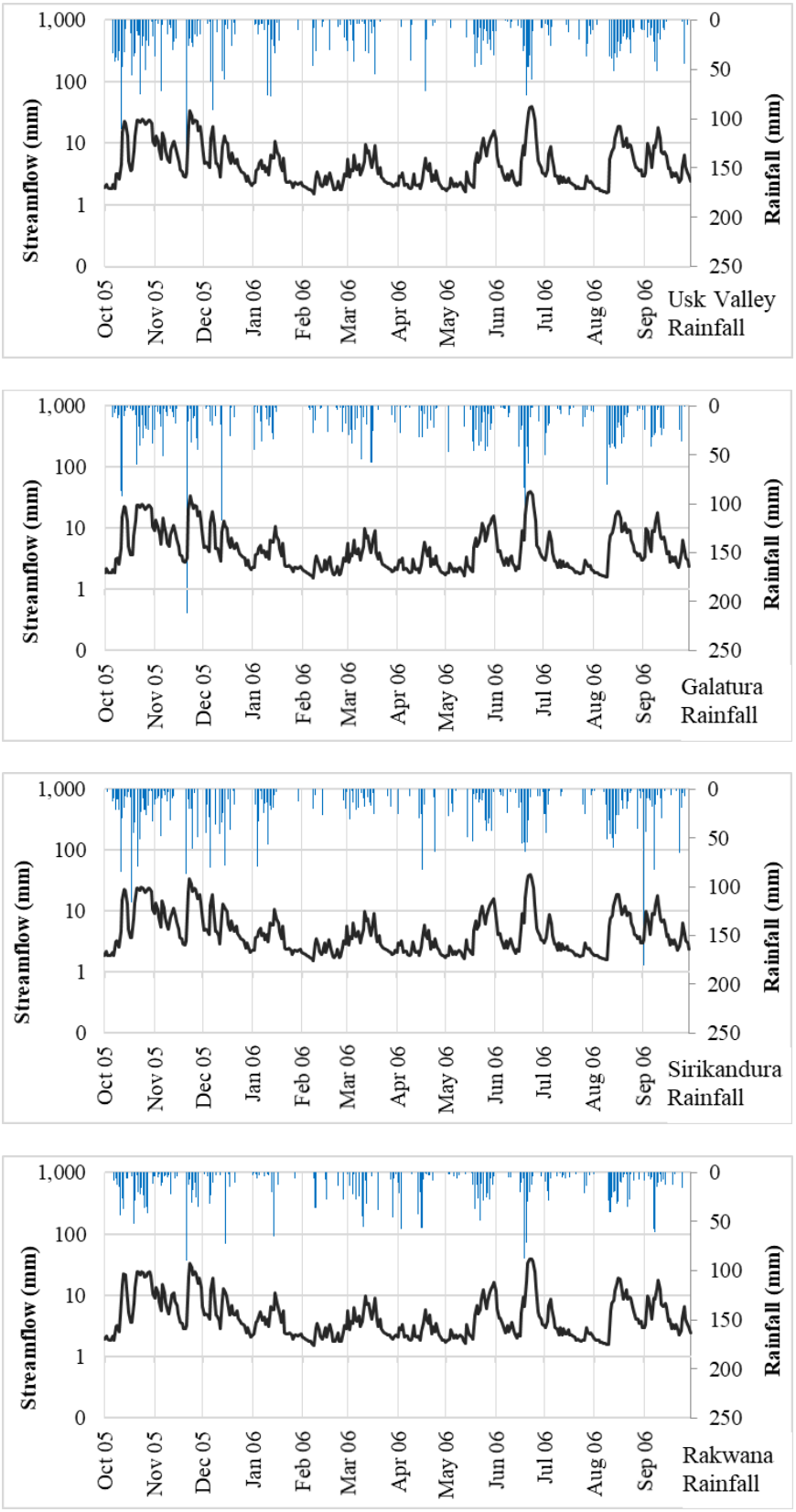

Figure I-2: Streamflow response to rainfall in Millakanda watershed in 2005/2006

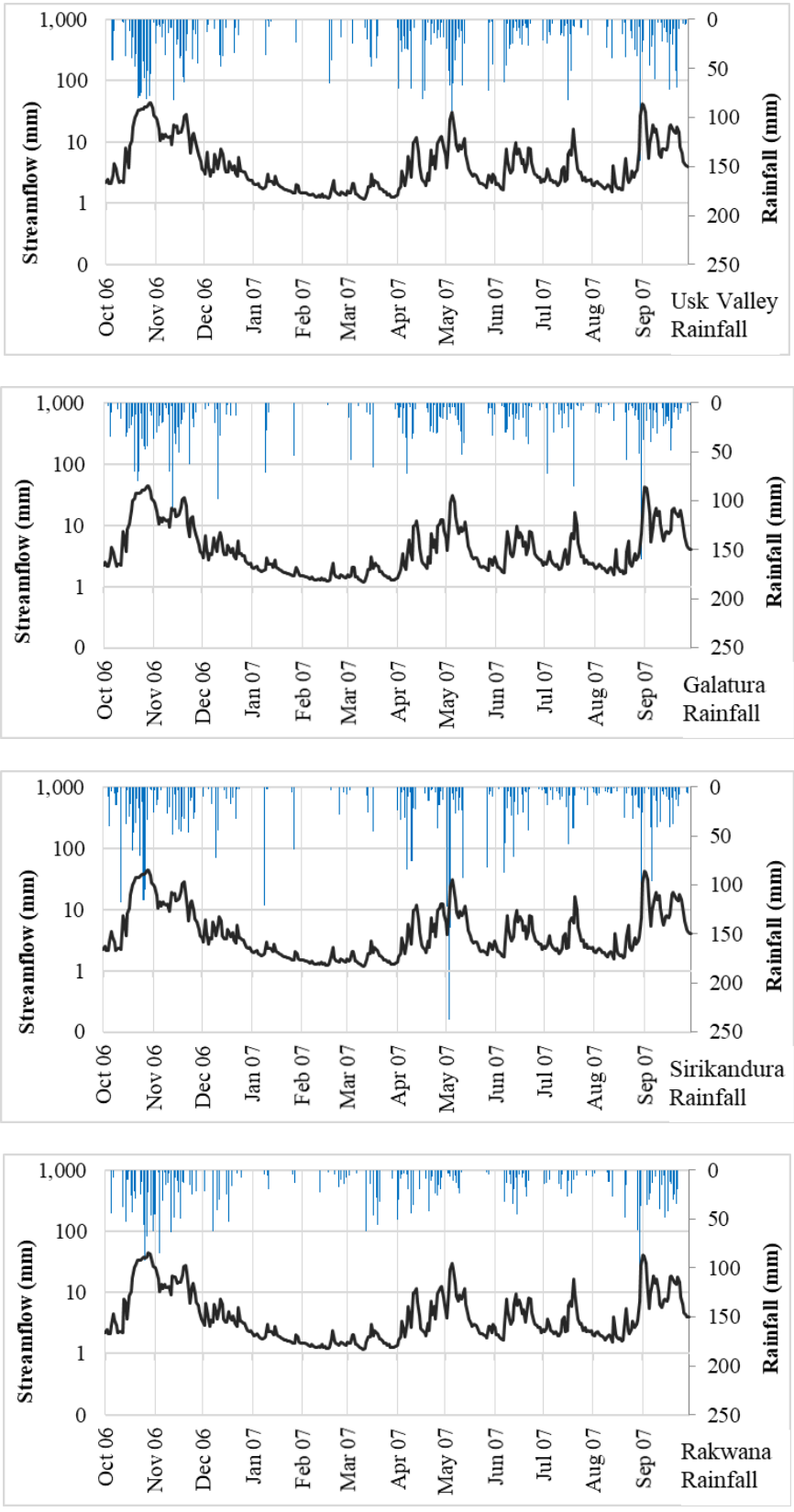

Figure I-3: Streamflow response to rainfall in Millakanda watershed in 2006/2007

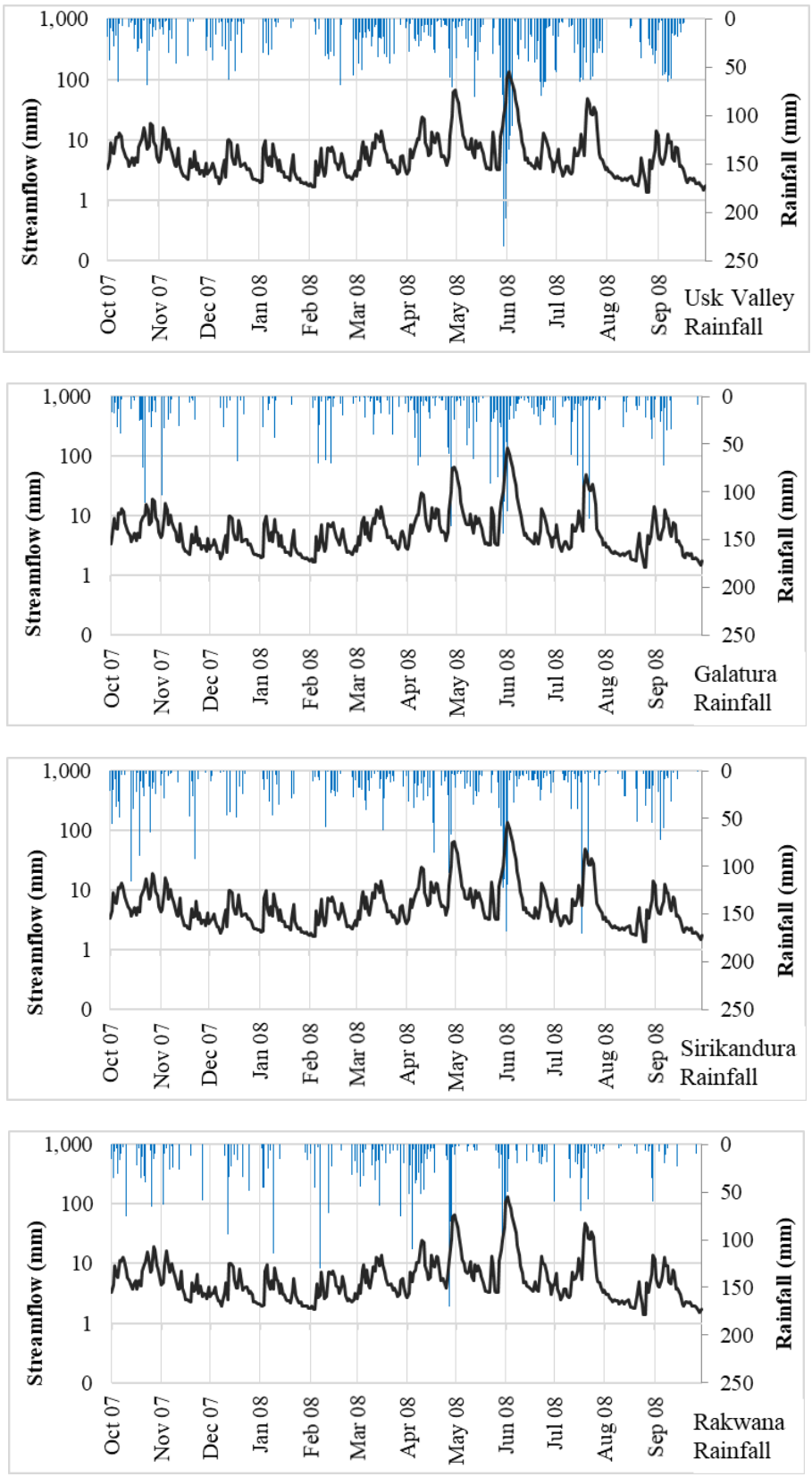

Figure I-4: Streamflow response to rainfall in Millakanda watershed in 2007/2008

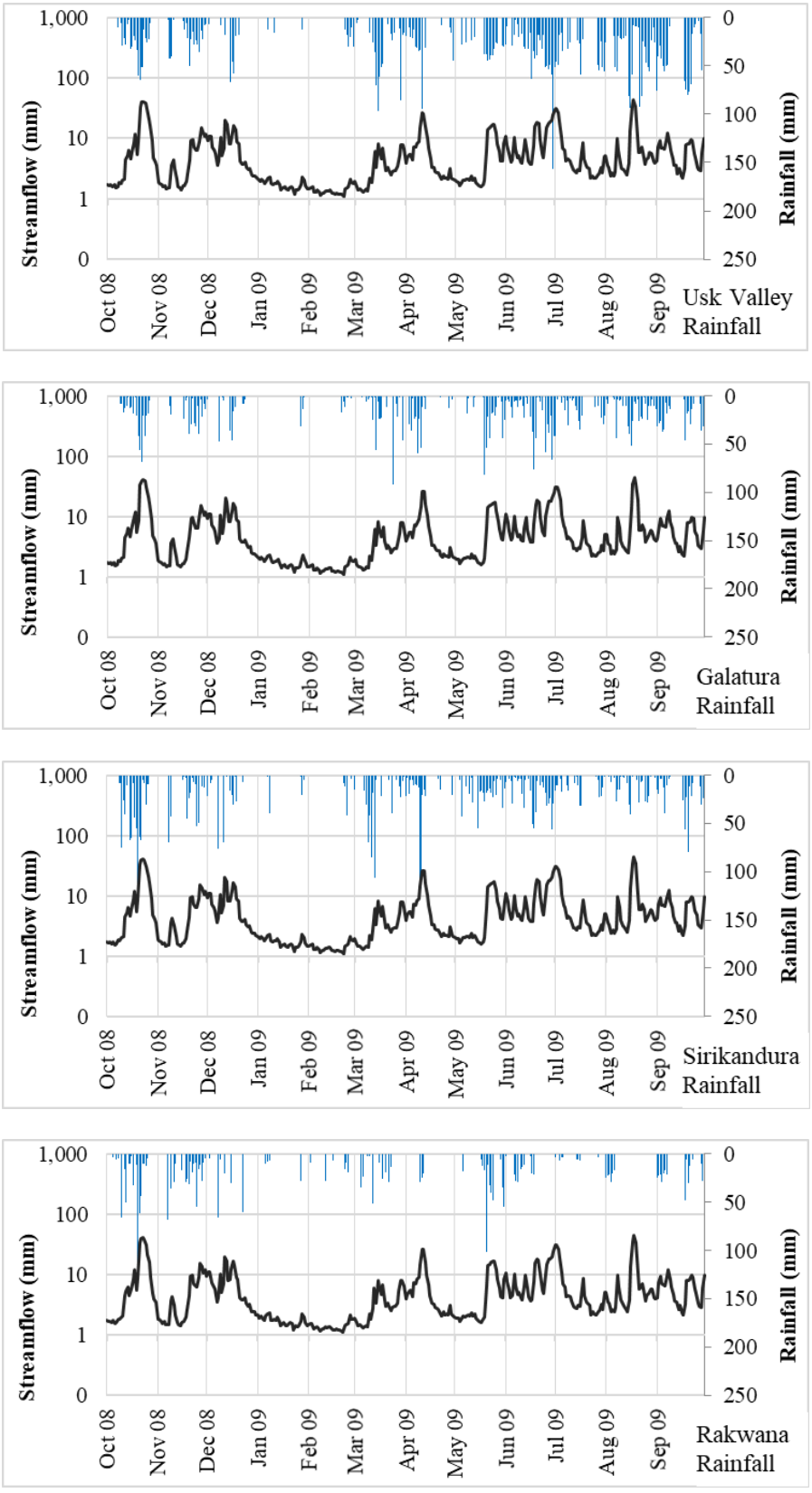

Figure I-5: Streamflow response to rainfall in Millakanda watershed in 2008/2009

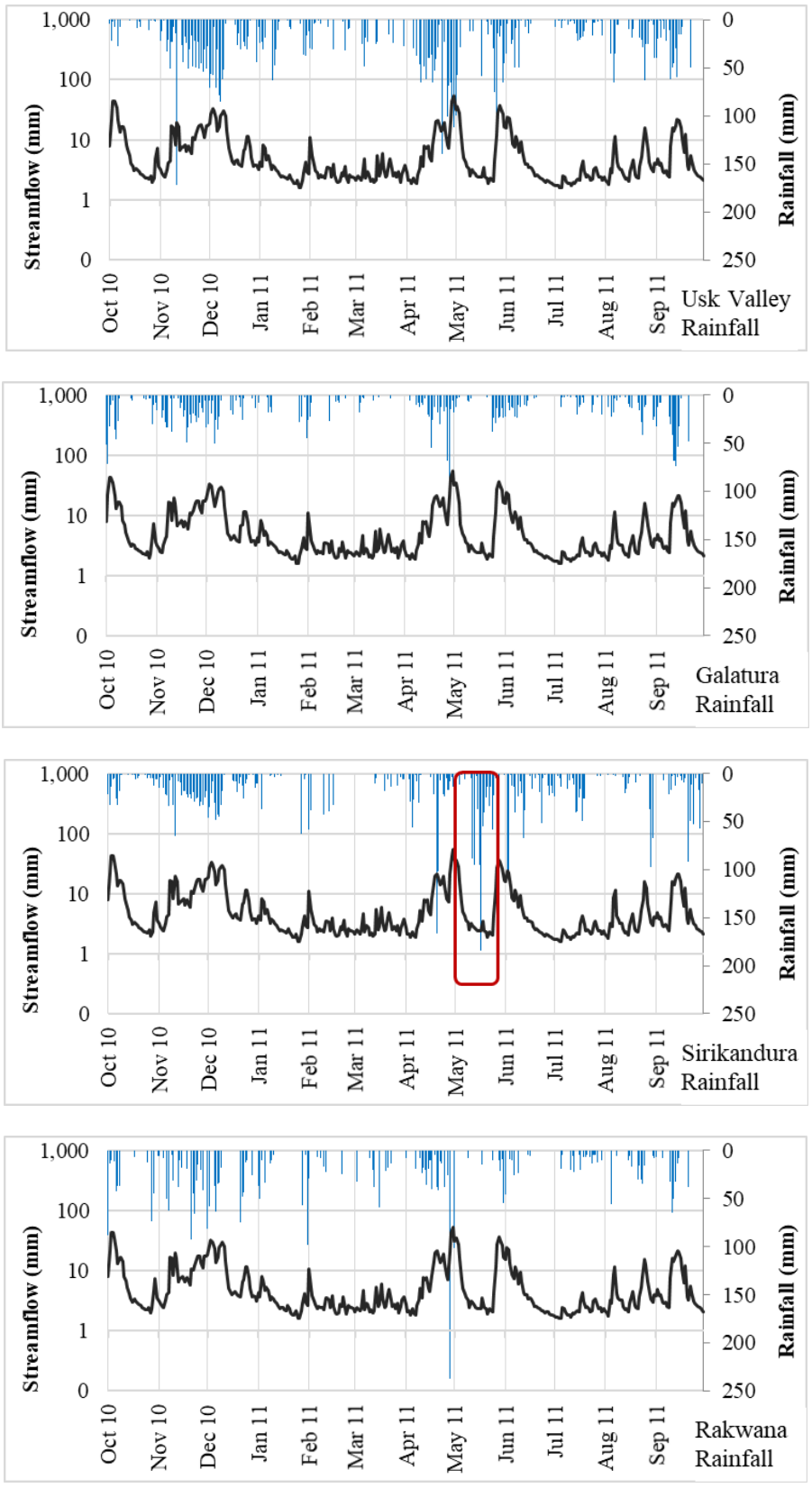

Figure I-6: Streamflow response to rainfall in Millakanda watershed in 2010/2011

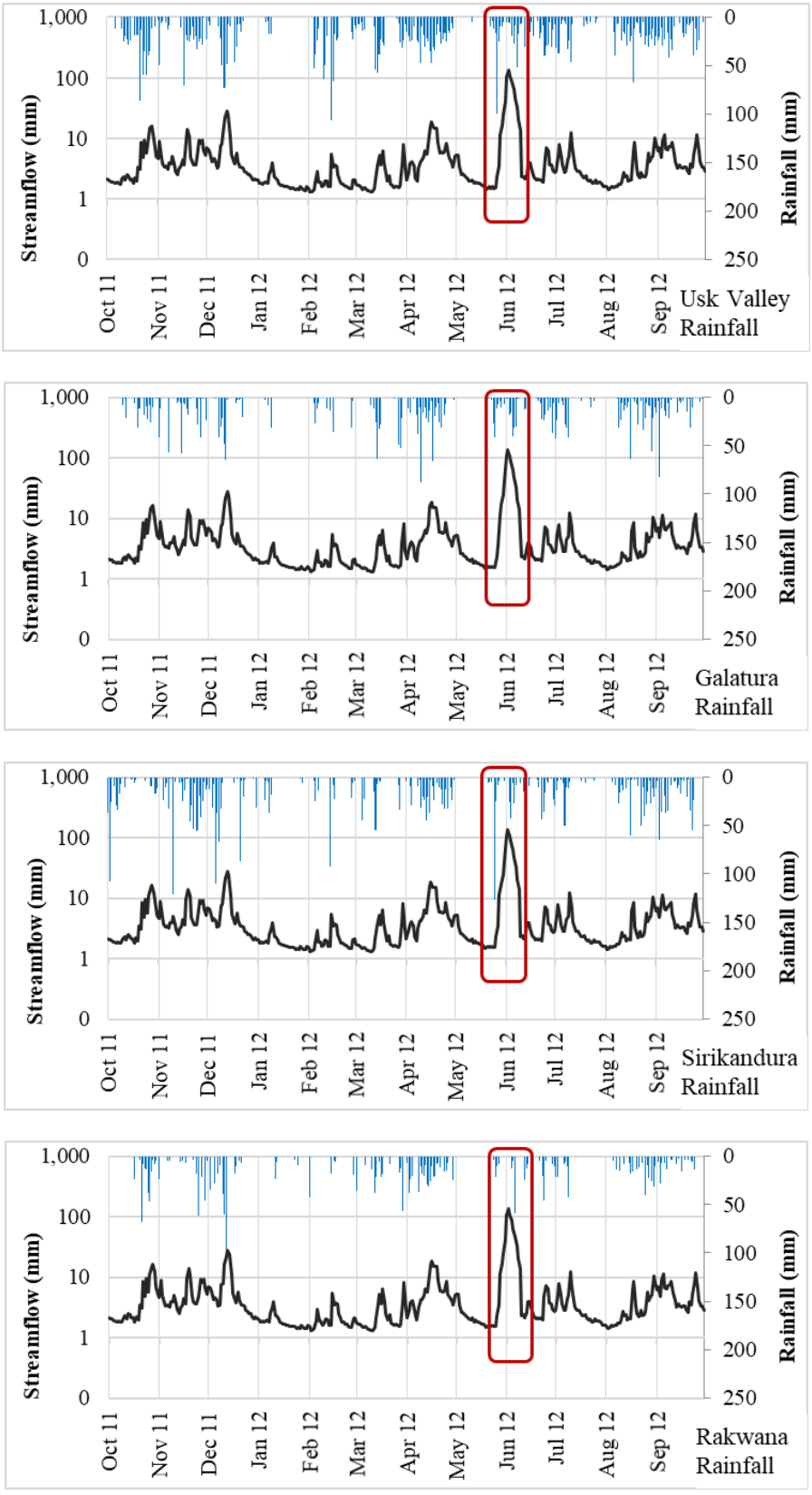

Figure I-7: Streamflow response to rainfall in Millakanda watershed in 2011/2012

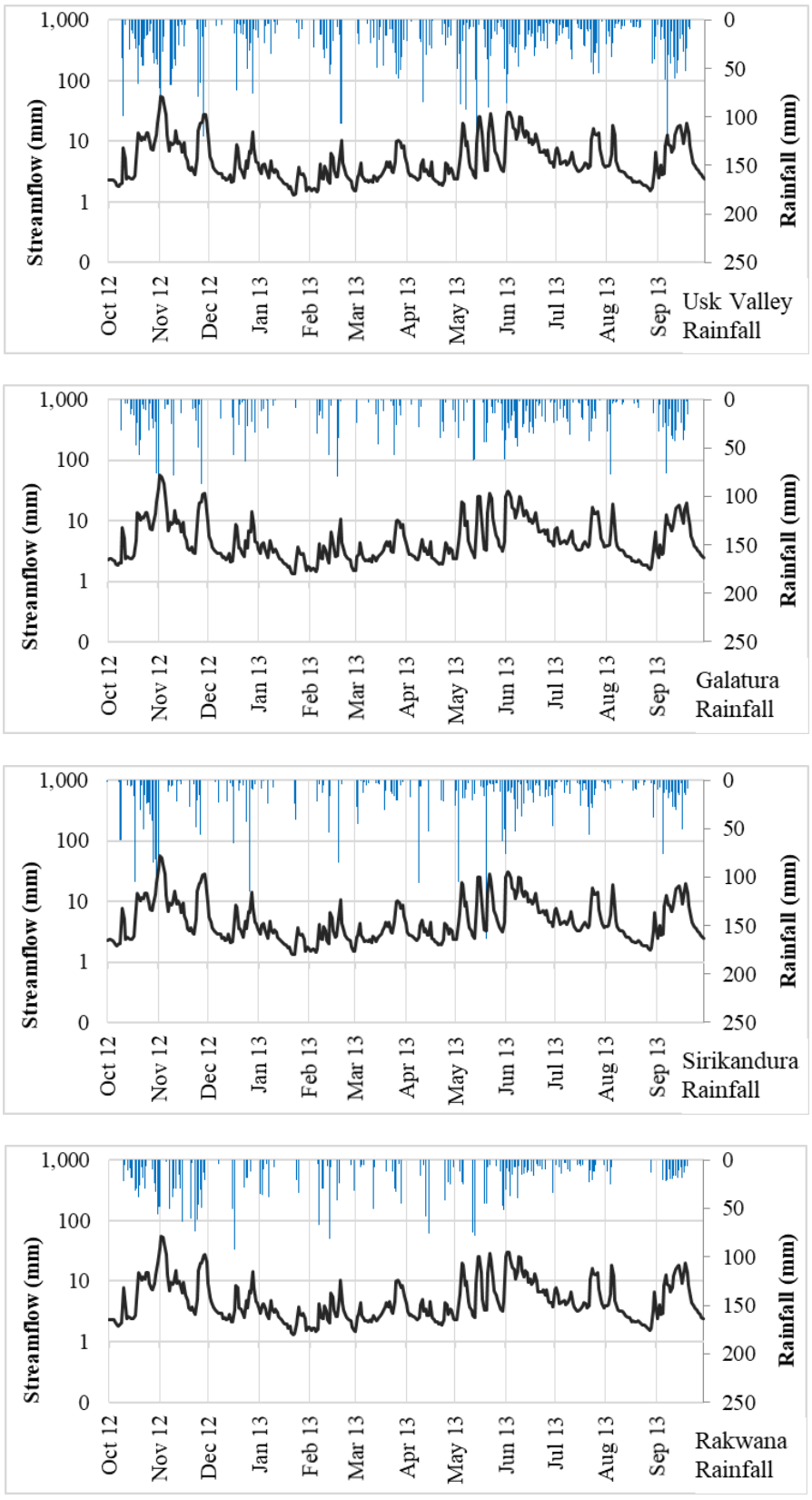

Figure I-8: Streamflow response to rainfall in Millakanda watershed in 2012/2013

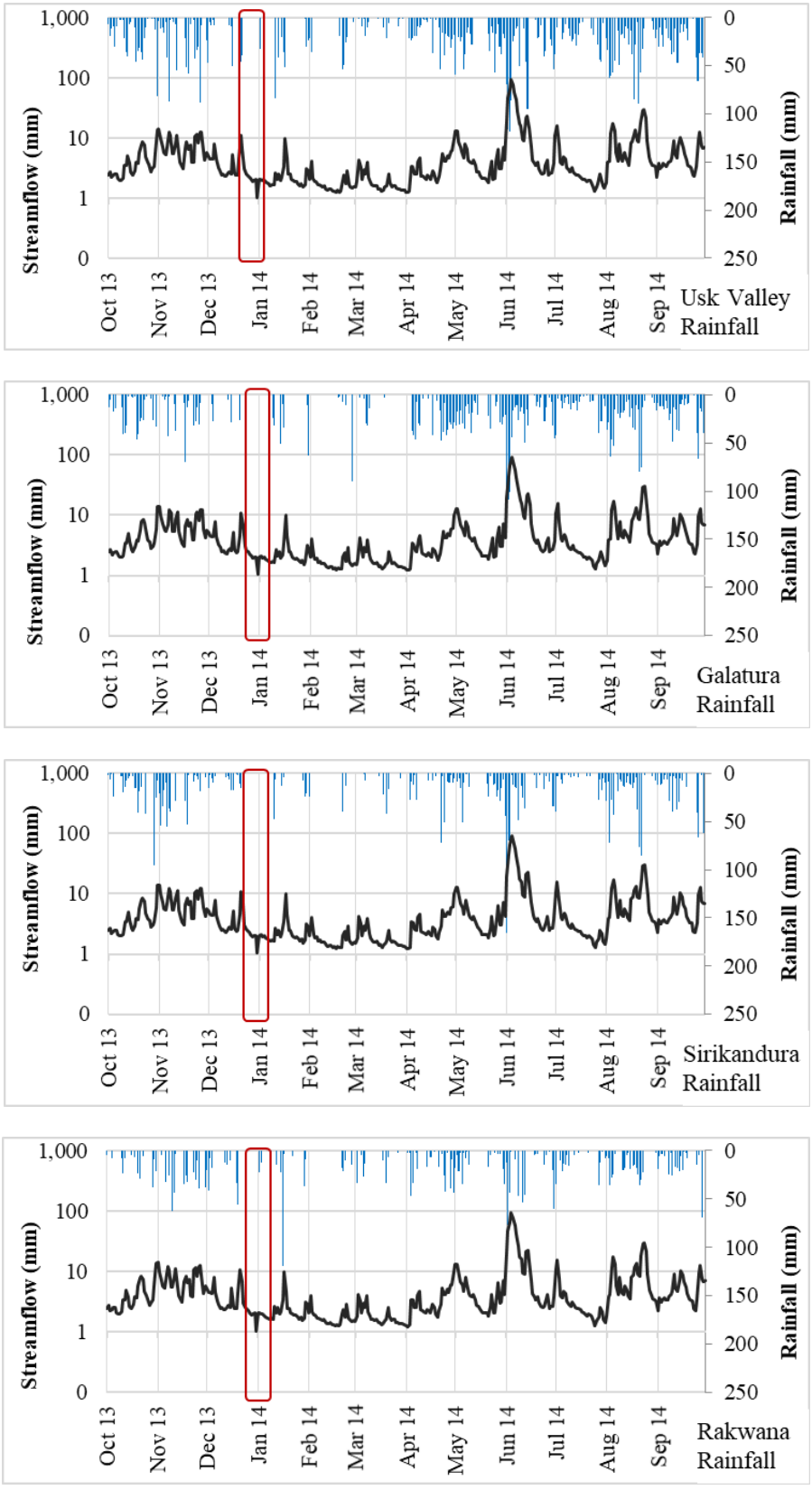

Figure I-9: Streamflow response to rainfall in Millakanda watershed in 2013/2014

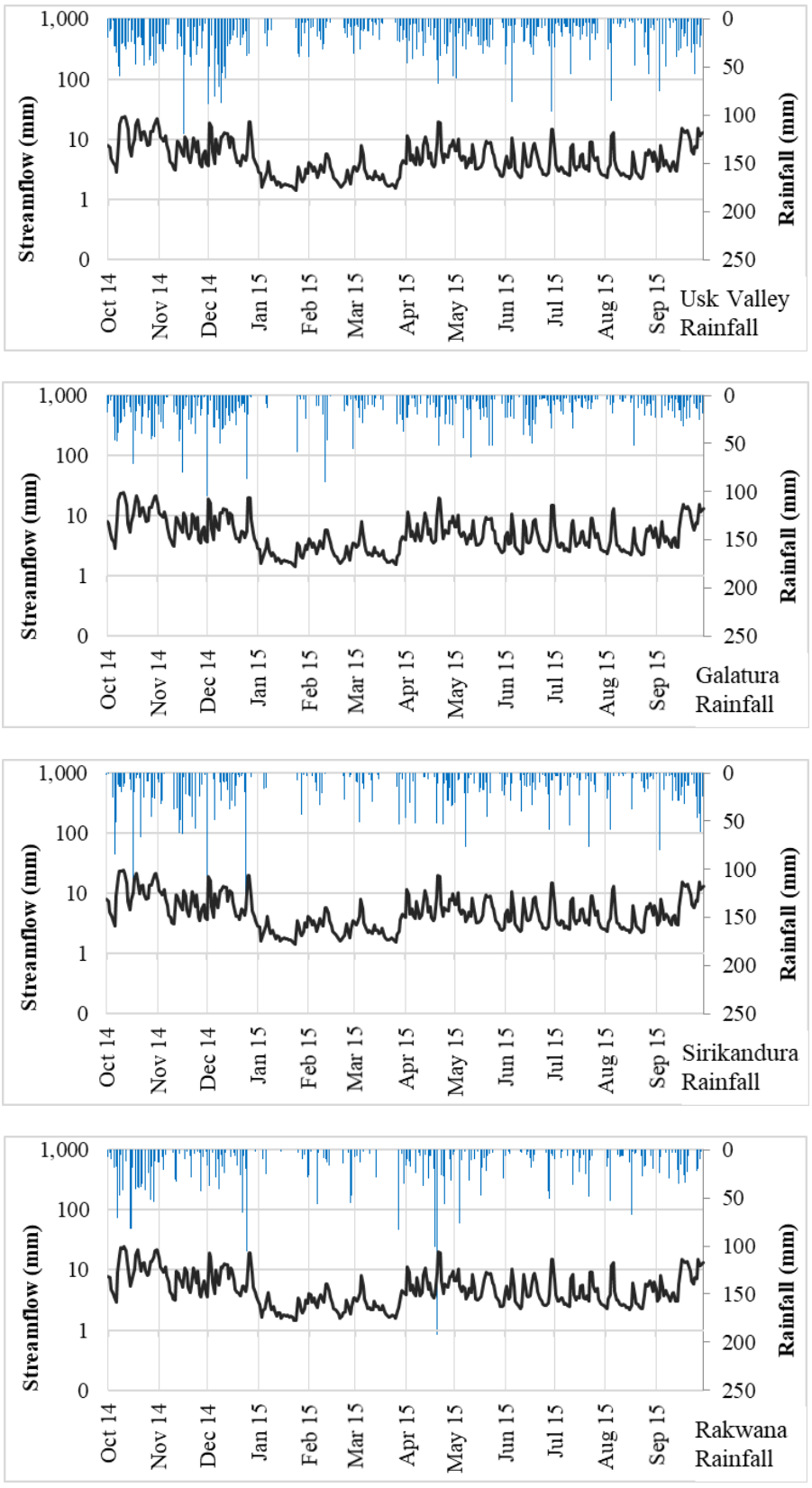

Figure I-10: Streamflow response to rainfall in Millakanda watershed in 2014/2015

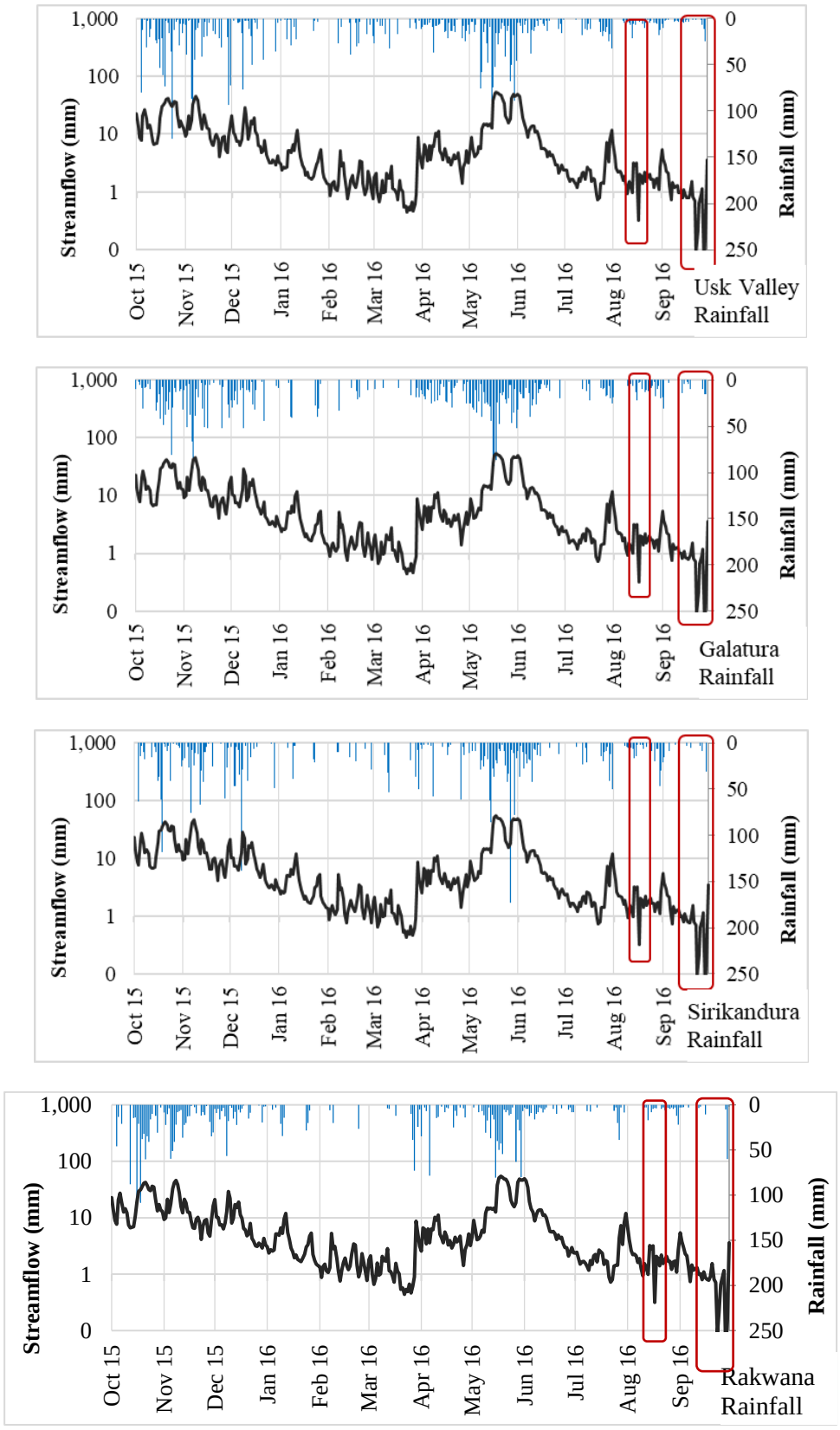

Figure I-11: Streamflow response to rainfall in Millakanda watershed in 2015/2016

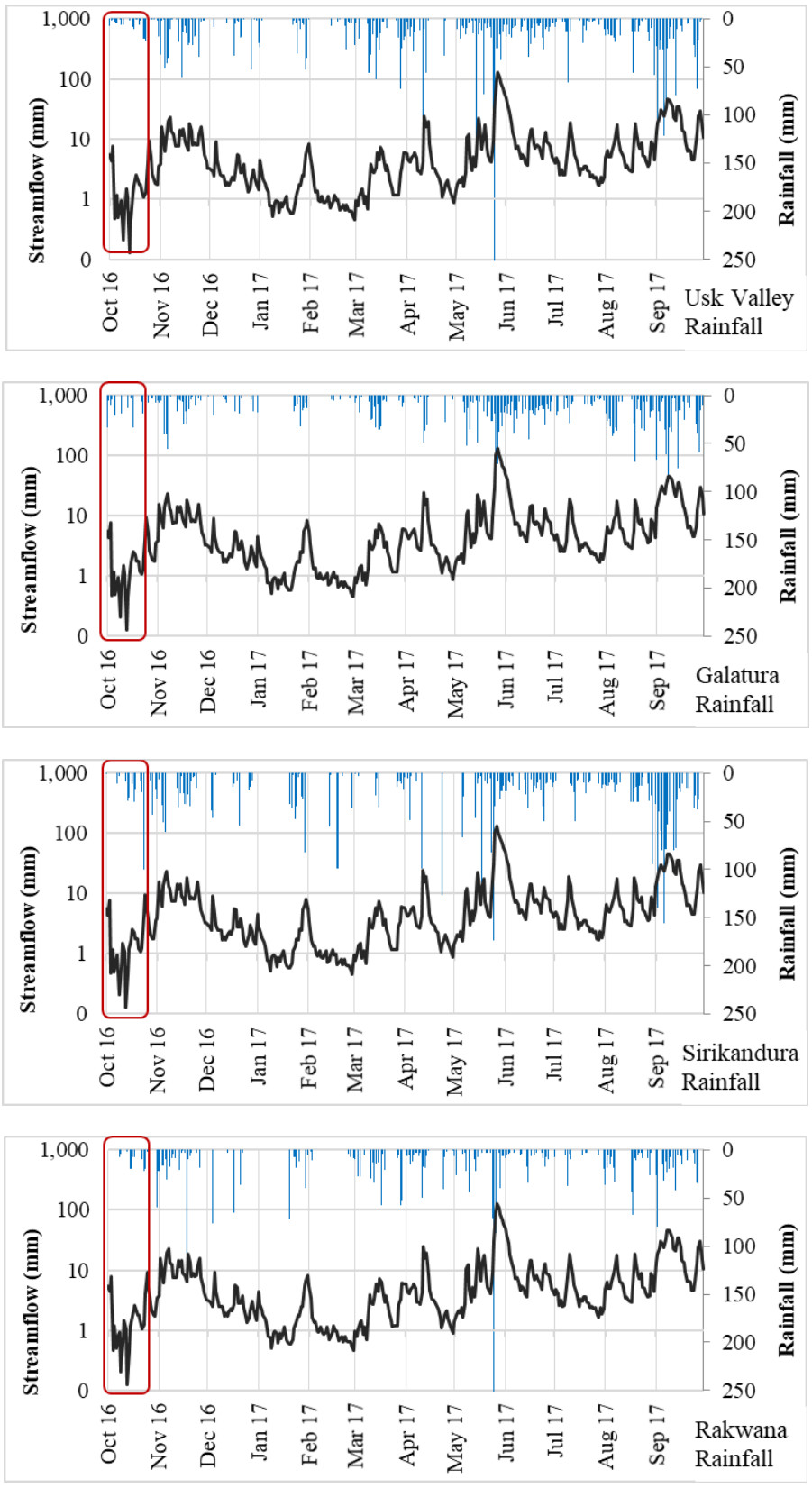

Figure I-12: Streamflow response to rainfall in Millakanda watershed in 2016/2017

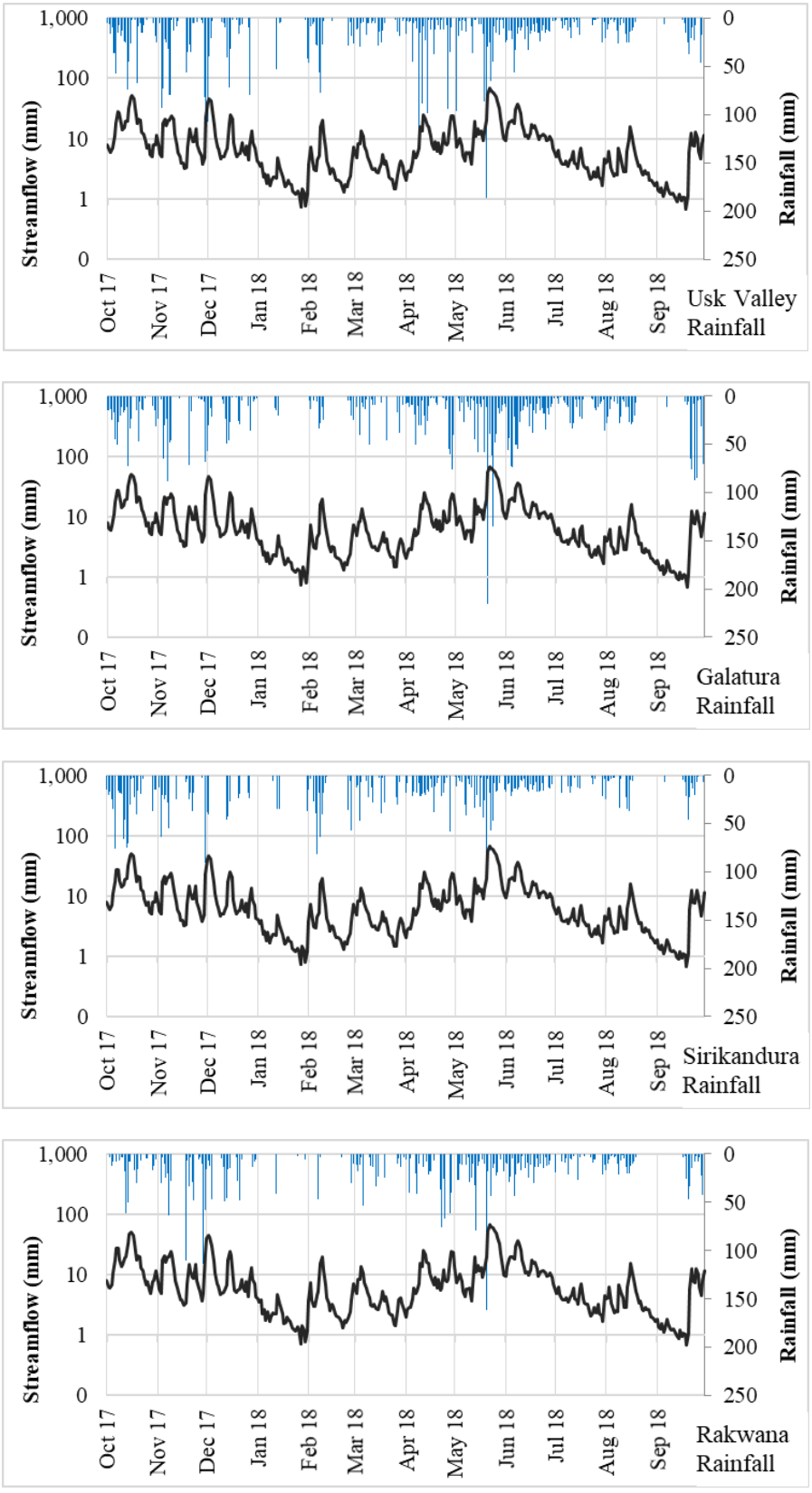

Figure I-13: Streamflow response to rainfall in Millakanda watershed in 2017/2018

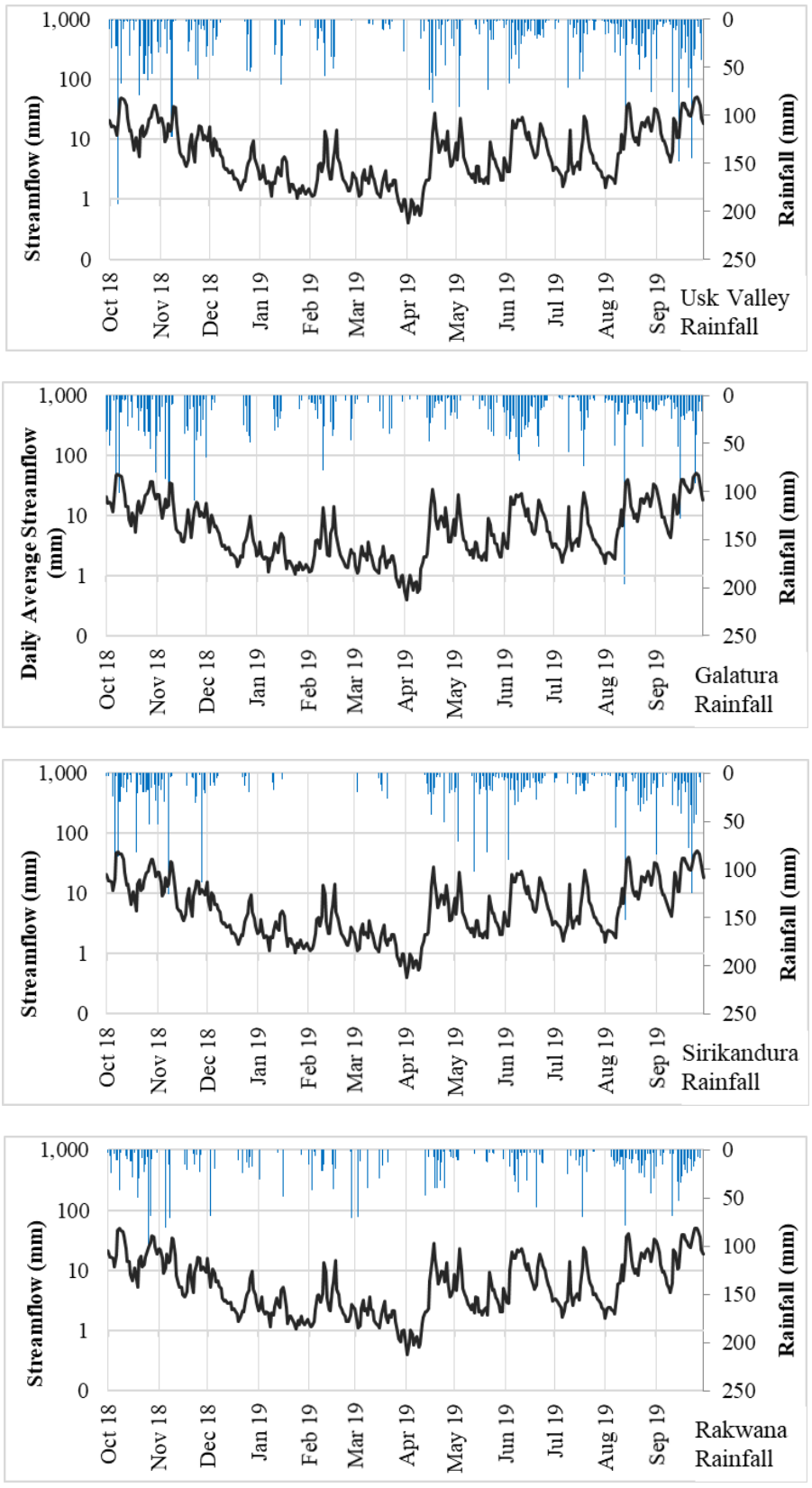

Figure I-14: Streamflow response to rainfall in Millakanda watershed in 2018/2019

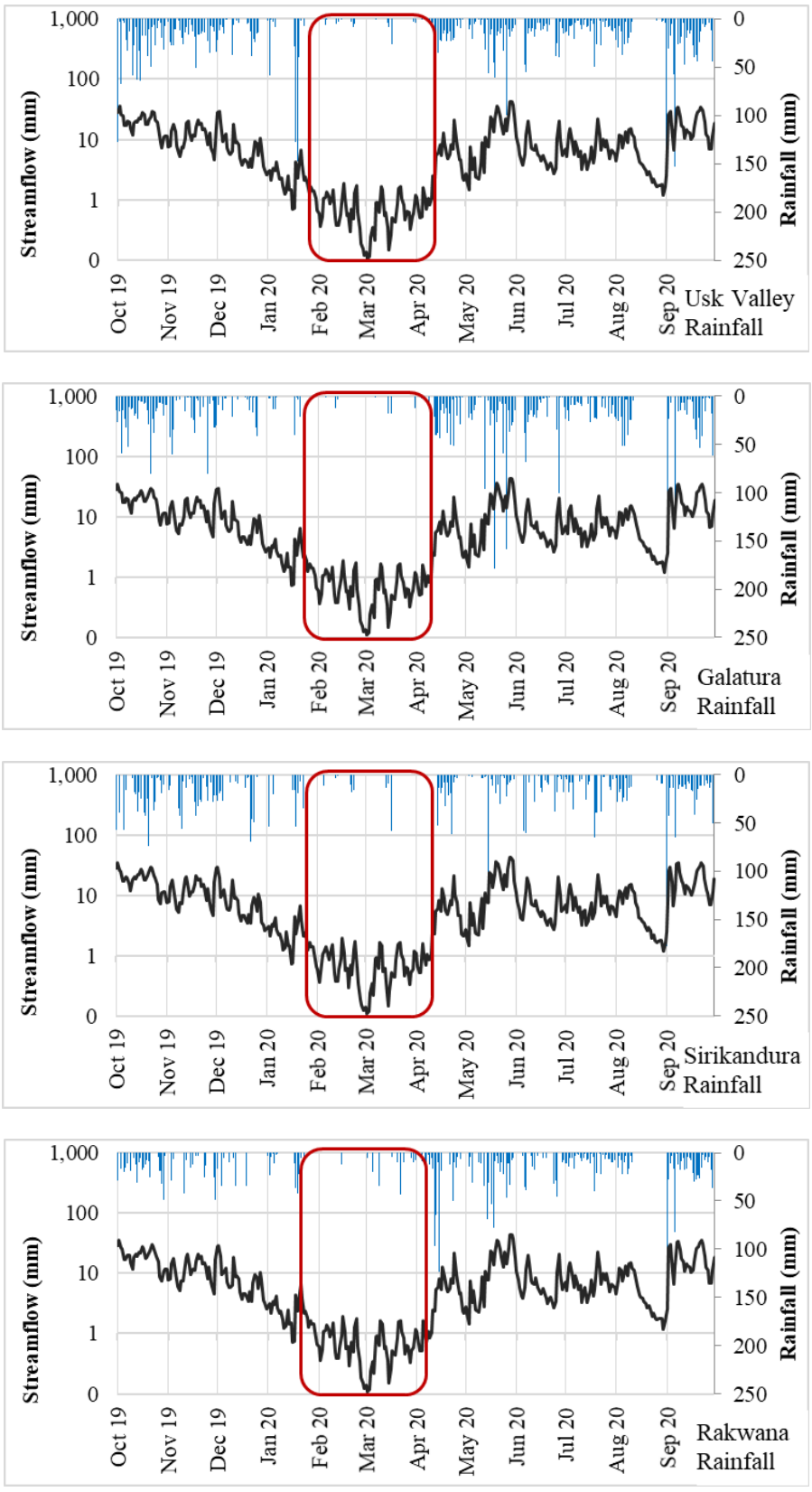

Figure I-15: Streamflow response to rainfall in Millakanda watershed in 2019/2020

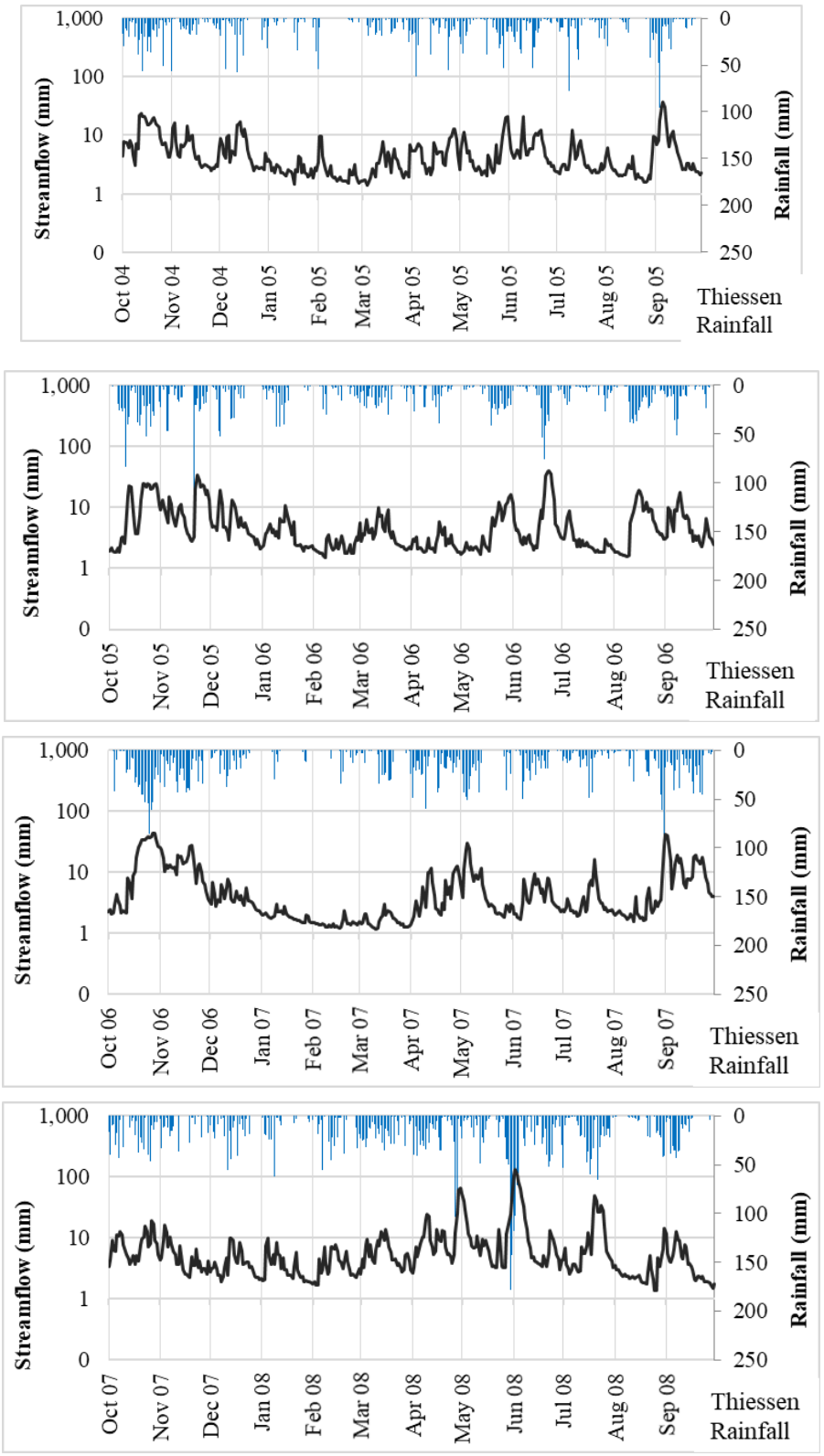

Figure I-16: Streamflow response to Thiessen Average rainfall in Millakanda watershed in Oct/2004 – Sep/2008

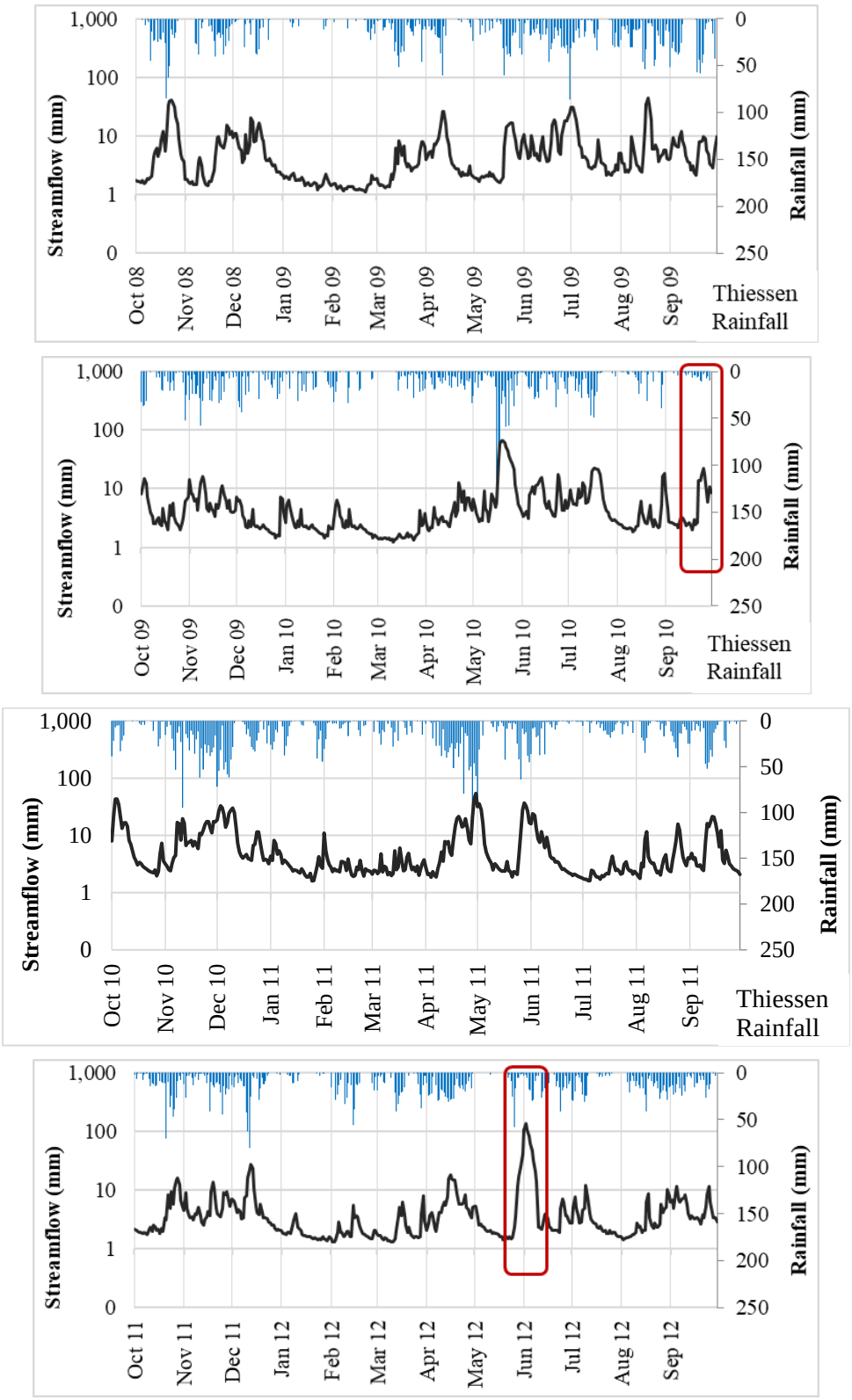

Figure I-17: Streamflow response to Thiessen Average rainfall in Millakanda watershed in Oct/2008 – Sep/2012

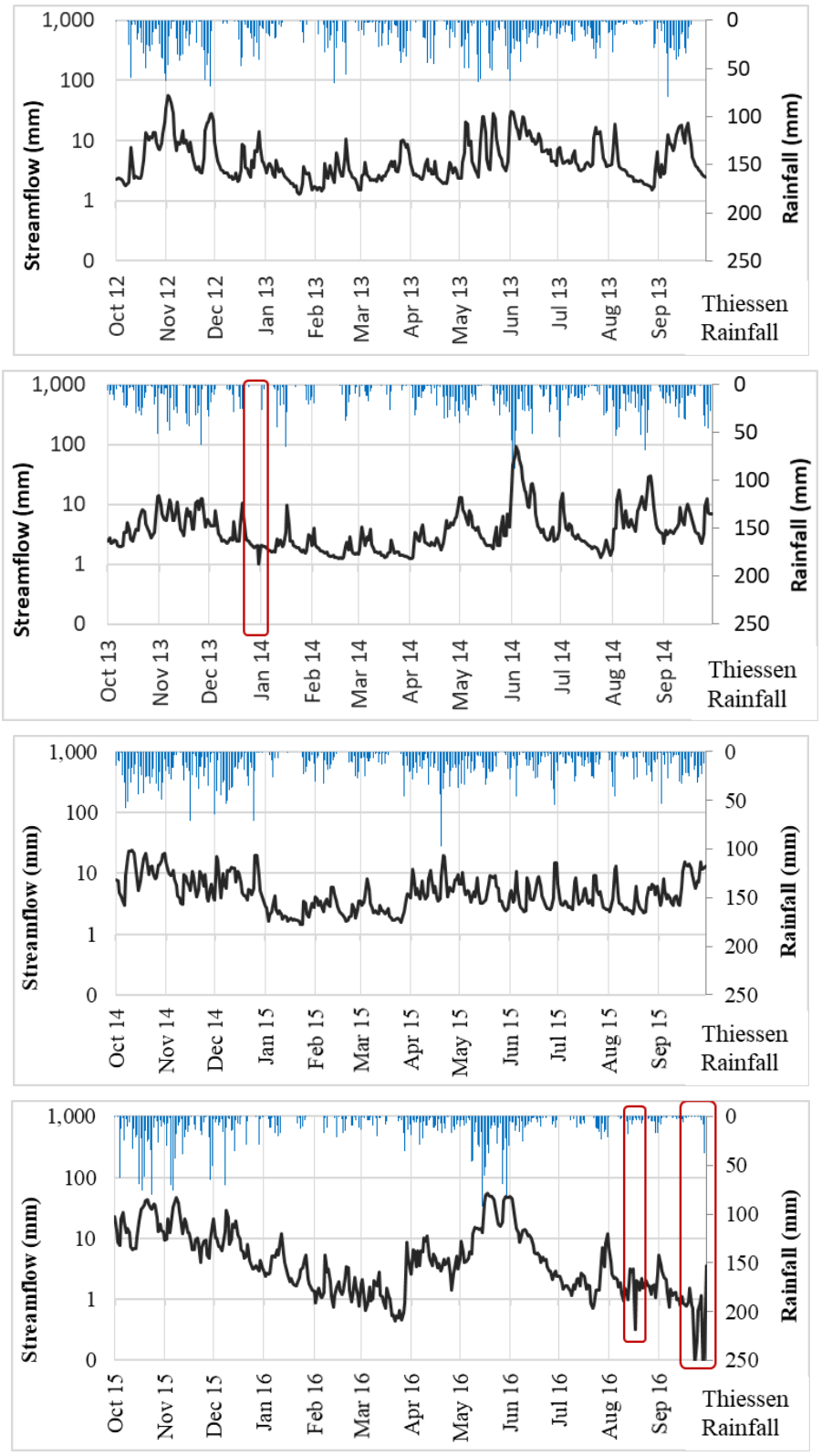

Figure I-18: Streamflow response to Thiessen Average rainfall in Millakanda watershed in Oct/2012 – Sep/2016

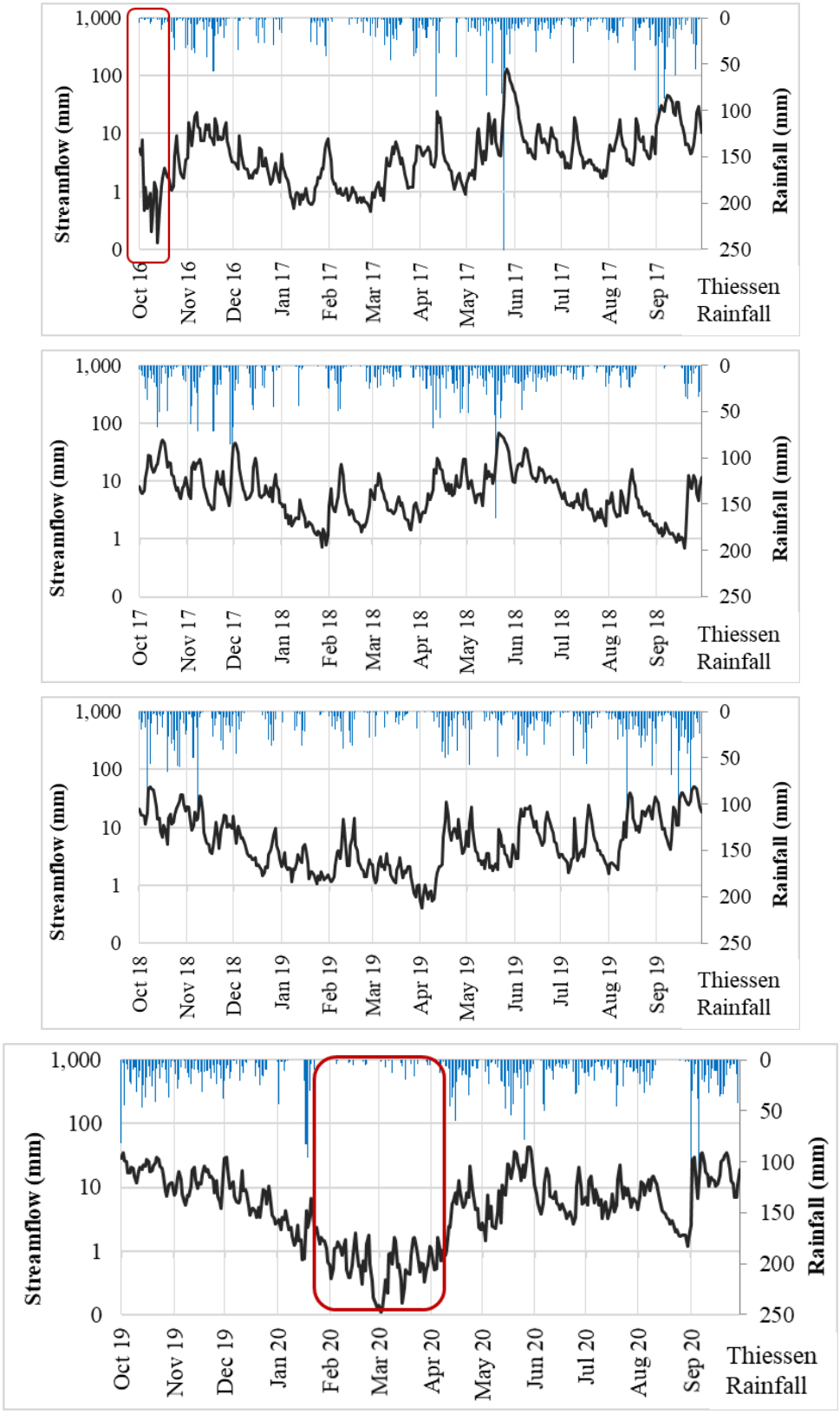

Figure I-19: Streamflow response to Thiessen Average rainfall in Millakanda watershed in Oct/2016 – Sep/2020

ANNEXURE II

II. SINGLE MASS CURVE AND DOUBLE MASS CURVE

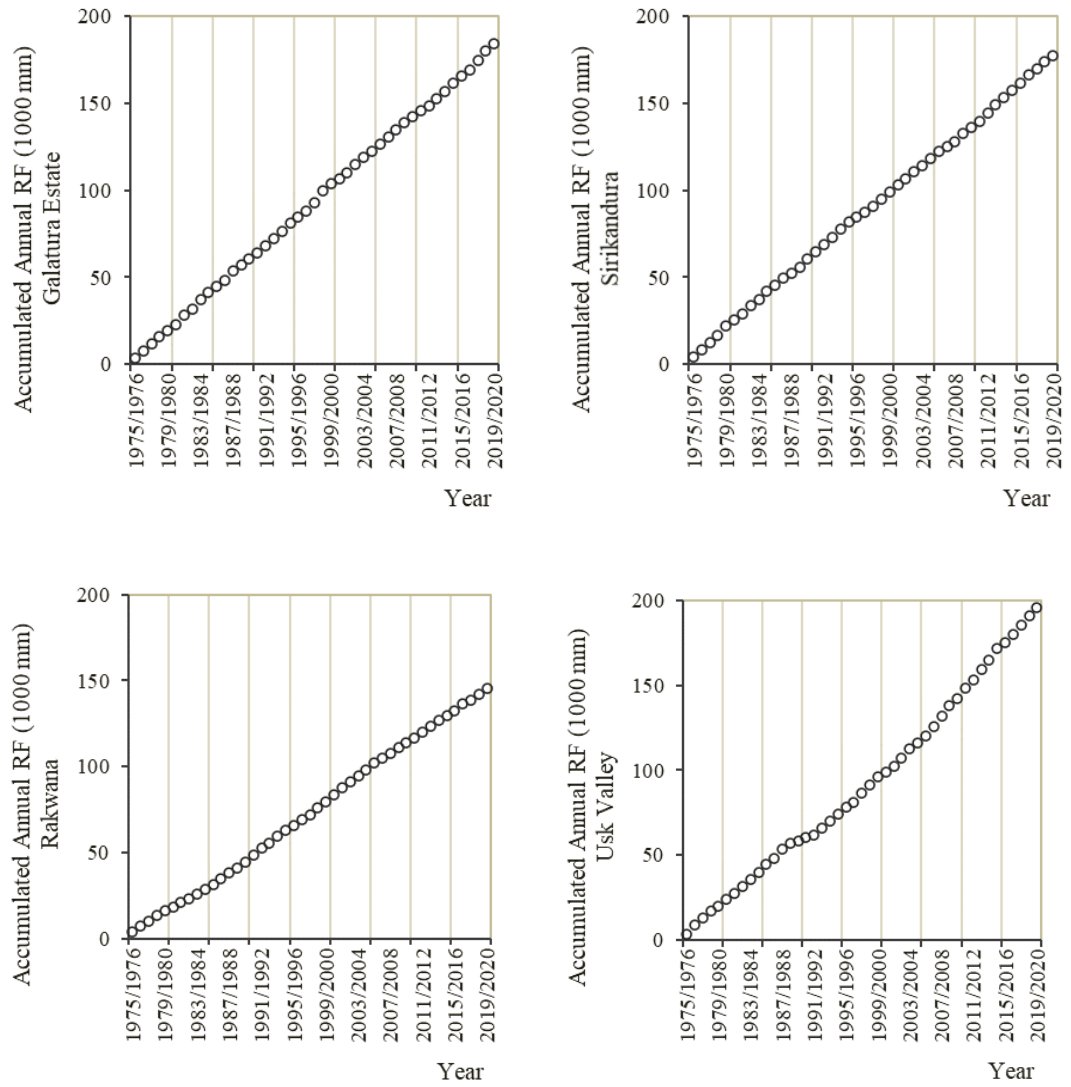

Figure II-1: Single mass curves

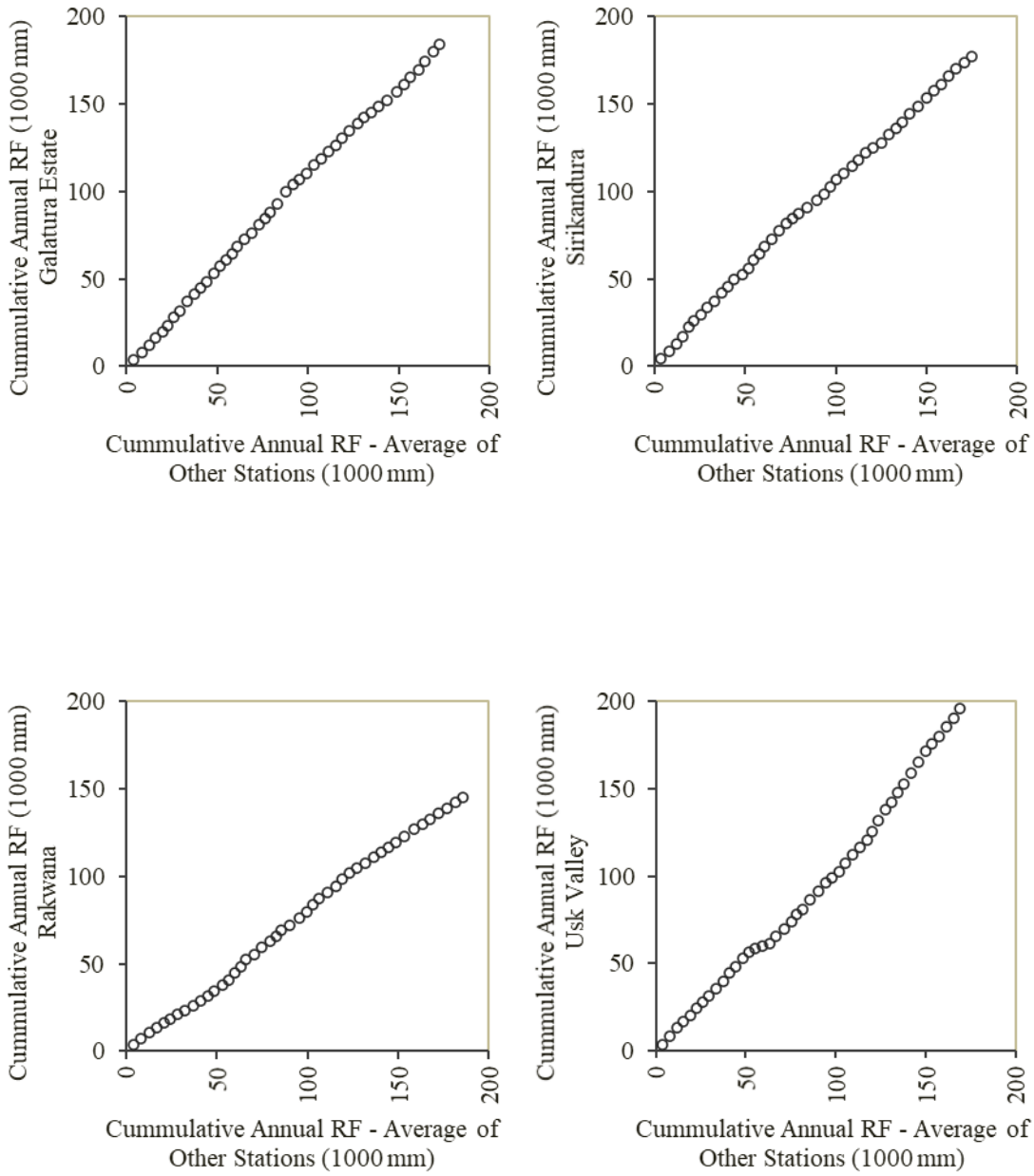

Figure II-2: Double mass curves

ANNEXURE III

III. DRY SPELL CHARACTERISTICS OF HISTORICAL PERIOD (COMPARING OBSERVED AND BIAS-CORRECTED RCM DATA)

Table III-1: Comparison of the response of the average dry spell length between the bias coerced RCM precipitation data and the observed precipitation data (1976 to 2005).

Month	Average dry spell length (days)		
	Observed	Bias Corrected RCM	Difference
January	8.0	7.0	1
February	9.0	15.0	-6
March	6.0	7.0	-1
April	4.0	4.0	0
May	3.0	4.0	-1
June	4.0	4.0	0
July	4.0	4.0	0
August	6.0	6.0	0
September	4.0	2.0	2
October	3.0	7.0	-4
November	3.0	2.0	1
December	4.0	3.0	1

Table III-2: Comparison of the response of the maximum dry spell length between the bias coerced RCM precipitation data and the observed precipitation data (1976 to 2005)

Month	Max. dry spell length (days)		
	Observed	Bias Corrected RCM	Difference
January	44.0	45.0	-1
February	64.0	82.0	-18
March	47.0	60.0	-13
April	19.0	18.0	1
May	17.0	21.0	-4
June	23.0	19.0	4
July	39.0	23.0	16
August	32.0	33.0	-1
September	40.0	25.0	15
October	21.0	60.0	-39
November	22.0	8.0	14
December	17.0	18.0	-1

Table III-3: Comparison of the response of the standard deviation of dry spell length between the bias coerced RCM precipitation data and the observed precipitation data (1976 to 2005)

Month	Standard deviation of dry spell length (days)		
	Observed	Bias Corrected RCM	Difference
January	8.0	7.0	1
February	12.0	18.0	-6
March	8.0	8.0	0
April	3.0	4.0	-1
May	3.0	4.0	-1
June	4.0	4.0	0
July	5.0	4.0	1
August	6.0	7.0	-1
September	6.0	3.0	3
October	3.0	8.0	-5
November	3.0	1.0	2
December	4.0	3.0	1

Table III-4: Comparison of the response of the 90th percentile dry spell length between the bias coerced RCM precipitation data and the observed precipitation data (1976 to 2005)

Month	90th percentile dry spell length (days)		
	Observed	Bias Corrected RCM	Difference
January	18.0	16.0	2
February	20.0	31.0	-11
March	14.0	16.0	-2
April	9.0	12.0	-3
May	7.0	10.0	-3
June	8.0	11.0	-3
July	9.0	9.0	0
August	14.0	16.0	-2
September	10.0	3.0	7
October	7.0	15.0	-8
November	6.0	3.0	3
December	9.0	6.0	3

Table III-5: Comparison of the response of the 95th percentile dry spell length between the bias coerced RCM precipitation data and the observed precipitation data (1976 to 2005)

Month	95th percentile dry spell length (days)		
	Observed	Bias Corrected RCM	Difference
January	21.0	21.0	0
February	35.0	51.0	-16
March	18.0	19.0	-1
April	10.0	16.0	-6
May	9.0	12.0	-3
June	10.0	13.0	-3
July	13.0	11.0	2
August	19.0	24.0	-5
September	16.0	7.0	9
October	10.0	21.0	-11
November	8.0	4.0	4
December	12.0	9.0	3

Table III-6: Comparison of the response of the 99th percentile dry spell length between the bias coerced RCM precipitation data and the observed precipitation data (1976 to 2005)

Month	99th percentile dry spell length (days)		
	Observed	Bias Corrected RCM	Difference
January	29.0	28.0	1
February	56.0	81.0	-25
March	39.0	27.0	12
April	16.0	16.0	0
May	14.0	17.0	-3
June	19.0	19.0	0
July	21.0	20.0	1
August	28.0	28.0	0
September	25.0	12.0	13
October	15.0	34.0	-19
November	14.0	6.0	8
December	17.0	14.0	3

ANNEXURE IV

IV. ANALYSIS OF MONTHLY AND SEASONAL MEANS OF OBSERVED, RCM, AND BIAS-CORRECTED RCM RAINFALL

Table IV-1: S1 - Monthly and seasonal means of observed rainfall, RCM rainfall, and bias-corrected RCM rainfall over evaluation period (2001 to 2005)

Type	Month	Precipitation (mm)		
		Observed	RCM raw data	Bias corrected RCM data
Monthly Means	October	205	143	205
	November	131	126	131
	December	251	234	251
	January	403	323	403
	February	451	371	451
	March	285	362	285
	April	279	244	279
	May	159	244	159
	June	342	372	342
	July	528	475	528
	August	368	392	368
	September	292	290	292
Seasonal Means	SWM	1,515	1,593	1,515
	NEM	629	560	629
	1st IM	654	558	654
	2nd IM	896	867	896

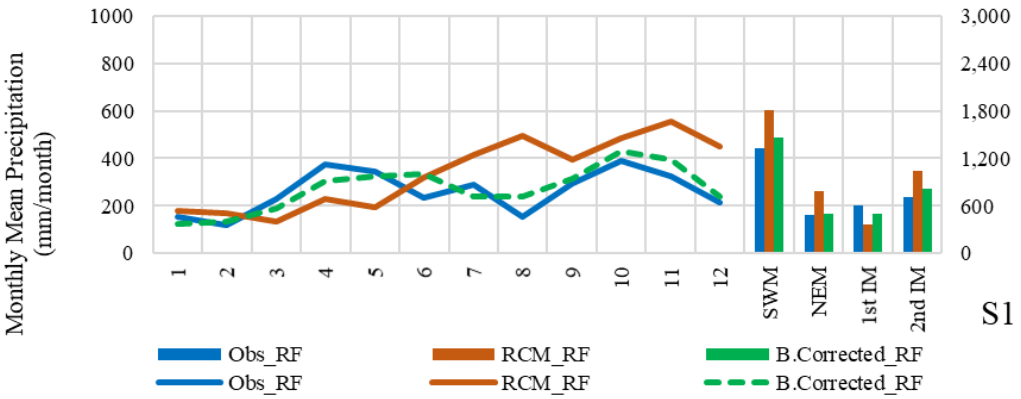

Figure IV-1: S1 - Variation of monthly and seasonal means of observed rainfall, RCM rainfall, and bias-corrected RCM rainfall over evaluation period (2001 to 2005)

Table IV-2: S2 - Monthly and seasonal means of observed rainfall, RCM rainfall, and bias-corrected RCM rainfall over evaluation period (2001 to 2005)

Type	Month	Precipitation (mm)		
		Observed	RCM raw data	Bias corrected RCM data
Monthly Means	October	237	178	155
	November	139	111	118
	December	269	115	264
	January	420	184	326
	February	518	198	400
	March	306	548	375
	April	263	728	247
	May	158	873	248
	June	367	599	402
	July	615	390	497
	August	392	470	390
	September	341	438	315
Seasonal Means	SWM	1,611	2,945	1,673
	NEM	717	727	588
	1st IM	688	299	590
	2nd IM	1,008	859	887

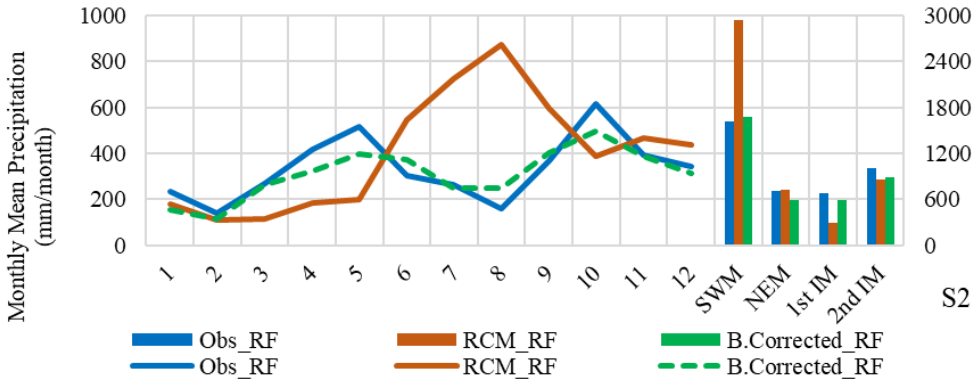

Figure IV-2: S2- Variation of monthly and seasonal means of observed rainfall, RCM rainfall, and bias-corrected RCM rainfall over evaluation period (2001 to 2005)

Table IV-3: S3 - Monthly and seasonal means of observed rainfall, RCM rainfall, and bias-corrected RCM rainfall over evaluation period (2001 to 2005)

Type	Month	Precipitation (mm)		
		Observed	RCM raw data	Bias corrected RCM data
Monthly Means	October	263	218	163
	November	148	126	120
	December	270	134	282
	January	448	226	343
	February	555	222	406
	March	328	547	374
	April	264	717	237
	May	157	851	246
	June	368	603	410
	July	639	458	518
	August	414	541	391
	September	364	507	338
Seasonal Means	SWM	1,672	2,939	1,672
	NEM	775	851	621
	1st IM	718	360	625
	2nd IM	1,053	1,000	909

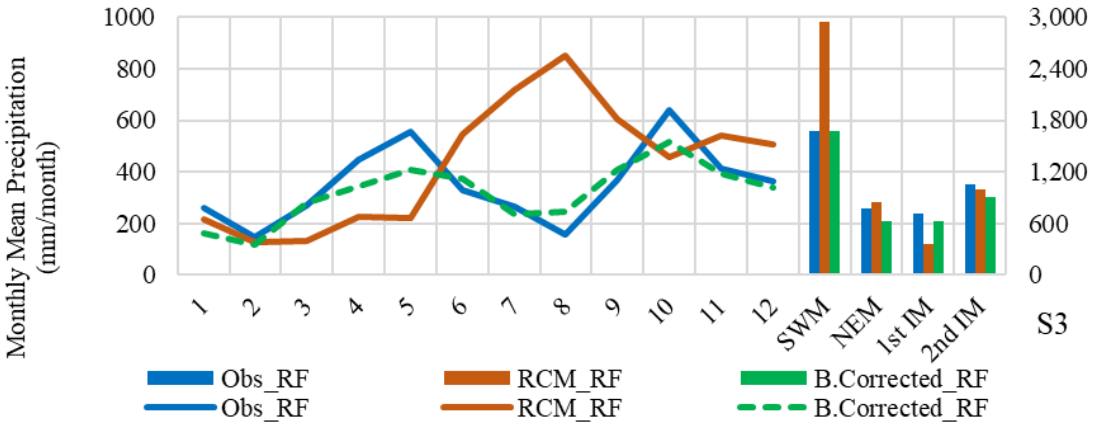

Figure IV-3: S3-Variation of monthly and seasonal means of observed rainfall, RCM rainfall, and bias-corrected RCM rainfall over evaluation period (2001 to 2005)

Table IV-4: S4 - Monthly and seasonal means of observed rainfall, RCM rainfall, and bias-corrected RCM rainfall over evaluation period (2001 to 2005)

Type	Month	Precipitation (mm)		
		Observed	RCM raw data	Bias corrected RCM data
Monthly Means	October	223	224	149
	November	138	116	119
	December	255	130	277
	January	421	216	344
	February	477	225	374
	March	294	599	357
	April	274	784	237
	May	156	927	237
	June	340	647	378
	July	547	436	479
	August	381	526	390
	September	308	508	302
Seasonal Means	SWM	1,541	3,181	1,584
	NEM	669	847	570
	1st IM	676	347	622
	2nd IM	928	962	869

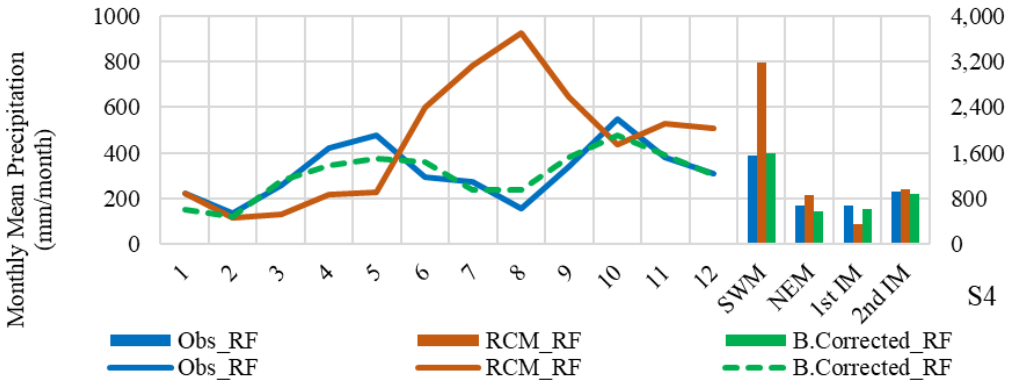

Figure IV-4: S4-Variation of monthly and seasonal means of observed rainfall, RCM rainfall, and bias-corrected RCM rainfall over evaluation period (2001 to 2005)

Table IV-5: S5 - Monthly and seasonal means of observed rainfall, RCM rainfall, and bias-corrected RCM rainfall over evaluation period (2001 to 2005)

Type	Month	Precipitation (mm)		
		Observed	RCM raw data	Bias corrected RCM data
Monthly Means	October	263	224	164
	November	148	116	117
	December	270	130	296
	January	448	216	349
	February	555	225	406
	March	328	599	373
	April	264	784	237
	May	157	927	245
	June	368	647	411
	July	639	436	513
	August	414	526	390
	September	364	508	337
Seasonal Means	SWM	1,672	3,181	1,671
	NEM	775	847	618
	1st IM	718	347	644
	2nd IM	1,053	962	904

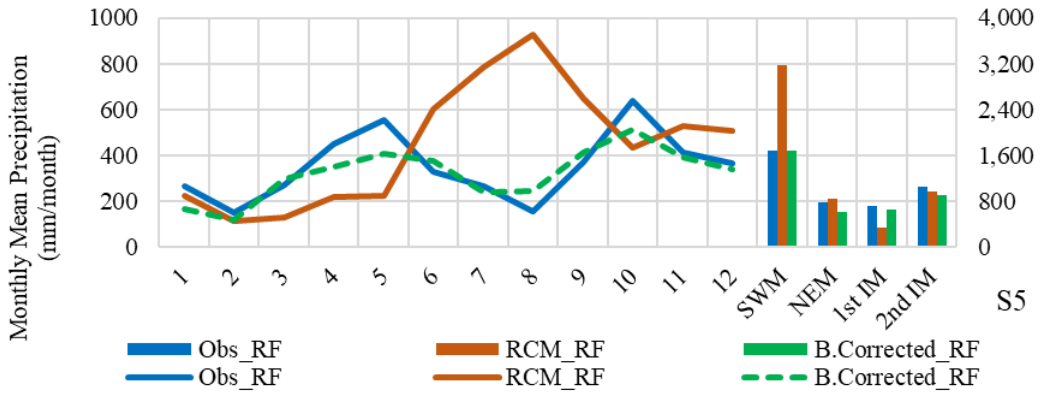

Figure IV-5: S5-Variation of monthly and seasonal means of observed rainfall, RCM rainfall, and bias-corrected RCM rainfall over evaluation period (2001 to 2005)

Table IV-6: S6 - Monthly and seasonal means of observed rainfall, RCM rainfall, and bias-corrected RCM rainfall over evaluation period (2001 to 2005)

Type	Month	Precipitation (mm)		
		Observed	RCM raw data	Bias corrected RCM data
Monthly Means	October	212	224	156
	November	128	116	118
	December	271	130	274
	January	384	216	350
	February	499	225	420
	March	295	599	361
	April	263	784	251
	May	164	927	241
	June	389	647	417
	July	631	436	512
	August	376	526	385
	September	335	508	319
Seasonal Means	SWM	1,611	3,181	1,690
	NEM	675	847	593
	1st IM	655	347	624
	2nd IM	1,007	962	898

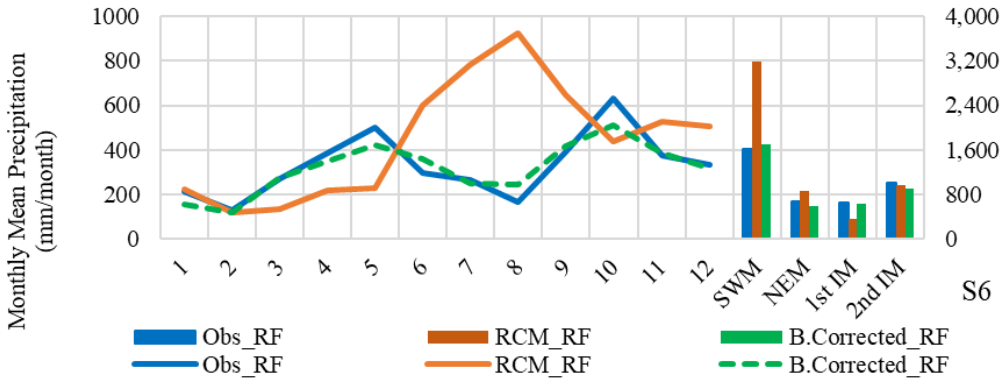

Figure IV-6: S6-Variation of monthly and seasonal means of observed rainfall, RCM rainfall, and bias-corrected RCM rainfall over evaluation period (2001 to 2005)

ANNEXURE V

V. HEC HMS MODEL DEVELOPMENT

Table V-1: Sample calculation of canopy storage for Kukule Ganga sub-basin S1

Landuse Type	Area (A) (Ha)	Canopy Storage (CS) (mm)	A x CS
Chena	9,931.0	1.8	17,875.9
Coconut	3.1	1.27	3.9
Forest - Unclassified	12,265.5	2.54	31,154.2
Homesteads/Garden	1,364.4	1.27	1,732.8
Marshy	5.7	1	5.7
Other Cultivation	691.0	1.27	877.6
Paddy	1,394.5	1	1,394.5
River	604.1	0	-
Rock	22.7	0	-
Rubber	1,488.3	2.032	3,024.2
Scrub land	2,064.1	2.032	4,194.3
Tea	2,297.1	2.032	4,667.8
Total	22,524,212.0		45,517,995.4
Canopy storage for Kukule Ganga (S1) sub-basin $(\sum(AxCS)/\sum A$			2.02 mm

Table V-2: Estimated canopy storage value for each sub-basin

Sub-basin	Estimated canopy storage (mm)
S1	2.02
S2	2.08
S3	2.23
S4	1.97
S5	1.96
S6	1.95

Table V-3: Calculation of basin average surface storage for sub-basins

Sub-basin	Surface Storage (mm)	Area (km^2)	Weight coefficient	Basin Average Surface Storage (mm)	(mm)
S1 - Kukule	1.02	23.134	0.072	0.07	**12.71**
	9	265.006	0.825	7.43	
	50.8	32.899	0.102	5.21	
		321.039			
S2	1.02	10.170	0.045	0.05	**15.71**
	9	179.288	0.786	7.08	
	50.8	38.568	0.169	8.59	
		228.025			
S3	1.02	4.661	0.060	0.06	**13.16**
	9	64.591	0.829	7.46	
	50.8	8.650	0.111	5.64	
		77.902			
S4	1.02	7.021	0.061	0.06	**14.00**
	9	93.215	0.808	7.27	
	50.8	15.148	0.131	6.67	
		115.384			
S5	1.02	1.500	0.039	0.04	**20.27**
	9	25.946	0.683	6.15	
	50.8	10.527	0.277	14.08	
		37.973			
S6	1.02	2.027	0.015	0.02	**18.72**
	9	101.107	0.750	6.75	
	50.8	31.734	0.235	11.95	
		134.867			

Table V-4: Calculation of constant rate or saturated hydraulic conductivity, and maximum deficit for Kukule Ganga sub-basin (S1)

Survey department Soil Map	Kukule Sub Watershed		Details of soil	Texture	Saturated Hydraulic Conductivity			Effective Porosity			Wilting Point			Max. Deficit (mm)
	Area km^2	%			(in/hr)	Assume soil Layer 24 inches	Basin Average (mm/Hr)	(in^3/in^3)	Assume soil Layer 24 inches	Basin average (in^3/in^3)	(in^3/in^3)	Assume soil Layer 24 inches	Basin average (in^3/in^3)	
Alluvial soils of variable texture and drainage; flat terrain		0.0%												
Red-Yellow podzolic soils with prominent A1 or semi-prominent A1	113.09	35.2%	A1 - 0-10 inches; Note 2	Sandy Clay Loam	0.06	0.043	**0.85**	0.33	0.318	**0.320**	0.15	0.179	**0.179**	**85.99**
			A2 10-21 inches; Note 3	Clay Loam	0.03			0.31			0.2			
			Bit 21-32 inches; Note 4	Clay Loam	0.03			0.31			0.2			
Red-Yellow podzolic soils, steeply dissected,hilly and rolling te'	208.23	64.8%	Ap 0-3 inches ; Note 5	Sandy Clay Loam	0.06	0.029		0.33	0.321		0.15	0.179		
			A2 3-15 inches ; Note 6	Sandy Clay	0.02			0.32			0.2			
			Bit 15 - 23 inches ; Note 7	Sandy Clay	0.03			0.32			0.2			
Total Area	***321.32***	100%												

Notes

1. Details of soil according to Soils of Ceylon by Moormakn & Panabokke, (1961)
2. Very dark gray-brown (10 YR 3/?) fine gravelly sandy clay loam, lateritic concretions, fine angular quartz gravel, some rock fragments; moderate fine granular; very friable; many fine random interstitial pores; many roots; smooth, clear transition to
3. Brown (10 YR 4/3) fine gravelly clay loam, less laterite concretions; structureless; friable; common fine pores; some signs of clay or clay-humus movement; few roots; smooth, clear transition to:
4. Brown (7.5 YR 5/5) fine gravelly clay loam; moderately weak fine subangular blocky; distinct clay coatings; friable; few root; smooth, clear transition
5. Dark brown (10 YE 4/3) fine gravelly sandy clay loam, latentie pebbles, bleached white sand grains; moderate crumb;.friable; common interstitial exped pores; many roots; smooth, clear transition to :
6. Yellowish-brown (10 YE 5/5) fine gravelly sandy clay, lateritic pebbles; very weak fine subangular blocky; friable; common fine and medium interstitial exped pores; many roots; smooth, clear transition to:
7. Strong brown (7.5 YR 5/6) fine gravelly sandy clay, lateritic pebbles and quartz gravel; moderate fine subangular blocky; clay coatings; friable to firm; pores as above; less roots; smooth, clear transition

Table V-5: Calculation of percentage impervious for Kukule Ganga sub-basin (S1)

Land use type	Impervious category (Prisloe et al., 2000)	Impervious Surface coefficient (C) (%)	Area (A) (Ha)	Impervious Area (C x A) (Ha)
Chena	Exposed Soil / Cropland	2.9	9,931.0	290.0
Coconut	Scrub & Shrub	1.4	3.1	0.0
Forest - Unclassified	Mixed Forest	0.4	12,265.5	45.4
Homesteads/Garden	Rural Residential	38.5	1,500.8	577.4
Marshy	Shallow Water & Mud Flats	2.9	5.7	0.2
Other Cultivation	Exposed Soil / Cropland	2.9	691.0	20.2
Paddy	Non-forested Wetland	2.5	1,394.5	35.1
River	NA	0.0	604.1	0.0
Rock	NA	0.0	22.7	0.0
Rubber	Deciduous Forest	3.5	1,453.6	50.6
Scrub land	Scrub & Shrub	1.4	2,064.1	27.9
Tea	Scrub & Shrub & Exposed Soil / Cropland	4.3	2,297.1	98.1
Total Area			32,233.30	1,144.80
Percentage impervious of Kukule Ganga sub-basin (S1)				3.55%

Table V-6: Estimated basin average deficit and constant parameters for each sub-basin

Sub-basin	Constant rate (mm/hr)	Maximum deficit (mm)	Percentage impervious (%)
S1	0.85	86.0	3.55
S2	0.72	84.7	5.23
S3	0.72	84.7	3.07
S4	0.72	84.7	6.18
S5	0.72	84.7	6.69
S6	0.72	84.7	6.68

Table V-7: Calibrated parameters of the HEC HMS model

Name of the Parameter	Unit	Sub-basin 1	Sub-basin 2	Sub-basin 3	Sub-basin 4	Sub-basin 5	Sub-basin 6
Initial Deficit	mm	25.00	25.00	25.00	25.00	25.00	25.00
Maximum Deficit	mm	81.73	8 0.51	80.51	80.51	80.51	80.51
Constant Rate	mm/hr	1.18	1.12	1.12	1.03	1.03	1.03
% Impervious	%	5.00	5.00	5.00	7.00	7.00	7.00
Standard Lag	hr	30.45	30.34	14.21	13.31	14.47	14.47
Peaking Coefficient	-	0.55	0.50	0.50	0.50	0.50	0.50
GW 1 Initial Discharge	$m^3/s/km^2$	0.00	0.00	0.00	0.00	0.00	0.00
GW 1 Fraction	-	0.05	0.05	0.05	0.05	0.05	0.05
GW 1 Coefficient	hr	114.31	136.65	50.43	53.97	55.91	67.47
GW 2 Initial Discharge	$m^3/s/km^2$	0.04	0.04	0.04	0.04	0.04	0.04
GW 2 Fraction	-	0.40	0.40	0.40	0.40	0.40	0.40
GW 2 Coefficient	hr	910.61	1088.63	401.69	430	445.46	537.61
		Reach 1	Reach 2	Reach 3	Reach 4	Reach 5	
K	hr	9.95	1.70	6.19	7.78	4.64	
X	-	0.20	0.20	0.20	0.20	0.20	

ANNEXURE VI

VI. MODEL SIMULATIONS FOR THE DESIGN PERIOD USING BIAS-CORRECTED RCM DATA UNDER RCP 2.6 AND 8.5

Table VI-1: Variation of MAM7 with projected streamflow under RCP 2.6 scenario relative to the base period 2005 to 2020

Period of Time	MAM7 (m^3/s)					% Difference relative to the base				
	SWM	NEM	1st IM	2nd IM	Annual	SWM	NEM	1st IM	2nd IM	Annual
Base 2010's	18.14	11.07	16.72	37.30	8.85					
2030's	19.02	7.45	7.73	47.94	6.27	4.87	-32.67	-53.77	28.53	-29.11
2040's	24.43	8.76	11.39	40.18	7.91	34.69	-20.85	-31.87	7.74	-10.62
2050's	22.74	15.51	10.86	48.58	8.73	25.37	40.11	-35.03	30.25	-1.37

Table VI-2: Variation of MAM30 with projected streamflow under RCP 2.6 scenario relative to the base period 2005 to 2020

Period of Time	MAM30 (m^3/s)					% Difference relative to the base				
	SWM	NEM	1st IM	2nd IM	Annual	SWM	NEM	1st IM	2nd IM	Annual
Base 2010's	33.44	18.35	30.01	67.15	16.56					
2030's	26.76	12.54	16.56	55.82	9.85	-19.98	-31.68	-44.80	-16.86	-40.47
2040's	30.23	11.47	19.68	51.62	11.04	-9.60	-37.53	-34.40	-23.13	-33.34
2050's	29.23	20.82	18.55	59.57	14.57	-12.61	13.43	-38.19	-11.28	-12.00

Table VI-3: Variation of MAM7 with projected streamflow under RCP 8.5 scenario relative to the base period 2005 to 2020

Period of Time	MAM7 (m^3/s)					% Difference relative to the base				
	SWM	NEM	1st IM	2nd IM	Annual	SWM	NEM	1st IM	2nd IM	Annual
Base 2010's	18.14	11.07	16.72	37.30	8.85					
2030's	24.66	5.40	4.56	48.15	4.02	35.96	-51.22	-72.74	29.08	-54.57
2040's	28.49	10.77	7.03	48.03	6.83	57.05	-2.71	-57.92	28.77	-22.76
2050's	24.46	11.43	15.19	53.03	7.95	34.85	3.27	-9.11	42.18	-10.14

Table VI-4: Variation of MAM30 with projected streamflow under RCP 8.5 scenario relative to the base period 2005 to 2020

	MAM30 (m^3/s)					% Difference relative to the base				
Period of Time	SWM	NEM	1st IM	2nd IM	Annual	SWM	NEM	1st IM	2nd IM	Annual
Base 2010's	33.44	18.35	30.01	67.15	16.56					
2030's	30.43	6.89	8.65	57.47	5.75	-9.01	-62.44	-71.17	-14.40	-65.25
2040's	35.73	13.49	14.08	57.14	11.46	6.84	-26.49	-53.06	-14.90	-30.76
2050's	30.52	14.31	25.45	62.52	11.48	-8.74	-22.06	-15.18	-6.90	-30.64

Table VI-5: Average annual and seasonal baseflow index (BFI) variation and percentage change in relative to the base period 2005-2015 under RCP 2.6

	BFI					% Difference relative to the base				
Period of Time	SWM	NEM	1st IM	2nd IM	Annual	SWM	NEM	1st IM	2nd IM	Annual
Base 2010's	0.58	0.64	0.61	0.54	0.58					
2030's	0.79	0.88	0.68	0.77	0.78	35.52	37.94	10.19	41.54	34.40
2040's	0.84	0.89	0.70	0.83	0.81	43.26	39.36	13.32	52.78	41.18
2050's	0.81	0.88	0.72	0.84	0.81	38.06	38.02	17.79	55.09	41.09

Table VI-6: Average annual and seasonal baseflow index (BFI) variation and percentage change relative to the base period 2005-2015 under RCP 8.5

	BFI					% Difference relative to the base				
Period of Time	SWM	NEM	1st IM	2nd IM	Annual	SWM	NEM	1st IM	2nd IM	Annual
Base 2010's	0.58	0.64	0.61	0.54	0.58					
2030's	0.78	0.89	0.73	0.85	0.80	34.31	39.39	18.96	55.75	39.11
2040's	0.75	0.91	0.62	0.80	0.76	29.30	43.33	0.08	47.03	32.18
2050's	0.75	0.88	0.73	0.82	0.77	28.60	38.11	18.37	51.56	33.18

The findings, interpretations and conclusions expressed in this thesis/dissertation are entirely based on the results of the individual research study and should not be attributed in any manner to or do neither necessarily reflect the views of UNESCO Madanjeet Singh Centre for South Asia Water Management (UMCSAWM), nor of the individual members of the MSc panel, nor of their respective organizations.